

Isabele Fattori Moretti

**Exploração da via de sinalização do Receptor do
Tipo
Toll 4 (TLR4) para o tratamento de Glioblastoma**

**São Paulo
2023**

Isabele Fattori Moretti

**Exploração da via de sinalização do Receptor do Tipo
Toll 4 (TLR4) para o tratamento de Glioblastoma**

Tese apresentada à Faculdade de Medicina da
Universidade de São Paulo para obtenção de título de
doutora em Ciências

Programa de Neurologia

Orientadora: Profa. Dra. Suely Kazue Nagahashi Marie

**São Paulo
2023**

Ficha Catalográfica

Dados Internacionais de Catalogação na Publicação (CIP)

Preparada pela Biblioteca da
Faculdade de Medicina da Universidade de São Paulo

©reprodução autorizada pelo autor

Moretti, Isabele Fattori
Exploração da via de sinalização do Receptor do
Tipo Toll 4 (TLR4) para o tratamento de
glioblastoma / Isabele Fattori Moretti. -- São
Paulo, 2023.
Tese(doutorado)--Faculdade de Medicina da
Universidade de São Paulo.
Programa de Neurologia.
Orientadora: Suely Kazue Nagahashi Marie.

Descritores: 1.Glioblastoma 2.Metformina
3.Receptores de lipopolissacarídeos 4.Pontos de
checagem do ciclo celular 5.Apoptose 6.NF-kappa B
7.Receptor 4 toll-like

USP/FM/DBD-126/23

Responsável: Erinalva da Conceição Batista, CRB-8 6755

Dedicatória

Aos meus familiares, em especial aos meus pais e minha irmã que sempre estiveram comigo, pelo apoio inabalável e incondicional.

Aos meus amigos que foram muito presentes, por me acompanharem e me compreenderem quando eu precisei. À Alessandra do Amaral, Aline Ferraz, Amanda Batista, Arthur de Lima, Caio Mendes, Gabriella Cardoso, Ligia Kyiuna, Moreno Pereira, Matheus Silva, Ricardo Pires e Yasmin Palulian.

Com todo meu carinho e amor dedico a vocês.

Agradecimentos

À minha orientadora Profa. Dra. Suely Kazue Nagahashi Marie meus mais sinceros agradecimentos, por ter me encorajado a seguir em frente. Todo o seu incentivo foi muito valioso para meu crescimento profissional e pessoal. Agradeço todo o tempo e empenho dedicados e espero que possa continuar com a sua ajuda no que vier pela frente.

À Dra. Sueli Mieko Oba-Shinjo por toda a contribuição, toda a atenção e cuidados que me motivaram para chegar até aqui.

À pesquisadora Dra. Roseli da Silva e à funcionária Paula Sola por toda ajuda e ensinamentos, agradeço toda a dedicação e prontidão em me ajudar.

Ao Dr. Antonio Lerário por todas análises de transcriptoma que permitiu que tivéssemos publicações aprimoradas e com grande aprofundamento de resultados, além de todo apoio e sugestões que foram muito relevantes.

Ao Prof. Dr. Giuseppe Palmisano por toda a disponibilidade e colaboração. Agradeço também aos funcionários e alunos do laboratório de GlicoProteômica que sempre me receberam de portas abertas. Em especial à Janaína Macedo, Veronica Feijoli e Lívia Fernandes.

À Profa. Dra. Marisa Passarelli que fez a doação da Metformina que foi essencial para nossa publicação, e ainda acredito que proporcionará outras possibilidades.

À Profa Dra. Maria Lúcia Giannela por toda a colaboração com o grupo da Profa Suely.

Ao Prof. Dr. Maurício Baptista que abriu seu laboratório e permitiu que nós trabalhássemos com o equipamento Seahorse, agradeço aos funcionários e alunos do seu laboratório em especial à Márcia Franco por toda sua assistência.

À Profa. Dra. Alícia J Kowaltowski e funcionária Camille Caldeiras por todo auxílio e disponibilidade com o equipamento Seahorse.

Ao Prof. Dr. Esper Kallas, a seus funcionários e alunos por toda a ajuda com a citometria de fluxo.

Ao CEFAP pelo uso do confocal, especialmente ao técnico Mário Cruz.

Ao laboratório de sequenciamento em larga escala (SELA), agradeço à Amanda Narcizo.

Às alunas do LIM-15 Stella Cavalcante, Talita Laurentino, Adaliana Moussessian, Yollanda Franco, Camila Dantas e Vanessa Futema. Foi um privilégio trabalhar e compartilhar esses anos com vocês.

Aos funcionários do LIM15, Dra. Christiane Ohzaki, Luís Roberto Silva, Rosa Martins, Maria Eunice, Camila, Darcy e Eliene. E aos funcionários do departamento de Neurologia principalmente à secretária Thais Figueira.

O presente trabalho foi realizado com apoio da Coordenação de Aperfeiçoamento de Pessoal de Nível Superior -Brasil (CAPES/PROEX) - Código de Financiamento 88887.600107/2021-00 e (CAPES/NUFFIC) 88887.351607/2019-00.

Resumo

Moretti IF. Exploração da via de sinalização do Receptor do Tipo Toll 4 (TLR4) para o tratamento de Glioblastoma [tese]. São Paulo: Faculdade de Medicina, Universidade de São Paulo; 2023.

Glioblastomas (GBM) são astrocitomas grau 4 e apresentam sobrevida média de 15 meses após o diagnóstico mesmo como tratamento padrão que consiste na ressecção cirúrgica, radioterapia e quimioterapia com temozolamida (TMZ). Previamente, nosso grupo reportou o aumento da expressão de receptores do tipo Toll (TLR) de membrana plasmática em GBMs, especialmente no subtipo mesenquimal (MES), que apresenta o pior prognóstico. TLR4 é um receptor do sistema imunológico responsável em reconhecer moléculas associadas a patógenos e a dano. Diferentes vias de sinalização são descritas para o TLR4 que podem ser pró-sobrevivência ou pró-morte. O objetivo principal deste trabalho foi a análise da sinalização do TLR4 em células de GBM e explorar possíveis alvos terapêuticos. Inicialmente confirmou-se a presença de TLR4 em astrocitomas humanos e nas linhagens celulares de GBM do subtipo MES, U87MG e A172. O tratamento com lipossacarídeo (LPS), ativador clássico da via TLR4, levou a translocamento para o núcleo tardio do NF- κ B, um dos principais fatores de transcrição da via do TLR4, com aumento da expressão de *IL1B* e genes relacionados ao reparo do DNA. Observou-se ainda aumento da expressão de genes associados a vias não canônicas do TLR4, inflamassomo e ripoptossomo, que foram validados em análise *in silico* em banco de dados públicos do Atlas do Genoma do Câncer (TCGA). O tratamento combinado com LPS+TMZ aumentou a apoptose das células U87MG, no entanto, houve um incremento significativo maior da morte celular com o acréscimo de inibidor do reparo do DNA, anti-RAD51 / Amuvatinib, em comparação a cada tratamento único. A seguir, o efeito combinado de LPS com metformina (MET) foi analisada em U87MG e A172 por RNASeq. MET é um medicamento conhecido para tratamento de diabetes e inibi o complexo I da fosforilação oxidativa e também pode causar uma resposta anti-inflamatória, incluindo diminuição da ativação do NF- κ B. MET levou à diminuição da viabilidade celular e estresse mitocondrial em ambas linhagens. Na U87MG, LPS+MET aumentou a expressão de genes pró-apoptóticos e diminuiu de genes pró-sobrevivência e o tratamento combinado LPS+MET+TMZ aumentou significativamente a apoptose das células tumorais. Já nas células A172, com aumento da expressão de genes anti-

oxidantes, o nível de apoptose do tratamento combinado foi muito similar ao tratamento só com TMZ. No entanto, o tratamento com MET diminui a expressão de genes relacionados a segregação cromossômica, o que foi compatível com a parada do ciclo celular observado após tratamento MET+TMZ. O aumento da expressão de genes de anti-oxidação, especialmente SOD1 foi validado *in silico* nos dados de TCGA no subtipo mitocondrial (MTC), com perfil de expressão similar à linhagem A172. A ativação da via TLR4 foi confirmada no subtipo glicolítico/plurimetabólico (GPM), compatível com perfil de expressão da linhagem U87MG. Os resultados do presente estudo sugerem que os GBM-GPM são elegíveis ao tratamento com MET e a associação com inibidores de reparo do DNA poderá incrementar a morte da célula tumoral, enquanto os GBM-MTC poderão se beneficiar com tratamento combinado com inibidores de anti-oxidantes, como anti-SOD1.

Palavras-chave: Glioblastoma. Metformina. Receptores de lipopolissacarídeos. Pontos de checagem do ciclo celular. Apoptose. NF-kappa B. Receptor 4 toll-like.

Abstract

Moretti IF. Exploitation of Toll like rector 4 (TLR4) signaling pathway for Glioblastoma treatment [thesis]. São Paulo: “Faculdade de Medicina, Universidade São Paulo”; 2023

Glioblastomas are grade 4 astrocytomas, presenting a medium overall survival of 15 months with standard treatment which consists in tumor resection, radiotherapy and chemotherapy with temozolomide (TMZ). Previously, our group showed upregulation of plasmatic membrane Toll-like receptors (TLRs) in human astrocytoma samples, particularly in GBM of mesenchymal (MES) subtype, presenting the poorest outcome. TLR4 is an important immune receptor, responsible to recognize molecules associated to pathogens and cellular damage. TLR4 stimulation may activate different pathways leading either to cell survival or cell death. The general aim of the present study was to analyze TLR4 signaling pathways in GBM cells and explore possible druggable targets. First, we confirmed TLR4 presence in human astrocytoma samples, and GBM cell lines of MES subtype, U87MG and A172. The lipopolysaccharide (LPS) treatment, TLR4 classical activator, led to late nuclear translocation of NF- κ B, one of the main transcription factor downstream of TLR4 activation, with upregulation of *IL1B* and gene related to DNA repair. Genes associated to non-canonical TLR4 pathway, as ripoptosome and inflammasome, were also upregulated, which were validated *in silico* analysis of the public The Cancer Genome Atlas (TCGA) GBM RNASeq database. The combined LPS+TMZ treatment increased apoptotic rate of U87MG cells, however, a further increment was observed with the addition of the DNA repair inhibitor, anti-RAD51 / Amuvatinib, compared to each treatment alone. Next, the effect of the combined therapy with LPS and metformin (MET) was analyzed in U87MG and A172 by RNASeq. MET is a known medication for diabetes and inhibits complex I of oxidative phosphorylation, and also may cause an anti-inflammatory response, including NF- κ B activation. MET led to a decrease of tumor cell viability and mitochondrial stress in both lineages. In U87MG, LPS+MET upregulated pro-apoptotic gene expressions and downregulated pro-survival gene expressions and the combined treatment LPS+MET+TMZ increased significantly the apoptosis of tumor cells. In contrast, in A172, with upregulation of anti-oxidative genes, the apoptotic rate of the combined treatment was similar to TMZ alone. However, MET treatment decreased the expression of genes related to chromosome segregation, which was compatible to observed cell cycle arrest after MET+TMZ treatment. Upregulation of anti-oxidative

genes, mainly *SOD1*, was validated *in silico* in the TCGA dataset in the mitochondrial (MTC) GBM subtype, with similar expression profile detected in A172. TLR4 activation was confirmed in the glycolytic/plurimetabolic (GPM) GBM subtype, compatible with the expression profile observed in U87MG. Therefore, the results of the present study suggested that GBM-GPM are eligible for MET treatment and an association with DNA repair inhibitors may increment tumoral cell death, while GBM-MTC may benefit from combined treatment with anti-oxidative inhibitors as anti-SOD1.

Keywords: Glioblastoma. Metformina. Lipopolysaccharide receptors. Cell cycle checkpoints. Apoptosis. NF-kappa B. Toll-like receptor 4.

Summary

1	Introduction – TLR4 and GBM.....	12
1.1	Toll-like Receptor 4.....	13
1.2	Glioblastoma.....	15
1.3	TLR4 and GBM.....	17
2	Aims.....	18
3	Experimental design and the studies.....	18
4	Publication 1 - Late p65 nuclear translocation in glioblastoma cells indicates non-canonical TLR4 signaling and activation of DNA repair genes.....	19
5	Publication 2 - GBM Cells Exhibit Susceptibility to Metformin Treatment According to TLR4 Pathway Activation and Metabolic and Antioxidant Status....	37
6	Discussion – TLR4 and Glioblastoma – final remarks.....	63
7	Conclusion.....	68
8	References for introduction and discussion.....	69
9	Anexos.....	75

Introduction

TLR4 and Glioblastoma

1 Introduction

Toll like receptor 4 (TLR4) is classically described as present in immune system cells, and it binds to molecules commonly present in pathogens or to endogenous molecules derived from cellular damage. Initially, TLR4 activation leads to a pro-inflammatory response through the production of interleukin-6 (IL-6), interleukin-1 β (IL-1 β), interleukin-8 (IL-8) cytokines and tumor necrosis factor (TNF), which assures cell survival and promotes cell proliferation. TLR4 can also activate an anti-inflammatory signal increasing interleukin-10 (IL-10) expression or by interferon type I signaling pathway (1). Moreover, TLR4 activation can promote cellular death (2).

In the tumor context, phenotypically anti- and/or pro-inflammatory cells infiltrate the tumor configuring a complex microenvironment (3, 4). Besides, tumor cells may “re-educate” immune cells to a pro-tumoral phenotype to promote tumor growth and proliferation (4). Additionally, TLR4 has been detected not only in inflammatory cells, but also in tumor cells (5, 6, 7, 8). Therefore, the present work was designed to address the question how the activation of TLR4 in GBM cells impact in tumor progression.

1.1 Toll like receptor 4

TLR4, among receptors, is the first molecule in the innate immunity capable of recognizing cell stress or pathogens invasion. Ten TLRs are described in humans, TLR1-10, and are structurally similar

The basic structure of these receptors comprises a recognition domain in the amino- terminal portion, presenting leucin repetitions; followed by a transmembrane helix, and a cytoplasmic domain, denominated Toll-interleukin receptor (TIR) in the carboxy-terminal portion (9, 10, 11).

Each TLR presents specific roles and characteristics for recognition, as TLR 1, 2, 4, 5, and 6, located in plasmatic membrane, bind to bacterial and fungal structures, while TLR 3, 7, 8, and 9, located in endosomes, recognize bacterial and viral molecules (9, 10, 12).

Pathogens molecules recognized by these receptors are nominated as Pathogens Associated Molecular Patterns (PAMPs), and endogenous molecules from damage or necrotic cells and tissues are designated as Danger Associated Molecular Patterns (DAMPs). Several molecules are classified as DAMPS, such as, high mobility

protein B1 (HMGB1) (13); hyaluronic acid (9); uric acid, heat shock proteins, surfactant protein A and extracellular matrix products like fibronectin, heparan sulfate, and fibrinogen (10, 14). DAMPs are recognized by TLR2 and TLR4, and they play an immunogenic role repairing the damaged area (15). The signaling pathway activated by DAMPs and PAMPs are similar, differing only for the co-receptors associated to the recognition (16).

Interestingly, TLR4 has the ability to activate two distinct pathways, via Myeloid Differentiation primary response gene 88 (MyD88) and TIR-domain-containing adapter-inducing interferon- β (TRIF). After MyD88 activation, transcription factor Nuclear *kappa* B (NF- κ B) and the family Mitogen Activated Protein Kinases (MAPKs) are activated.

The NF- κ B is an important transcription factor in TLR4 pathway. The NF- κ B family consists of five subunits. Structurally, NF- κ B family present a transactivation domain responsible for gene transcription. The five subunits can form homo and heterodimers, and are named RelA, also known as p65; RelB, c-Rel, p50 and p52(17). TLRs are known to activate the NF- κ B canonical pathway. Briefly, in the canonical pathway, the signal starts after NF- κ B p50/p65 is released from the inhibitor kappa B (IKB), and subsequently phosphorylated by IKB kinase complex (IKK), the IKB is ubiquitinated and degraded (18). The subunit p65 plays the major role and it forms heterodimer with p50 and c-Rel, being part of the canonical pathway (19). In this pathway, the NF- κ B induces a pro-inflammatory phenotype by expressing IL-6, TNF, IL-1 β and IL-8, chemokines, adhesion molecules, acute phase proteins, and co-stimulation molecules (20, 21). This signaling pathway is related to cell proliferation, with activation of proliferation factors as cyclin D1 (22), c-JUN (6, 23) and c-myc (24). In addition, cell proliferation can be also increased indirectly by IL-6 and IL-8 secretion (25, 26). This pro-survival signaling is essential for immune cells to fulfill their protective role (10, 27). For IL-1 β maturation is necessary the inflammasome complex, composed by NLRP3 (NLR Family Pyrin Domain Containing 3), CASP1 (Caspase 1) and PYCARD (PYD And CARD Domain Containing). The Inflammasome is an important process that activates the innate immune response, adaptative response and also lead to a type of cell death, named pyroptosis (28).

The non-canonical pathway of TLR4 involves the TLR4 endocytosis under phosphoinositide 3-kinase (PI3K) modulation. Once inside the endosome, TLR4 signals by TRIF (29). TRIF activation leads to an anti-inflammatory response, resulting in the activation of the transcription factors interferon-3 and 7 (IRF3/7). IRF3/7 induces the expression of interferon type I cytokines (IFN- α and IFN- β) and IL-10 (9, 10, 30, 31). TRIF pathway is responsible to end the inflammatory process. Furthermore, TRIF orchestrates a death signaling pathway by interaction with RIPK1 (Receptor interacting protein kinase 1), RIPK3 (Receptor interacting protein kinase 3), and FADD (Fas Adaptor Death Domain). This complex activates CASP8 (caspase 8), starting the apoptotic cell signaling (32). CASP8 inhibition may result in a necroptosis response (33).

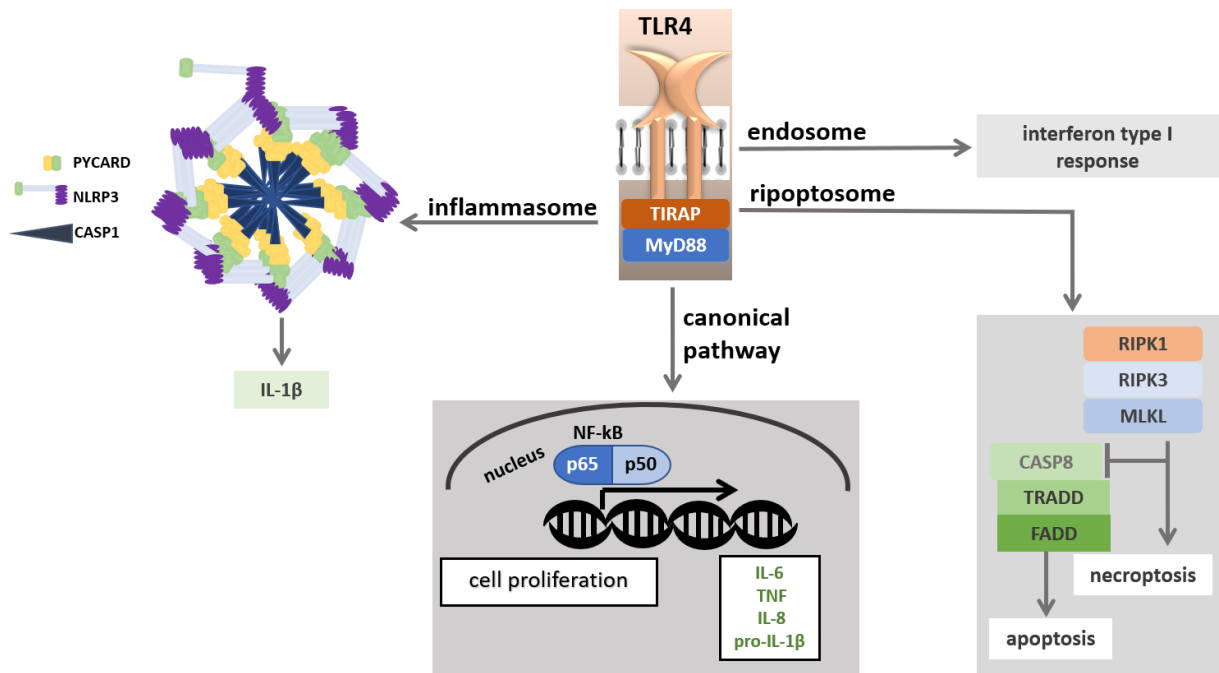


Figure 1 Schematic of TLR4 signaling. After activation of TLR4 the canonical signaling pathway activates NF- κ B, that translocates to the nucleus and starts the transcription of cell proliferation genes, and inflammatory cytokines. TLR4 activates the inflammasome complex to produce the functional IL-1 β . TLR4 endocytosis is another pathway signaling for Interferon type I response. Further, TLR4 activates the ripoptosome complex leading to either necroptosis with the inhibition of CASP8 or apoptosis in its presence.

1.2 Glioblastoma

The present work will analyze TLR4 role in Glioblastoma (GBM) cells. GBM is classified as astrocytoma grade 4 according to the World Health Organization (WHO), with overall survival of 15 months with current standard of care which includes surgical tumor resection, radiotherapy, and chemotherapy with temozolomide (TMZ) (34, 35).

GBM is a very heterogeneous tumor, with high proliferative cells rate, nuclear atypia, neovascularization, and necrosis. GBM is restricted to the central nervous system, and is highly invasive to the surrounding normal brain tissue (36, 37).

The *de novo* GBM corresponds to primary GBM, whereas secondary GBM evolves from a lower grade astrocytoma (38). GBM was one of the first solid tumor analyzed by high throughput sequencing which determined different molecular subtypes based on mutational status with impact on patient's overall survival. The proneural (PN) subtype presents a molecular pattern related to progenitor or neural stem cells and correlated with better overall survival. The PN subtype harbours mutations in *PDGFRA* (platelet derived growth factor receptor alpha), *TP53* (tumor protein p53) and *IDH1* (isocitrate dehydrogenase 1) genes. The classical subtype (CS) presents proliferative markers, mostly *EGFR* (epidermal growth factor receptor) amplification, but also deletion in chromosome 10 and amplification in chromosome 7. The mesenchymal (MES) subtype is associated to mesenchymal markers, as *MET*, *NF1* (neurofibromin 1) mutations, and presents the worst prognosis (39, 40, 41). WHO added *IDH1* mutation status for classification purposes and the majority of secondary GBMs presents *IDH1* mutation and characteristics of PN subtype (42). GBM with *IDH1* mutation will be designated as grade 4 astrocytoma with *IDH1* mutation, according the most recent WHO classification (43).

Several high throughput analyses were performed to try to identify expression signatures and correlation to overall survival. In the present work the classification proposed in Garofano *et al's* study, 2021 (44) was applied to analyze the impact of our results based in a metabolic stratification of GBM. Four pathways based on metabolic and development molecular signatures were identified in GBM by the authors. Two subtypes were based in metabolic phenotypes, one presenting complex I of the mitochondrial oxidative phosphorylation system (OXPHOS) upregulated genes, named as Mitochondrial (MTC), and the other with upregulation of glycolytic pathway targets, named as glycolytic/plurimetabolic. The two other subtypes were classified according to developmental markers, one being neuronal (NEU), presenting upregulation of genes responsible for axogenesis and synaptic transmission, and the other denominated as proliferative/progenitor subtype (PPR), with markers of progenitor neural cells, and upregulation of genes related with cell cycle progression and DNA repair (44).

1.3 TLR4 and GBM

Several roles have been described for TLR4 in tumor cells, as cell survival and proliferation (7, 45, 46, 47, 48, 49, 50), migration (49, 51), and a pro-inflammatory phenotype (50, 52, 53, 54, 55). In glioma animal models (52, 56, 57), TLR4 activation by LPS, a known agonist for TLR4, resulted in tumor remission, where the anti-tumor response was attributed to the infiltration of inflammatory cells (45).

TLR4 role was also evaluated in glioma stem cells (GSCs). TLR4 upregulation was reported in differentiating glioma stem cells (GSCs) and its blockage led to decreased number and viability of differentiate cells. The transcription factor, NF- κ B, was associated to TLR4 activation in differentiating GSCs cells. A positive loop of autocrine signaling through secreted hyaluronic acid, a DAMP TLR4-agonist, was described to increment this pathway (58). However, newly differentiated GBM cells showed no effect in their viability, when treated with LPS and TMZ (59). Moreover, non-differentiated GSCs with downregulated TLR4, presented self-renewal and survival by avoiding the activation of inflammatory pathways (60). In animal models, microglia secretion of IL-6 via TLR4, increased glioma growth through IL-6 intake by GSCs cells (61).

Previously, we also evaluated the expression of plasmatic membrane TLRs in human astrocytoma samples and observed higher TLRs expression in the tumor samples compared to non-tumor samples. Interestingly, TLRs expressions were upregulated in MES-GBM subtype. Our findings confirmed the TLRs presence in tumor cells (8), that motivated our interest to better understand their role in the tumor context. We focused our studies in TLR4 because it was highly upregulated in tumor samples, and presented a particular cell compartment distribution, including a nuclear localization.

2 Aims

We aimed to evaluate the TLR4 role in GBM cells in search for druggable targets in the TLR4 signaling pathways.

3 Experimental design and the studies

We designed the present work with *in vitro* experiments in GBM cell lines to address the TLR4 signaling pathways activated by LPS, and the effects on these pathways with combined treatment with metformin (MET) and TMZ. The corresponding results were presented in publication 1 and publication 2, respectively.

4 Publication 1 - Late p65 nuclear translocation in glioblastoma cells indicates non-canonical TLR4 signaling and activation of DNA repair genes

In **publication 1**, we evaluated the role of TLR4 in GBM, aiming to analyze:

- a) TLR4 expression in human astrocytoma cases
- b) TLR4 gene and protein expression in U87MG-GBM cell line
- b) U87MG cells behavior after stimulus with LPS in U87MG cells
- c) involved signaling pathways in U87MG cells after LPS stimulus by Next Generation Sequencing-RNASeq (NGS-RNA-seq)
- d) effect of combined treatment with LPS + TMZ and LPS + inhibitor of DNA repair + TMZ in U87MG cells.
- e) the identified signaling pathways *in silico* in the Cancer Genome Atlas (TCGA)-GBM-RNASeq dataset


This study was published in the Scientific Reports (62), where methodology, results and discussion were detailed. In brief, we observed, unexpectedly, a late NF- κ B translocation to nucleus after 12hs of LPS stimulation, in contrast to a translocation within 100min after canonical activation of TLR4 previously described in immune cells. An increased expression of *IL1B* was observed after this time interval, and, interestingly, DNA repair genes expressions were concomitantly increased, and TLR4 was detected in nuclei of U87MG cells. A TLR4-non-canonical pathway activation was observed after LPS stimulation by the transcriptomic analysis, with upregulation of ripoptosome and inflammasome components. The combined treatment with LPS and TMZ led to an increased apoptotic rate in comparison to TMZ alone, and the addition of a DNA repair inhibitor, Amuvatinib, RAD51 inhibitor, further reduced tumor cell viability more than with each treatment alone. These results suggested that for GBM cases presenting stimulation of TLR4, a combinatory treatment with pharmacological inhibition of the DNA repair pathway may be complementary treatment to the current standard of care. The publication 1 (PMID: 33446690) is presented below.

Publication 1

Late p65 nuclear translocation in glioblastoma cells
indicates non-canonical TLR4 signaling and activation of
DNA repair genes



OPEN Late p65 nuclear translocation in glioblastoma cells indicates non-canonical TLR4 signaling and activation of DNA repair genes

Isabele F. Moretti¹, Antonio M. Lerario², Marina Trombetta-Lima¹, Paula R. Sola¹, Roseli da Silva Soares¹, Sueli M. Oba-Shinjo¹ & Sueli K. N. Marie¹

Glioblastoma (GBM) is the most aggressive brain primary malignancy. Toll-like receptor 4 (TLR4) has a dual role in cell fate, promoting cell survival or death depending on the context. Here, we analyzed *TLR4* expression in different grades of astrocytoma, and observed increased expression in tumors, mainly in GBM, compared to non-neoplastic brain tissue. TLR4 role was investigated in U87MG, a GBM mesenchymal subtype cell line, upon LPS stimulation. p65 nuclear translocation was observed in late phase, suggesting TLR4-non-canonical pathway activation. In fact, components of ripoptosome and inflammasome cascades were upregulated and they were significantly correlated in GBMs of the TCGA-RNASeq dataset. Moreover, an increased apoptotic rate was observed when the GBM-derived U87MG cells were co-treated with LPS and Temozolomide (TMZ) in comparison to TMZ alone. Increased TLR4 immunostaining was detected in nuclei of U87MG cells 12 h after LPS treatment, concomitant to activation of DNA repair genes. Time-dependent increased *RAD51*, *FEN1* and *UNG* expression levels were confirmed after LPS stimulation, which may contribute to tumor cell fitness. Moreover, the combined treatment with the *RAD51* inhibitor, Amuvatinib in combination with TMZ after LPS stimulation reduced tumor cell viability more than with each treatment alone. In conclusion, our results suggest that stimulation of TLR4 combined with pharmacological inhibition of the DNA repair pathway may be an alternative treatment for GBM patients.

Toll-like receptor 4 (TLR4) is part of the receptor family for innate immunity that first recognizes endogenous (damage-associated molecular patterns—DAMPs) and exogenous (pathogen-associated molecular patterns—PAMPs) molecules¹. This family is composed of 10 known receptors in humans, which are structurally similar (TLR1-10)². Depending on the context, TLR4 activation may induce a pro-inflammatory and pro-survival response, which translates into a proliferative phenotype or may induce an anti-inflammatory response leading to cell death^{3,4}.

TLR4 downstream signaling includes two distinct pathways: the myeloid differentiation primary response gene 88 (MyD88; "canonical" pathway) and TIR-domain-containing adapter-inducing interferon- β (TRIF; "non-canonical" pathway). Signaling through the canonical TLR4 leads to the activation of the transcription factor nuclear kappa B (NF- κ B) by means of the translocation of its heterodimeric complex p50/p65 to the nucleus⁵. Once in the nucleus, NF- κ B induces the transcription of pro-inflammatory genes coding for interleukins 6 (IL6) and 1 β (IL-1 β), tumor necrosis factor (TNF), adhesion molecules, and chemokines⁶⁻⁷, as well as genes coding for a proliferative response⁸⁻¹². On the other hand, the non-canonical pathway consists of the TLR4 internalization to the endosome compartment by a phosphoinositide 3-kinase (PI3K)-dependent mechanism¹³. This process results in the activation of TRIF, which promotes an anti-inflammatory response by inducing the expression of interferon type I, interferon regulatory factor 3 and 7 (IRF3/7), and IL-10¹⁴. TRIF may also trigger a cell death pathway by interacting with receptor interacting protein kinase 1 and 3 (RIPK1, RIPK3), and the fas adaptor death domain (FADD), which in turn activate caspase 8 (CASP8), leading to apoptosis. In the absence of CASP8, the necroptosis pathway is activated^{15,16}.

¹Laboratory of Molecular and Cellular Biology (LIM15), Department of Neurology, Faculdade de Medicina FMUSP, Universidade de São Paulo, São Paulo, SP, Brazil. ²Department of Internal Medicine, Division of Metabolism, Endocrinology and Diabetes, University of Michigan, Ann Arbor, MI, USA. [✉]email: imoretti@usp.br

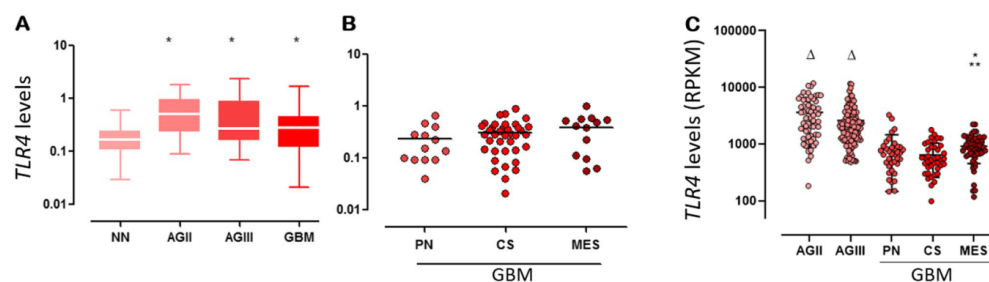


Figure 1. The *TLR4* mRNA expression level was upregulated in human astrocytoma. **(A)** Box plot representation of *TLR4* expression levels in our cohort of different astrocytoma malignant grades (AGII, AGIII, and GBM) and non-neoplastic (NN) brain samples ($*p < 0.05$ Kruskal–Wallis and Dunn tests). *TLR4* expression levels ($2^{-\Delta Ct}$) are log10 transformed, and the horizontal bars represent the median values. **(B)** The expression levels of *TLR4* in the GBM molecular subtypes: proneural (PN), classical (CS), and mesenchymal (MES) in our cohort. **(C)** *TLR4* expression analysis in the TCGA RNASeq data set is demonstrated by reads per kilobase per million mapped reads (RPKM), transformed in log10, including values for AGII, AGIII and GBM molecular subtypes. AGII and AGIII presented higher expression values (Δ) compared to GBM, and MES subtype presented significant higher than CS (*) and PN (**)($p = 0.001$, Kruskal–Wallis, $p = 0.001$ Dunn tests).

TLR4 stimulation may also lead to NACHT, LRR, and PYD domains-containing protein 3 (NLRP3) inflammasome activation by either MyD88 or the TRIF-dependent pathway^{17,18}. The NLRP3 inflammasome complex comprises NLRP3, a sensing molecule with a pyrin domain (PYD), which interacts with an adaptor protein (ASC) with a CARD domain. The resulting combined ASC-CARD domain interacts with pro-CASP1¹⁹, which cleaves and releases interleukin-1 family members such as IL-1 β and interleukin-18 (IL18)²⁰.

Inflammatory cells in a solid tumor microenvironment may exhibit a pro- or anti-inflammatory profile depending on the stimuli²¹. Moreover, inflammatory receptors such as *TLR4* are also expressed in tumor cells, adding another layer of complexity that results from potentially distinct effects of *TLR4* downstream signaling in each cell compartment²². We previously demonstrated an increased *TLR4* expression in human astrocytoma, particularly glioblastoma (WHO-grade IV astrocytoma). Glioblastoma (GBM) is the most common and the most aggressive primary brain malignancy in adults²³, and due to its relevant heterogeneity and the invasive feature, the outcomes of current therapeutic strategies have remained almost invariably lethal. In fact, the standard of care, including surgical tumor cytoreduction followed by radiotherapy and adjunct chemotherapy with Temozolomide (TMZ), and several combinatorial rescue trials have not improved the median overall survival time of approximately 15 months²⁴. Among the GBM molecular subtypes, the mesenchymal (MES) subtype, which harbors *neurofibromin 1* (*NF1*) and *RB transcription corepressor 1* (*RB1*) mutations, presents the poorest outcome, compared to the proneural (PN) subtype harboring somatic mutations in *tumor protein p53* (*TP53*), *platelet-derived growth factor receptor A* (*PDGFRA*), and *isocitrate dehydrogenase 1* (*IDH1*), and to the classical subtype with *epidermal growth factor receptor* (*EGFR*) mutations^{25,26}.

In this context, we aimed to analyze the impact of *TLR4* stimulation in a MES-GBM tumor cell. We worked with the hypothesis that activating the *TLR4* downstream cascade might activate a cell death pathway and contribute to a better outcome for GBM patients, mainly with the MES subtype.

Results

***TLR4* expression in human astrocytoma.** The upregulation of plasmatic membrane TLRs have been previously demonstrated in astrocytoma, particularly in GBM by our group²⁷. Here, we first recapitulated *TLR4* expression in our cohort of 140 human astrocytoma of different grades of malignancy (26 AGII, 18 AGIII, and 96 GBM compared to 22 non-neoplastic [NN] brain tissue), and we next analyzed *TLR4* signaling pathways. *TLR4* expression was significantly higher in AGII, AGIII, and GBM when compared to NN ($p < 0.05$, Kruskal–Wallis and Dunn tests). Interestingly, among GBM molecular subtypes (14 PN, 36 CS, and 16 MES)²⁶, *TLR4* expression was higher in MES than in PN and CS subtypes, however a statistical significance was not reached in our cohort due to the small number of cases in each subtype. Then, we validated this result in a larger dataset of the TCGA cohort, and a significant difference of *TLR4* expression was confirmed among GBM subtypes ($p < 0.0001$ Kruskal–Wallis test), being higher in MES subtype compared to PN and to CS subtypes ($p = 0.001$ for both comparisons, Dunn test) (Fig. 1) Lower grade astrocytomas (AGII and AGIII) presented *TLR4* higher expression levels when compared to GBM samples ($p = 0.001$ for both comparisons, Dunn test).

***TLR4* canonical signaling pathway in U87MG cells.** To access *TLR4* role in a GBM cell line, we treated U87MG cells with LPS and observed NF- κ B activation aiming to analyze the canonical *TLR4* signaling pathway. The NF- κ B translocation to the nucleus was assessed by the presence of the p65 subunit in the nucleus. In immune cells, NF- κ B translocation to the nucleus has been detected 30–100 min after TNF stimulation²⁸. However, in our experiment the nuclear translocation was not observed at 30 min or 2 h after LPS stimulation, the time interval expected for NF- κ B translocation to occur through the MyD88/TRAF6 canonical pathway. It

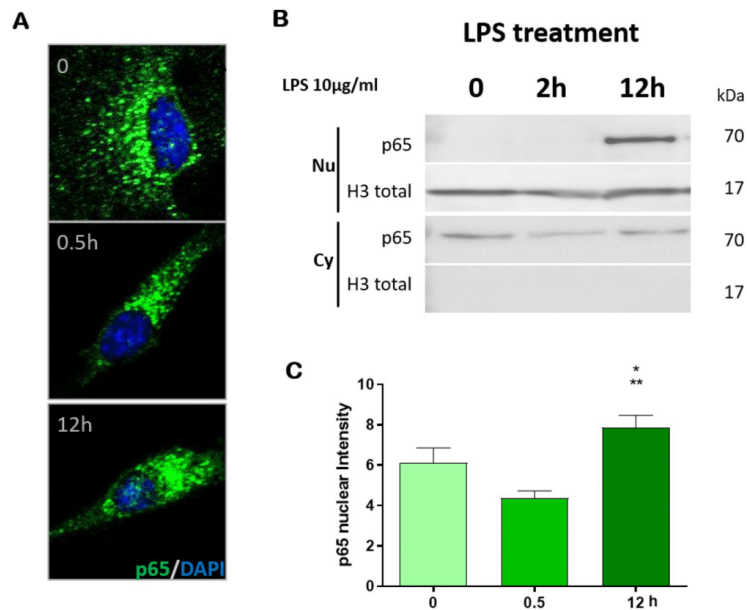


Figure 2. Translocation of the p65 subunit of NF- κ B to the nucleus of U87MG cells after LPS treatment. (A) Immunofluorescence confocal images at three different time points (0, 0.5, 12 h) of U87MG cells treated with LPS showed p65 translocation to nucleus after 12 h of treatment. Cells were incubated with anti-p65, followed by a secondary antibody anti-rabbit-Alexa Fluor 488, in green, and with DAPI, in blue. 400 \times magnification (B) Western blot analysis of p65 with nuclear (Nu) and cytoplasmic (Cy) extracts of U87MG cells after 2 and 12 h of LPS treatment. Histone H3 was used as a loading control for nuclear extract. (C) Quantification of nuclear fluorescence intensity of p65 staining ($n=30$) at the three time points ($*p<0.05$ compared to 0 h and $**p<0.05$ compared to 0.5 h by one-way Anova, Tukey test).

occurred only after 12 h, being considered a late translocation, as demonstrated by immunofluorescence analysis and Western blotting (Fig. 2A–C).

TLR4 non-canonical signaling pathway in U87MG cells. To further investigate the TLR4-signaling pathways after LPS stimulation of U87MG cells, considering the late translocation of NF- κ B to the nucleus, we performed a qRT-PCR for the *MYD88*, and *TRAF6* of the canonical pathway; *SRF*⁹, and *JUN*²⁹ for the proliferative response; *TRIF*³⁰ for the endosome; *NLRP3*¹⁷ and *IL1B*³¹ for inflammasome; and *RIPK1* and *RIPK3* for ripoptosome pathways³², at different time points: 0, 0.5, 12, 24 and 48 h, in three independent experiments. *MYD88*, *SRF*, *JUN*, *IL1B*, *NLRP3*, and *RIPK1* expression levels increased after 12 h of LPS stimulation, and *IL1B* expression reached the largest fold change of 5.83 times compared to basal expression level. Interestingly, *TRAF6* was the only analyzed target presenting a peak of increased expression within 30 min of stimulation ($p=0.052$, One-way Anova post-hoc Tukey test), but it was not related to the NF- κ B translocation to the nucleus, as shown by the Western blot analysis (Fig. 2B). The mRNAs expression alterations at 12 h after LPS stimulation corroborated the activation of TLR4-inflammasome, and -rioptosome pathways, with increase of *SRF*, *JUN* and particularly *IL1B* ($p<0.05$ One-way Anova, $p=0.012$ Tukey test) transcripts levels. (Fig. 3A). We next checked the expression level of these targets in the TCGA RNASeq dataset to validate the activation of these pathways in human astrocytoma (Fig. 3B). In fact, significant upregulations of *MYD88*, *SRF*, *JUN*, *IL1B*, *TRIF*, *RIPK1*, *NLRP3* were detected in GBM cases compared to lower grade astrocytomas (AGII and AGIII) (Supplementary Fig. 1). When the expression pattern of these genes was compared among the GBM subtypes, MES subtype presented higher *MYD88*, *IL1B*, *RIPK3* and *NLRP3* expression levels than PN and CS subtypes (Supplementary Fig. 1), in a similar pattern to *TLR4* expression (Fig. 1C).

Therefore, these observations of the TCGA dataset were convergent to U87MG expression profile after LPS stimulation, indicating upregulation of inflammasome and ripoptosome pathways in GBM, particularly in MES subtype.

As a next step, we checked whether the activation of TLR4 by LPS presented a co-stimulatory effect to TMZ, the alkylating agent used in the standard of care of GBM patients. Interestingly, U87MG cells presented a more significant early cell death after combined stimulation than either TMZ- or LPS-alone treatment after

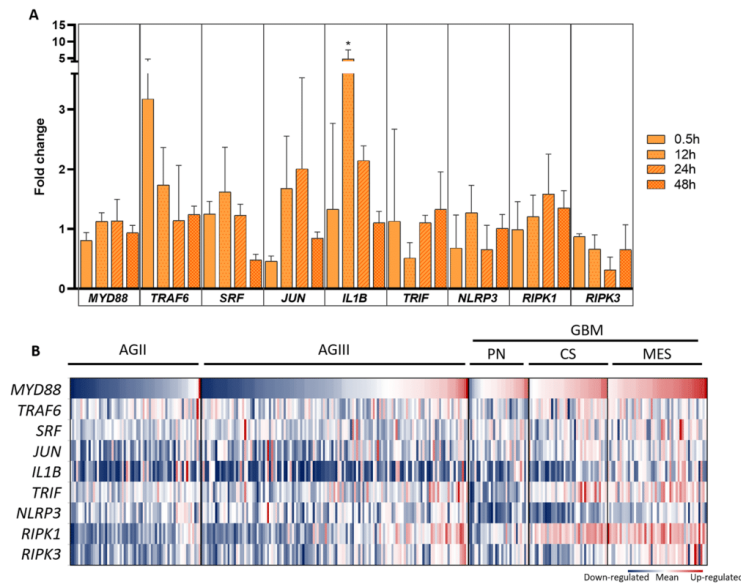


Figure 3. Canonical and non-canonical gene expression profile after LPS stimulation of U87MG cells and of TCGA astrocytoma RNASeq data. (A) *MYD88*, *TRAF6*, *JUN*, *SRF*, *IL1B*, *TRIF*, *NLRP3*, *RIPK1*, *RIPK3* expression ratio with the non-treated cell were accessed by qRT-PCR, at different time points (0.5, 12, 24, 48 h) in three independent experiments. The fold change values were calculated by the ratio of the value obtained by $2^{-\Delta\Delta C_t}$ formula of treated cells compared to control cells (time point 0). (B) Heatmap of the RPKM values from the TCGA RNASeq dataset, normalized by z-score for the selected genes of astrocytoma cases of different malignant grades (AGII, AGIII, and GBM). GBM cases were subdivided by molecular subtypes proneural (PN), classical (CS), and mesenchymal (MES). Upregulated values are in red and downregulated in blue.

48 h (Fig. 4A). We observed an approximately 10% increase in the initial cell death by the combined treatment in comparison to the TMZ single treatment (Fig. 4B). No differences among the stimulation conditions were observed for the number of cells in late cell death.

TLR4 localization in nuclei of U87MG cells. We also analyzed TLR4 protein distribution within U87MG cells upon 12 h of LPS stimulation compared to control. Unexpectedly, immunofluorescence analysis showed a granular pattern of TLR4 expression in nuclei in addition to its distribution in cytosol and plasma membrane in these cells (Fig. 5B), with increased immunostaining after 12 h of LPS stimulation (Fig. 5C) ($p < 0.05$, Mann Whitney). Such nuclear TLR4 distribution was also confirmed by Western blot in non-treated cells (Fig. 5A).

Increased mRNA expression of DNA repair genes related to TLR4 stimulation. To better understand the role of TLR4 in the nucleus, we performed RNASeq in U87MG cell lines after 12 h of LPS stimulation and compared to non-treated cells. This transcriptomic analysis showed 286 upregulated genes and 232 downregulated genes ($\log_{2}FC > |0.5|$, $p < 0.05$, and adjusted $p < 0.1$). The enrichment analysis by Hallmark gene sets³³ showed statistical significance for 25 pathways, including the pathway for DNA repair (HALLMARK_DNA_REPAIR), that was upregulated in the treated cells with a $\log_{2}FC$ of 0.244 (Fig. 6A). Eighteen differentially expressed genes included in this Hallmark group were detected, 16 genes upregulated and 2 genes downregulated after LPS treatment compared to control cells (Fig. 6B). These genes were grouped according to their biological function by GO classification as: DNA repair, DNA dependent DNA replication, regulation of DNA binding, mRNA splicing via spliceosome and transcription by RNA polymerase III. The analysis with the String Consortium tool showed high connectivity among them (Fig. 6C). Additionally, in the TCGA dataset of astrocytoma, their expressions were significantly higher in GBM compared to lower grade astrocytoma (AGII and AGI), ($p < 0.0001$, Kruskal-Wallis test), except for *XRCC1* and *POLA1*. Among them, *MBD4* (methyl-CpG binding domain 4), *PLAUR* (urokinase plasminogen activator receptor), *POLE* (DNA polymerase epsilon, catalytic subunit) and *RAD51* (*RAD51* recombinase) expressions were significantly higher in GBM-MES subtype when compared to CS and PN subtypes ($p < 0.05$ Dunn test for all comparisons) (Supplementary Fig. 1). The DNA repair gene expressions correlated positively among themselves, particularly *RAD51* with *FEN1* (flap structure-specific endonuclease 1)

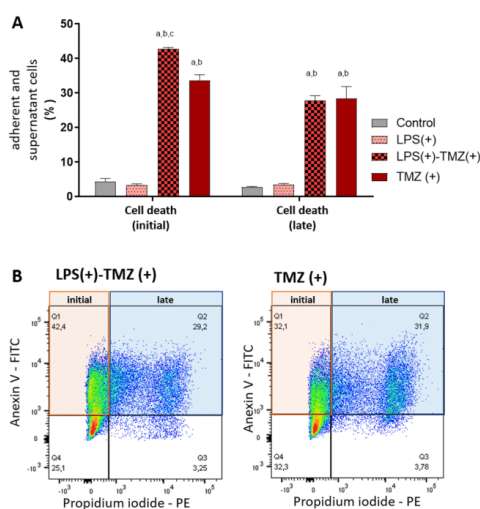


Figure 4. Cell death functional assay by flow cytometry. **(A)** U87MG cells were treated for 48 h with LPS, TMZ, and LPS together with TMZ. The cells were incubated with annexin V and propidium iodide (PI) and evaluated by flow cytometry for the adherent and supernatant cells. Statistical analysis was performed using a Two-way Anova $p < 0.001$ followed by Bonferroni post-test, where significance was ^a $p < 0.001$ compared to non-treated cells (control group), ^b $p < 0.001$ compared to cells treated with LPS, and ^c $p < 0.001$ in comparison to cells treated with TMZ. **(B)** Representative scatter plots of Annexin V-FITC/PI staining of U87MG cells with TMZ alone or in combination with LPS. The initial cell death phenotype was indicated when the cells were positive by annexin V (orange). Late cell death was given by the positivity for annexin V and PI (blue).

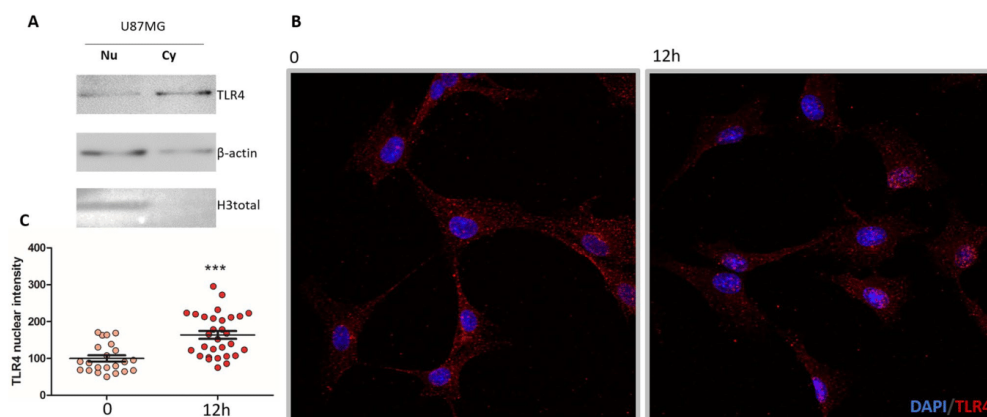


Figure 5. TLR4 localization in U87MG cells. **(A)** TLR4 presence was observed in nuclear (Nu) and cytoplasmic (Cy) protein fractions of U87MG cell line by Western blot analysis. Total H3 protein was used for nuclear protein enrichment control and β -actin for protein loading control. **(B)** The presence of TLR4 was detected in cytoplasmic and nuclear compartments in U87MG cells by immunofluorescence. TLR4 staining in the nucleus increased after 12 h of LPS stimulation. Cells incubated with anti-TLR4-secondary antibody anti-mouse-Alexa Fluor 568, in red, and with DAPI, in blue. 200 \times magnification. **(C)** Values for nuclear fluorescence intensity for each analyzed cell $n = 23$ at 0 h and $n = 25$ at 12 h (^{***} $p < 0.001$ compared to 0 h, Mann-Whitney).

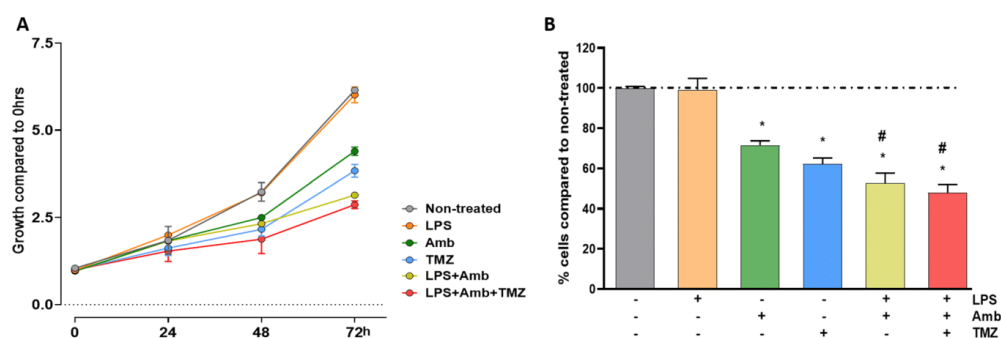


Figure 7. U87MG cell viability with LPS, Amb and TMZ combined treatment. **(A)** Cell viability curves with values normalized by the 0 h values at 0, 24, 48, 72 h with different treatments: LPS-alone, Amb-alone, TMZ-alone, LPS + Amb, LPS + Amb + TMZ compared to non-treated cells. **(B)** The percentage of cell viability decrease compared to non-treated cells after 72 h treatment. The bar graphs represent the fluorescence of viable cells normalized by the mean of non-treated cells (wherein * $p \leq 0.001$ compared with non-treated and # $p \leq 0.001$ compared with Amb-alone and TMZ-alone, Two-way Anova, followed by Tukey post-hoc test).

($r = 0.632$, $p = 0.0001$) and with *UNG* (uracil DNA glycosylase) ($r = 0.263$, $p = 0.003$) in GBM. In MES subtype, a stronger correlation was observed between *RAD51* and *FEN1* expression ($r = 0.758$, $p = 0.0001$, Spearman test).

Considering these correlation findings in the TCGA dataset and our observations of differential expression after LPS stimulus in U87MG cells, we checked the expression level of *RAD51*, *FEN1*, and *UNG* of U87MG cells after 0.5, 12, 24 and 48 h after LPS stimulation. These three genes presented an increase of their expressions in 24 h, with further increase of *UNG* expression in 48 h (Fig. 6D). Thus, these findings corroborated our transcriptomic data of DNA repair related genes upregulation upon LPS stimulation.

Decreased viability after *RAD51* inhibition and LPS stimulation of U87MG cells. Considering the upregulation of *RAD51* expression after TLR4 stimulation with LPS, we chose Amuvatinib (Amb), a *RAD51* inhibitor tested in clinical trial for advanced solid tumors³⁴ to check the impact on U87MG cells (Fig. 7A).

LPS treatment alone did not alter U87MG cell viability, however it significantly decreased with Amb single treatment (compared to non-treated in 48 and 72 h, $p < 0.001$). TMZ single treatment led to a sharper viability decrease in 72 h (compared to non-treated in 48 and 72 h, $p < 0.001$; compared to Amb in 72 h, $p < 0.001$). Moreover, a more pronounced decrease of cell viability was observed when Amb was combined to LPS stimulation (compared to non-treated in 48 and 72 h, $p < 0.001$; compared to Amb in 72 h, $p < 0.001$; compared to TMZ in 72 h, $p < 0.001$), which was comparable to Amb and TMZ combined treatment after LPS stimulation (compared to non-treated in 48 and 72 h, $p < 0.001$; compared to Amb in 72 h, $p < 0.001$; compared to TMZ in 72 h, $p < 0.001$) (Fig. 7B).

Discussion

In view of TLR4 dual role in cellular fate, which is a direct consequence of both the stimuli and microenvironmental context, we aimed to evaluate TLR4 molecular mechanism in human GBM cells. First, we determined *TLR4* expression in 140 human astrocytoma samples of different malignant grades. We observed that *TLR4* expression was higher in astrocytoma samples when compared to non-neoplastic samples. Moreover, when we focused on GBM samples, the analysis of the TCGA RNASeq dataset revealed that *TLR4* expression was higher in the MES subtype, with the poorest outcome when compared to PN and CS subtypes.

The function of TLR4 has been extensively described in immune cells³⁵. Nonetheless, TLR4 role in the tumor cell compartment is still lacking. To analyze TLR4 signaling pathways in GBM cells, the U87MG cell line, harboring *NFI* mutation³⁶, was chosen as a model for the MES-GBM subtype²⁵.

We observed that stimulation of U87MG cells with LPS, a traditional TLR4 agonist that activates pro-inflammatory pathways³⁷, led to NF- κ B (p65) nuclear translocation after 12 h. This was considered a late response because both tumor necrosis factor- α (TNF α) and LPS stimulation have been described to induce NF- κ B translocation to the nucleus through the MyD88/TRAF6 canonical pathway within 30 min to 2 h³⁸. Additionally, hyaluronic acid, a component of the brain extracellular matrix, has been described to trigger TLR4-NF- κ B pathway in GBM stem-like cell differentiation and maintenance in a proliferative astrocytic precursor state²². Furthermore, angiogenin has also induced a proliferative phenotype in U87MG cells through NF- κ B translocation to the nucleus³⁹. In opposition to these previous observations, an unequivocal proliferative effect was not observed in our experiments with U87MG. In another report, TLR4 was able to suppress tumor growth by decreasing the expression of a transcription factor responsible for the maintenance of cancer stem cells, the retinoblastoma binding protein 5⁴⁰.

A late NF- κ B translocation to nucleus was observed in U87MG cells stimulated by LPS, and the gene expression profile of our experiments was compatible to activation of inflammasome and ripoptosome pathways. TRIF

was described to interact with TRAF6, leading to a late-phase NF- κ B activation. Moreover, TLR4 signaling activates the TRIF-RIPK3 complex⁴¹ and leads to apoptosis in the presence of CASP8, or to necroptosis in its absence³². However, CASP8 activation can be prevented by its inhibitor, c-FLIP, or by blocking TLR4-pathway and inhibiting apoptosis⁴². Following TLR4 internalization, TRIF mediates the activation of inflammasome complexes⁴³. Two distinct inflammasome pathways have been described: a pro-proliferative through NLRP3 overexpression⁴⁴ and a cell death signaling pathway⁴⁵, a pyroptotic type of cell death triggered by persistent stimulation of IL-1 β ⁴⁶. Additionally, the TLR4 pathway has been described to trigger apoptosis in glioma in a TRIF-dependent pathway⁴⁷. Our transcriptomic data of U87MG cells 12 h after LPS stimulation and the TCGA RNASeq dataset of astrocytoma showed upregulation of genes related to inflammasome and ripoptosome pathways, namely *MYD88*, *NLRP3*, *RIPK1* and *RIPK3*, and also *SRF*, *JUN* and *IL1B*, the downstream regulated genes.

In this context, an increase of apoptosis of LPS stimulated U87MG cells was expected, however only an increase of approximately 10% in early apoptosis 48 h after the combined treatment of TMZ and LPS was observed. Moreover, we detected an increase of TLR4 distribution in the nucleus of U87MG, 12 h after LPS stimulation. In fact, portions of the TLR4 protein were predicted by computational analysis to be in the nucleus⁴⁸, and such nuclear distribution has already been reported in pancreatic cancer cells⁴⁹, as well as in non-neoplastic rat cells⁵⁰. Additionally, the combined TLR4 expression in nuclei and in cytosol has been associated with poor prognosis and metastasis⁵¹.

In an attempt to understand the mechanisms that lead to the low rate of apoptosis, and the role of TLR4 in the nucleus, NGS transcriptomic analysis of U87MG cells after 12 h of LPS stimulation was performed. Interestingly, among the enriched gene sets differentially expressed after TLR4 activation we found the DNA repair-related genes. Particularly, *UNG*, *FEN1* and *RAD51* presented a time-dependent pattern of upregulation after LPS stimulation in U87MG cells. Considering that the activation of DNA repair cascade may increase tumoral cell fitness, with consequent enhancement of tumor cell survival, we tested the impact of inhibiting this cascade in this model of TLR4-LPS stimulation. In fact, such strategy has already been proposed as targeting the phosphorylation of H2AX, a histone acting for the assembly of repair foci, through modification of TLR4 pathway²². Moreover, the activation of DNA repair signals has been associated with TMZ resistance, including the MGMT (O-6-methylguanine-DNA methyltransferase) repair system, which catalyzes the transference of the methyl group to the cysteine residue of the MGMT protein²⁴. Therefore, targeting DNA repair proteins has been pursued as interesting cancer therapeutic strategy.

Among the DNA repair related genes identified in our transcriptomic data, we selected RAD51 as its inhibition has already shown antitumor activity when combined with other therapeutic agents³⁴. RAD51 has a role in the DNA repair pathway of homologous recombination (HR), and it forms a complex in a single strand DNA break, allowing the homology search and the HR process to continue⁵². Amuvatinib (Amb) is a multi-kinase inhibitor, including RAD51, and it has been tested in a clinical trial for advanced solid tumors³⁴. Additionally, in several GBM cell lines, Amb had a radiosensitization effect and delayed tumor growth, as in U87MG subcutaneous xenograft mice model³⁵. Convergent to this previous finding, we observed a significant reduction of U87MG cell viability with Amb treatment after TLR4-LPS stimulation, in a similar fashion as the combined Amb and TMZ treatment after TLR4-LPS stimulation. Furthermore, TLR4 protective role against tumorigenesis by downregulation of DNA damage repair proteins was also described in a mouse hepatocellular carcinoma⁵⁴. Additionally, the absence of TLR4 was associated with DNA damage resistance after UV irradiation in mice skin cells⁵⁵. These cumulative pieces of evidence suggest TLR4 as a DNA repair pathway regulator due to its capacity to recognize DAMPs and to generate an auto-paracrine signal in the presence of DNA damage⁵⁶. Therefore, we speculate that the reduction of tumor cell viability by TLR4 stimulation combined with the downregulation of DNA repair genes may be an attractive complementary cancer therapeutic strategy, and a treatment alternative for tumor TMZ resistance, as hypermutated TMZ status⁵⁷. Further clarification of the involved mechanisms might enable TLR4-targeted therapies to be combined with the current standard of care to improve GBM patient outcomes.

Materials and methods

TLR4 expression in human astrocytoma and GBM cell line. Biological samples were collected during the neurosurgical procedure by the Neurosurgery Division of the Neurology Department of the Hospital das Clinicas, Faculdade de Medicina, Universidade de Sao Paulo (FMUSP) after informed and written consent from the patients following the Institutional Ethical Committee guidelines (process number: 691/05). The present study was approved by the HCFMUSP (process number: 059/15) and the FMUSP, ethical committee (process number: 278/15). The samples were snap frozen in liquid nitrogen and necrotic, gliotic, and non-neoplastic areas were previously macrodissected to guarantee presence of more than 90% of tumor cells in the processed tumor fragments as described previously²⁷.

Biological samples and cell line total RNA were extracted using the RNeasy Mini Kit (Qiagen, Hilden, Germany) following the manufacturer instructions. Purity and concentration were analyzed by NanoDrop (Thermo Fisher Scientific, Carlsbad, CA, USA), and 1.8–2.0 values for the absorbance ratio 260/280 were considered satisfactory. Electrophoresis in agarose gel was done to check RNA quality.

For the reverse transcription, 1 μ g of total RNA of each sample was used. Treatment with DNase I (FPLC-puro, GE Healthcare, Uppsala, Sweden) was performed, and RNA was reversely transcribed with random primers, oligodT oligonucleotides RNase inhibitor, and SuperScript III (Thermo Fisher Scientific). Lastly, the cDNA was treated with RNase H (GE Healthcare) and diluted in TE (Tris/EDTA) buffer.

We analyzed 22 non-neoplastic (NN) brain samples obtained from temporal lobectomy of epilepsy surgery, 26 astrocytoma grade II (AGII) samples, 18 astrocytoma grade III (AGIII) samples, and 96 GBM, classified 14 as PN, 38 CS and 16 MES subtype.

Cell culture. U87MG human GBM cell lineage was acquired from ATCC and authenticated by short tandem repeats (STR) analysis using the GenePrint 10 System (Promega, Madison, WI, USA). Cells were cultured in monolayer with DMEM medium (Dulbecco's Modified Eagle's Medium) (Thermo Fisher Scientific) supplemented with 10% fetal bovine serum and 100 µg/ml streptomycin and 100 IU/ml penicillin. The cells were kept in an incubator at 37 °C with 5% CO₂. U87MG cell line presents Neurofibromin 1 (NF1) mutation, with molecular pattern of MES subtype³⁶.

Western blotting. To analyze NF-κB activation by TLR4 stimulation, the translocation of the subunit p65 to the nucleus was evaluated by Western blot. Cytoplasmic and nuclear protein extractions were performed for U87MG cells after LPS treatment for 2 and 12 h. The cells were lysed with a buffer solution containing light detergents to separate the cytoplasmic proteins: Igepal-CA-630 (0,5%), Triton X-100 (0,25%), glycerol (10%) (Thermo Fisher Scientific), 1 mM EDTA, 50 mM Hepes, and 140 mM NaCl. After centrifugation, nuclei were lysed with a buffer containing strong detergent and sonicated 50 mM Tris-HCl, 10 mM EDTA and 1% SDS. The Western blotting was performed with the loading of 40 µg proteins in a 4–12% polyacrylamide gel (Thermo Fisher Scientific), using a buffer solution NuPAGE MOPS SDS (Thermo Fisher Scientific). The proteins were transferred to a polyvinylidene fluoride (PVDF) membrane through a semi-dry transfer system (Bio-Rad, Hercules, CA, USA). The antibodies used were anti-p65 (Abcam, Cambridge, UK, 1:500), TLR4 (, Santa Cruz Biotechnology, Santa Cruz, CA, USA, 1:500), β-actin (Sigma-Aldrich, 1:1000) and Histone H3 total (Abcam, 1:20,000). The secondary antibodies were anti-rabbit (p65), anti-mouse (TLR4 and β-actin) and anti-goat (Histone H3 total) (Sigma-Aldrich, 1:1000). The proteins were detected by the chemiluminescent reagent ECL (Western Lightning Chemiluminescence Reagent Plus, Perkin Elmer, Waltham, MA, USA) in the ImageQuant LAS4000 (GE Healthcare).

Immunofluorescence. Immunofluorescence analysis was performed to analyze p65 and TLR4 distribution in the cell compartments, 0,5 h and 12 h after LPS stimulation, and control with no stimulation. The cells were fixed with methanol and acetone (1:1), the cell membrane was permeabilized with Triton-X-100 (0.1%), and, to avoid unspecific reactions, the cells were treated with 2% bovine serum albumin. The primary antibodies anti-p65 (Abcam, 1:500), anti-TLR4 (Abcam, 1:800) were incubated overnight at 4°C. The secondary antibodies (Thermo Fisher Scientific) goat anti-Rabbit IgG H&L (Alexa Fluor 488, 1:400) and goat anti-Mouse IgG H&L (Alexa Fluor 546) were incubated overnight, and nuclei were stained with DAPI (Thermo Fisher Scientific, 1:1000 dilution). The preparations were analyzed in confocal microscope Zeiss 780-NLO (Thornwood, NY, USA). The retrieved images were analyzed by Image J/Fiji³⁸. The fluorescence values for TLR4 and p65 in the nuclei was delimited by DAPI staining.

Cell viability analysis. U87MG cells were plated in 96 wells (2 × 10³ cell/well), stimulated with LPS alone, Amuvatinib (Amb), a RAD51 inhibitor, alone, TMZ alone and the combined treatment, compared to the non-stimulated, and non-treated group. The plates were observed in four time periods of 24, 48 and 72 h. The concentrations for Amb and TMZ were 10 µM and TMZ 0.54 mM, respectively. The cell viability was analyzed by the Presto Blue reagent (Thermo Fisher Scientific), following the manufacturer instructions. The fluorescence of each well was measured by the Glomax (Promega). The samples were evaluated in triplicate in two independent experiments, and an additional spot with only the Presto Blue reagent was evaluated to normalize the fluorescence results.

Apoptosis assay. U87MG cells were treated with LPS and TMZ and the combined treatment LPS and TMZ for 48 h. Cells were washed with PBS and trypsinized. The adherent and non-adherent cells were collected for analysis. Annexin V conjugated with FITC and propidium iodide (PI) were used for the staining following the manufactures instructions (BD Biosciences, San Jose, CA, USA) and the measurements were done by the Flow Cytometry FACS Canto BD (BD Biosciences). The cells presenting the phosphatidylserine translocation with Annexin V positivity were considered as in early apoptosis. The cells with increased membrane permeability resulting in Annexin V and PI positivity were considered as in late apoptosis. The results were analyzed by Flow Jo version 10 (Flow Jo, LLC, Ashton, OR, USA).

Transcriptome analysis. We performed RNA-Seq to interrogate differentially expressed transcripts induced by LPS treatment for 12 h in the U87MG cell line. Control and LPS-treated cells were analyzed in triplicates. We used the QuantSeq 3' mRNA-Seq Library Prep kit FWD for Illumina (Lexogen, Vienna, Austria) to generate around 5 million 75 bp single-ended reads per library. Libraries for a given condition (control or LPS) were generated in triplicates. Sequencing was performed in the Illumina NextSeq 550 (Illumina, San Diego, CA, USA) platform at the Sequenciamento em Larga Escala (SELA) facility of FMUSP.

We used STAR to align sequencing data to the GRCh38 version of the human genome (downloaded from ftp.ensembl.org). We used the bamsort tool, from biobambam2, for downstream processing of the BAM file, including merging and sorting. To count the number of reads that overlap each gene, we used featureCounts. We obtained the GFF file containing the gene models from ftp.ensembl.org. We used fastQC and RNASEQC to assess sequencing quality and alignment metrics, respectively. To assess differential gene expression between LPS-treated and control cells, we used the R-Bioconductor package *limma*. Pathway analysis and gene-set enrichment analysis were performed using online tools such as GSEA (<http://software.broadinstitute.org/gsea>) and Web-Gestalt (<http://www.webgestalt.org/>), Gene Ontology Resources (accessed: 2020–02–10 <https://doi.org/10.5281/zenodo.2529950>)^{59,60} and String consortium to produce figure²⁸.

Validation of the transcriptomic analysis. The differentially expressed genes selected from the transcriptomic analysis was validated by qRT-PCRs. The cells were collected in four time points (0.5, 12, 24, 48 h). The genes of the DNA repair pathway analyzed were *UNG*, *FEN1*, and *RAD51*.

Gene expression analyses. Gene expression levels were evaluated by qRT-PCR using the Sybr green approach to in an ABI 7500 (Thermo Fisher Scientific), using the Power Sybr green PCR master mix (Thermo Fisher Scientific). The primers were synthesized by IDT (Coralville, IA, USA) and Thermo Fisher Scientific. The sequence of primers were: *TLR4* (F: TTTATCCAGGTGTGAAATCCAGAC; R: TCCAGAAAAGGCTCC CAGG), *TRAF6* (F: TGAAATGTCCAAATGAAGTTGTT; R: GAAGGGACGCTGGCATTG), *MYD88* (F: GGATGGTGGTGGTTGTCTCTG; R: CCTGTACTTGTATGGGGATCAGT), *SRF* (F: ACAGCAGCACAG ACCTCACG; R: CATGCGGGCTAGGGTACATC), *JUN* (F: CTCAGACAGTGCCGAGATG; R: TTCCTC TCCGCCTTGATCC), *NLRP3* (F: CGGAGACAAGGGGATCAAAC; R: AGCAGCAGTGTGACGTGAGG), *IL1B* (F: GGGACAGGATATGGAGCAACAA; R: TCAACACGACAGGACAGGTACA), *TRIF* (F: AAGCCGTGC CCACCTACTC; R: GAGGAAGGGAACAGGGAGGA), *RIPK1* (F: TTTGGGAAGGTGT CTCTGTGTTT; R: CATCATCTTCGCCTCTCCA), *RIPK3* (F: CAATATGAATGCTGCTGTCTCCA; R: CCATCCATTTCTGTC CCTCT), *UNG* (F: TTGCTCTGGGGCTCTTATGC; R: TGACAAAAGGGGAGGGATGAG), *FEN1* (F: GAA GGGAGAGCGAGCTTAGGA; R: GGCAACACAGAGGAGGGATG), *RAD51* (F: CGTTCAACACAGACCACC AGAC; R: GCGGTGGCACTGTCTACAATAA) *TBP* (F: AGGATAAGAGAGCCACGAACCA; R: CTTGCT GCCAGTCTGGACTGT), *HPRT* (F: TGAGGATTTGGAAAGGGTGT; R: AGCACACAGAGGGCTACAA), *GUSB* (F: GAAAATACGTGGTTGGAGAGCTCATT; R: CGAGTGAAGATCCCCTTTTAA). The expression levels for the tissues samples and cell samples were resulted by the formula $2^{-\Delta Ct}$ (where $\Delta Ct = TLR4 Ct - \text{geometric means of three housekeeping genes, TBP, HPRT and GUSB}$)²⁷. The cell samples were analyzed by one housekeeping gene (HPRT).

In silico analysis using TCGA dataset. Datasets from The Cancer Genome Atlas (TCGA-<http://cancer.genome.nih.gov/>) was downloaded from Genomics Data Commons Data Portal, and the data were normalized by DE-seq. Heatmap z-score of RPKM values were calculated for each gene, and the mean was used as cutoff value to determine whether up- and down-regulated. The TCGA cohorts consist of low grade astrocytomas (63 AGII and 128 AGIII cases), 29 GBM-PN, 38 GBM-CS, and 48 GBM-MES cases.

Statistical analysis. The program SPSS version 23.0 (IBM, Armonk, NY, USA) and Graph Pad Prism (Graph-Pad Software Inc, CA, USA) were used for the statistical analysis and graphs. The Normality of the data distribution was analyzed by the Kolmogorov–Smirnov test. Kruskal–Wallis and post hoc Dunn tests were used to analyze the differences among groups when non-parametric, and One-way Anova when parametric and multiple groups comparisons for the cellular treatment experiments, and Tukey as post hoc test (p65 nuclei staining and expression levels). For multiple variables comparison Two-way Anova was used, upon significance of interaction, column and row factor, Bonferroni post hoc test (apoptosis by flow cytometry) and Tukey post hoc (cellular viability assay) were applied. The test Mann Whitney was used for two groups comparison (TLR4 nuclear staining). The correlations were performed by Spearman's rho test. Differences were considered significant for $p < 0.05$.

Received: 16 March 2020; Accepted: 1 December 2020

Published online: 14 January 2021

References

- Kawasaki, T. & Kawai, T. Toll-like receptor signaling pathways. *Front. Immunol.* **5**, 461 (2014).
- Pradere, J. P., Dapito, D. H. & Schwabe, R. F. The Yin and Yang of toll-like receptors in cancer. *Oncogene* **33**, 3485–3495 (2014).
- Silke, J., Rickard, J. A. & Gerlic, M. The diverse role of RIP kinases in necroptosis and inflammation. *Nat. Immunol.* **16**, 689–697 (2015).
- Karin, M. & Ben-Neriah, Y. Phosphorylation meets ubiquitination: the control of NF- κ B activity. *Annu. Rev. Immunol.* **18**, 621–663 (2000).
- Beutler, B. Microbe sensing, positive feedback loops, and the pathogenesis of inflammatory diseases. *Immunol. Rev.* **227**, 248–263 (2009).
- Hedayat, M., Takeda, K. & Rezaei, N. Prophylactic and therapeutic implications of toll-like receptor ligands. *Med. Res. Rev.* **32**, 294–325 (2012).
- Ma, W.-W., Li, C.-Q., Zhao, L., Wang, Y.-S. & Xiao, R. NF- κ B-mediated inflammatory damage is differentially affected in SH-SY5Y and C6 cells treated with 27-hydroxycholesterol. *Food Sci. Nutr.* **7**, 1685–1694 (2019).
- Guttridge, D. C., Albanese, C., Reuther, J. Y., Pestell, R. G. & Baldwin, A. S., Jr. NF- κ B controls cell growth and differentiation through transcriptional regulation of cyclin D1. *Mol. Cell Biol.* **19**, 5785–5799 (1999).
- Schratt, G. *et al.* Serum response factor is required for immediate-early gene activation yet is dispensable for proliferation of embryonic stem cells. *Mol. Cell Biol.* **21**, 2933–2943 (2001).
- Chaturvedi, M. M., Sung, B., Yadav, V. R., Kannappan, R. & Aggarwal, B. B. NF- κ B addiction and its role in cancer: "one size does not fit all". *Oncogene* **30**, 1615–1630 (2011).
- Lin, C. Y. *et al.* Transcriptional amplification in tumor cells with elevated c-Myc. *Cell* **151**, 56–67 (2012).
- David, A. *et al.* c-Myc dysregulation is a co-transforming event for nuclear factor- κ B activated B cells. *Haematologica* **102**, 883–894 (2017).
- Aksay, E. *et al.* The p110delta isoform of the kinase PI(3)K controls the subcellular compartmentalization of TLR4 signaling and protects from endotoxic shock. *Nat. Immunol.* **13**, 1045–1054 (2012).

14. Kawai, T. & Akira, S. The role of pattern-recognition receptors in innate immunity: update on Toll-like receptors. *Nat. Immunol.* **11**, 373–384 (2010).
15. Hasan, U. A. *et al.* Cell proliferation and survival induced by Toll-like receptors is antagonized by type I IFNs. *Proc. Natl. Acad. Sci. U.S.A.* **104**, 8047–8052 (2007).
16. Vanlangenakker, N., Vanden Berghe, T. & Vandenabeele, P. Many stimuli pull the necrotic trigger, an overview. *Cell Death Differ.* **19**, 75–86 (2012).
17. Bauernfeind, F. G. *et al.* Cutting edge: NF- κ B activating pattern recognition and cytokine receptors license NLRP3 inflammasome activation by regulating NLRP3 expression. *J. Immunol. (Baltim., Md: 1950)* **183**, 787–791 (2009).
18. Shang, S., Wang, L., Zhang, Y., Lu, H. & Lu, X. The beta-hydroxybutyrate suppresses the migration of glioma cells by inhibition of NLRP3 inflammasome. *Cell. Mol. Neurobiol.* **38**, 1479–1489 (2018).
19. Yang, Y., Wang, H., Kouadir, M., Song, H. & Shi, F. Recent advances in the mechanisms of NLRP3 inflammasome activation and its inhibitors. *Cell Death Dis.* **10**, 128 (2019).
20. Martinon, F., Mayor, A. & Tschopp, J. The inflammasomes: guardians of the body. *Annu. Rev. Immunol.* **27**, 229–265 (2009).
21. Hanahan, D. & Robert, A. Weinberg, Hallmarks of cancer: the next generation. *Cell* **144**, 646–674 (2011).
22. Ferrandez, E., Gutierrez, O., Segundo, D. S. & Fernandez-Luna, J. L. NF κ B activation in differentiating glioblastoma stem-like cells is promoted by hyaluronic acid signaling through TLR4. *Sci. Rep.* **8**, 6341 (2018).
23. Louis, D. N. *et al.* The 2016 World Health Organization classification of tumors of the central nervous system: a summary. *Acta Neuropathol.* **131**, 803–820 (2016).
24. Karlsson, I. *et al.* Local delivery of temozolomide via a biologically inert carrier (Temodex) prolongs survival of glioma patients irrespectively of the MGMT methylation status. *Neoplasma* **66**(2), 288–293 (2018).
25. Verhaak, R. G. W. *et al.* Integrated genomic analysis identifies clinically relevant subtypes of glioblastoma characterized by abnormalities in *PDGFRA*, *IDH1*, *EGFR*, and *NF1*. *Cancer Cell* **17**, 98–110 (2010).
26. Galatro, T. F. *et al.* Correlation between molecular features and genetic subtypes of Glioblastoma: critical analysis in 109 cases. *MedicalExpress* M170505 (2017).
27. Moretti, I. F., Franco, D. G., de Almeida Galatro, T. F., Oba-Shinjo, S. M. & Marie, S. K. N. Plasmatic membrane toll-like receptor expressions in human astrocytomas. *PLoS ONE* **13**, 211 (2018).
28. Szklarczyk, D. *et al.* STRING v11: protein-protein association networks with increased coverage, supporting functional discovery in genome-wide experimental datasets. *Nucleic Acids Res.* **47**, D607–D613 (2019).
29. Dong, Y. Q. *et al.* Toll-like receptor 4 signaling promotes invasion of hepatocellular carcinoma cells through MKK4/JNK pathway. *Mol. Immunol.* **68**, 671–683 (2015).
30. Cusson-Hermance, N., Khurana, S., Lee, T. H., Fitzgerald, K. A. & Kelliher, M. A. Rip1 mediates the Trif-dependent toll-like receptor 3- and 4-induced NF- κ B activation but does not contribute to interferon regulatory factor 3 activation. *J. Biol. Chem.* **280**, 36560–36566 (2005).
31. Ghiringhelli, F. *et al.* Activation of the NLRP3 inflammasome in dendritic cells induces IL-1 β -dependent adaptive immunity against tumors. *Nat. Med.* **15**, 1170–1178 (2009).
32. Najjar, M. *et al.* RIPK1 and RIPK3 kinases promote cell-death-independent inflammation by toll-like receptor 4. *Immunity* **45**, 46–59 (2016).
33. Liberzon, A. *et al.* The molecular signatures database (MSigDB) hallmark gene set collection. *Cell Syst.* **1**, 417–425 (2015).
34. Mita, M. *et al.* Phase 1B study of amuvatinib in combination with five standard cancer therapies in adults with advanced solid tumors. *Cancer Chemother. Pharmacol.* **74**, 195–204 (2014).
35. Vaure, C. & Liu, Y. A comparative review of toll-like receptor 4 expression and functionality in different animal species. *Front. Immunol.* **5**, 316 (2014).
36. Forbes, S. A. *et al.* COSMIC: somatic cancer genetics at high-resolution. *Nucleic Acids Res.* **45**, D777–D783 (2017).
37. Cochet, F. & Peri, F. The role of carbohydrates in the lipopolysaccharide (LPS)/toll-like receptor 4 (TLR4) signalling. *Int. J. Mol. Sci.* **18**, 2318 (2017).
38. Korwek, Z. *et al.* Importins promote high-frequency NF- κ B oscillations increasing information channel capacity. *Biol. Direct* **11**, 61 (2016).
39. Xia, W. *et al.* Angiogenin promotes U87MG cell proliferation by activating NF- κ B signaling pathway and downregulating its binding partner FHL3. *PLoS ONE* **10**, e0116983 (2015).
40. Alvarado, A. G. *et al.* Glioblastoma cancer stem cells evade innate immune suppression of self-renewal through reduced TLR4 expression. *Cell Stem Cell* **20**, 450–461.e454 (2017).
41. He, S., Liang, Y., Shao, F. & Wang, X. Toll-like receptors activate programmed necrosis in macrophages through a receptor-interacting kinase-3-mediated pathway. *Proc. Natl. Acad. Sci. U.S.A.* **108**, 20054–20059 (2011).
42. Xu, W. *et al.* Long noncoding RNA UBE2R2-AS1 promotes glioma cell apoptosis via targeting the miR-877-3p/TLR4 axis. *Oncotargets Therapy* **12**, 3467–3480 (2019).
43. Chen, K. Q. *et al.* Toll-like receptors in inflammation, infection and cancer. *Int. Immunopharmacol.* **7**, 1271–1285 (2007).
44. Xue, L. *et al.* NLRP3 promotes glioma cell proliferation and invasion via the interleukin-1beta/NF- κ B p65 signals. *Oncol. Res.* **27**, 557–564 (2018).
45. Shimada, K. *et al.* Oxidized mitochondrial DNA Activates the NLRP3 inflammasome during apoptosis. *Immunity* **36**, 401–414 (2012).
46. Aarberg, L. D. *et al.* Interleukin-1 β Induces mtDNA release to activate innate immune signaling via cGAS-STING. *Mol. Cell* **74**, 801–815.e806 (2019).
47. Tewari, R., Choudhury, S. R., Ghosh, S., Mehta, V. S. & Sen, E. Involvement of TNF α -induced TLR4-NF- κ B and TLR4-HIF-1 α feed-forward loops in the regulation of inflammatory responses in glioma. *J. Mol. Med. (Berl.)* **90**, 67–80 (2012).
48. Dinkel, H. *et al.* ELM—the database of eukaryotic linear motifs. *Nucleic Acids Res.* **40**, D242–D251 (2012).
49. Leppanen, J. *et al.* Toll-like receptors 2, 4 and 9 and hypoxia markers HIF-1 α and CAIX in pancreatic intraepithelial neoplasia. *Appl. Immunol.* **126**, 852–863 (2018).
50. Wu, F.-X. *et al.* Intrathecal siRNA against Toll-like receptor 4 reduces nociception in a rat model of neuropathic pain. *Int. J. Med. Sci.* **7**, 251–259 (2010).
51. Huhta, H. *et al.* Toll-like receptors 1, 2, 4 and 6 in esophageal epithelium, Barrett's esophagus, dysplasia and adenocarcinoma. *Oncotarget* **7**, 23658–23667 (2016).
52. Sullivan, M. R. & Bernstein, K. A. RAD-ical new insights into RAD51 regulation. *Genes (Basel)* **9**, 629 (2018).
53. Welsh, J. W. *et al.* The c-Met receptor tyrosine kinase inhibitor MP470 radiosensitizes glioblastoma cells. *Radiat. Oncol.* **4**, 69 (2009).
54. Wang, Z. *et al.* Toll-like receptor 4 activity protects against hepatocellular tumorigenesis and progression by regulating expression of DNA repair protein Ku70 in mice. *Hepatology* **57**, 1869–1881 (2013).
55. Harberts, E., Zhou, H., Fischevich, R., Liu, J. & Gaspari, A. A. Ultraviolet radiation signaling through TLR4/MyD88 constrains DNA repair and plays a role in cutaneous immunosuppression. *J. Immunol.* **194**, 3127–3135 (2015).
56. Narayanaswamy, P. B., Tkachuk, S., Haller, H., Dumler, I. & Kiyay, Y. CHK1 and RAD51 activation after DNA damage is regulated via urokinase receptor/TLR4 signaling. *Cell Death Dis.* **7**, e2383 (2016).
57. Marie, S. K. N. *et al.* Maternal embryonic leucine zipper kinase transcript abundance correlates with malignancy grade in human astrocytomas. *Int. J. Cancer* **122**, 807–815 (2008).

58. Schindelin, J. *et al.* Fiji: an open-source platform for biological-image analysis. *Nat. Methods* **9**, 676–682 (2012).
59. Ashburner, M. *et al.* Gene ontology: tool for the unification of biology. The gene ontology consortium. *Nat. Genet.* **25**, 25–29 (2000).
60. Resource, T. G. O. 20 years and still going strong. *Nucleic Acids Res.* **47**, D330–d338 (2019).

Acknowledgements

We thank the doctors and residents from the Discipline of Neurosurgery of the Department of Neurology at Hospital das Clínicas of School of Medicine, University of São Paulo for their help in tumor sample collection. We are grateful to the São Paulo Research Foundation (FAPESP, grants processes n°2001/12898-4, 2004/12133-6, 2013/02162-8 (SKNM), 2014/50137-5 (SKNM), 2015/26328-8 (MTL) and 2016/14695-9 (IFM)); to the Conselho Nacional de Desenvolvimento Científico e Tecnológico (CNPq, grant number 305730/2015-0); to the Coordenação de Aperfeiçoamento de Pessoal de Nível Superior (CAPES, grant number NUFFIC 062/15 (SKNM), Processes n° 9999.001625/2015-02 (SKNM), 88887.321693/2019-00 (MTL) and 88887.351607/2019-00 (IFM)); and to FMUSP and the Fundação Faculdade de Medicina (FFM). We are also grateful to Prof. Esper Kallas, coordinator of the FMUSP flow cytometry facility, for the use of the equipment and excellent assistance provided by their staff.

Author contributions

Conceptualization, S.K.N.M., and I.F.M.; Data curation, I.F.M., and A.M.L.; Formal analysis, I.F.M., M.T.-L., A.M.L., and S.M.O.-S.; Investigation, I.F.M., A.M.L., M.T.-L., P.R.S., R.S.S., S.M.O.-S., and S.K.N.M.; Methodology, I.F.M., A.M.L., M.T.-L., P.R.S., R.S.S.; Project administration, S.K.N.M.; Supervision, S.K.N.M.; Validation, I.F.M., M.T.-L., P.R.S., R.S.S.; Visualization, I.F.M., M.T.-L., S.M.O.-S., and S.K.N.M.; Writing—original draft, I.F.M., and S.K.N.M.; Writing—review and editing, I.F.M., A.M.L., M.T.-S., S.M.O.-S., and S.K.N.M.

Competing interests

The authors declare no competing interests.


Additional information

Supplementary Information The online version contains supplementary material available at <https://doi.org/10.1038/s41598-020-79356-1>.

Correspondence and requests for materials should be addressed to I.F.M.

Reprints and permissions information is available at www.nature.com/reprints.

Publisher's note Springer Nature remains neutral with regard to jurisdictional claims in published maps and institutional affiliations.

 **Open Access** This article is licensed under a Creative Commons Attribution 4.0 International License, which permits use, sharing, adaptation, distribution and reproduction in any medium or format, as long as you give appropriate credit to the original author(s) and the source, provide a link to the Creative Commons licence, and indicate if changes were made. The images or other third party material in this article are included in the article's Creative Commons licence, unless indicated otherwise in a credit line to the material. If material is not included in the article's Creative Commons licence and your intended use is not permitted by statutory regulation or exceeds the permitted use, you will need to obtain permission directly from the copyright holder. To view a copy of this licence, visit <http://creativecommons.org/licenses/by/4.0/>.

© The Author(s) 2021

Publication 1 Supplementary information

Late p65 nuclear translocation in glioblastoma cells indicates non-canonical TLR4 signaling and activation of DNA repair genes

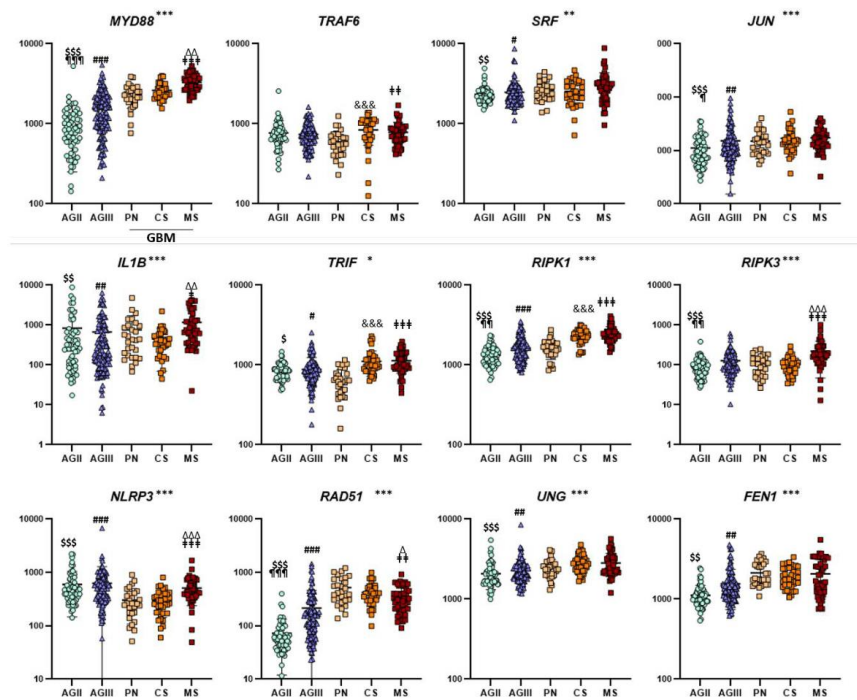
Isabele F. Moretti^{1*}, Antonio M. Lerario², Marina Trombetta-Lima¹, Paula R. Sola¹, Roseli da Silva Soares¹, Sueli M. Oba-Shinjo¹, and Sueli K.N. Marie¹

1. Laboratory of Molecular and Cellular Biology (LIM15), Department of Neurology, Faculdade de Medicina FMUSP, Universidade de Sao Paulo, SP, BR

2. Department of Internal Medicine, Division of Metabolism, Endocrinology and Diabetes, University of Michigan, Ann Arbor, Michigan, USA.

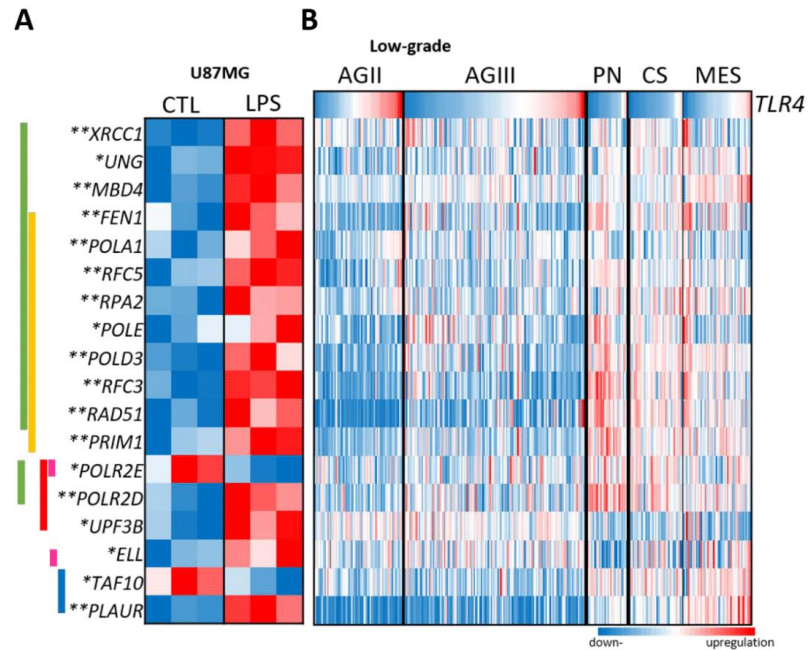
*Corresponding author e-mail address: imoretti@usp.br

• Supplementary information

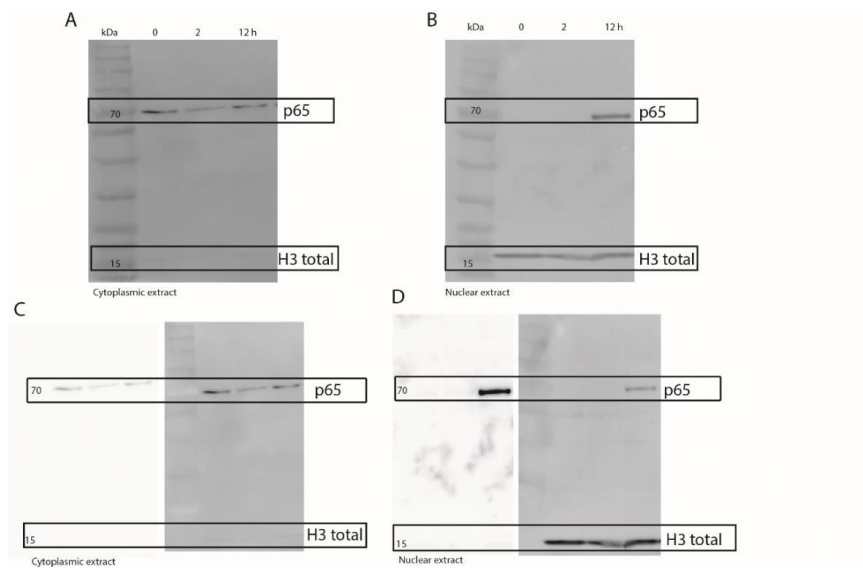


Supplementary Figure 1. Expression analysis in the TCGA RNAseq data set for the different genes analyzed throughout the study. For TLR4 canonical and non-canonical pathways targets. The data is demonstrated by reads per kilobase per million mapped reads (RPKM), presented in the graph by log10, including values for low grade astrocytomas and GBM molecular subtypes. Statistical significance were analyzed and demonstrated by (*) for Kruskal-Wallis test, and followed of post hoc Dunn tests, wherein: ¶ AGII in comparison with AGIII; § AGII in comparison

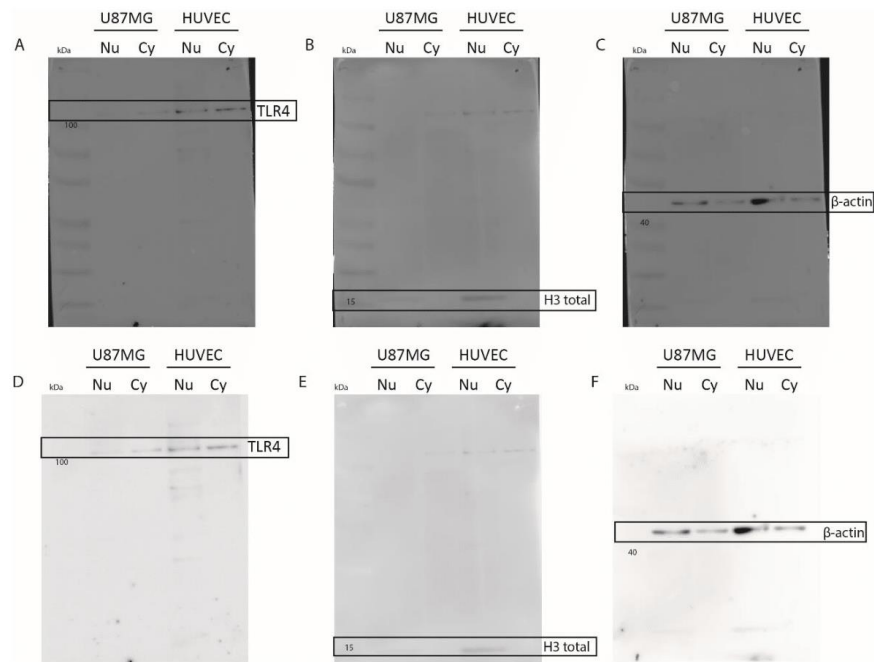
with GBM; # AGIII compared to GBM; (‡ PN compared to MS; Δ CS compared to MS and & PN compared to CS. The quantity of symbols is proportional to p value, as one symbol $p < 0.0$, two symbols $p < 0.00$, and three symbols $p < 0.000$.



Supplementary Figure 2. (A) Heatmap representing the expression of genes coding for proteins with biological functions for DNA repair (genes selected from the gene set enrichment analysis - GSEA). Each group was analyzed in triplicates for CTL and LPS treated. *p-value < 0.05 ** adjusted $p < 0.05$ (B) Heatmap representing the expression of selected genes from TCGA RNAseq dataset from astrocytoma cases (AGII, AGIII, and AGIV). GBM cases were subdivided by the molecular subtypes (PN, CS, MES). Up-regulated values are in red and down-regulated in blue. The \log_2 CPM values were normalized by z-score.



Supplementary Figure 3- Western blot full length images highlighting the areas presented in figure 3 B. Both images were merged with the protein ladder for size localization. (A) Cytoplasmic extract incubated with anti-p65 and anti-H3 total and (B) nuclear extract incubated with anti-p65 and anti-H3 total. The antibodies were incubated in different times in the same membrane in (C) Cytoplasmic extract for anti-p65, left membrane exposed for 1 minutes and anti-H3 total right membrane, exposed for 1 minute and (D) nuclear extract for anti-p65, left membrane, exposed for 2 minutes and anti-H3 total right membrane, exposed for 1 minute.



Supplementary Figure 4- Western blot full length images highlighting the areas presented in figure 6 D merged with the protein ladder image, the antibodies were incubated in different times in the same membrane in (A) anti-TLR4 first incubated antibody with the membrane exposition for 5 min. In (B) anti-H3 total image exposed for 1min30s and (C) anti- β -actin exposed for 1 minute. (D-F) Same images without the ladder image merged.

5 Publication 2 - GBM Cells Exhibit Susceptibility to Metformin Treatment According to TLR4 Pathway Activation and Metabolic and Antioxidant Status





In **Publication 2**, we aimed to analyze the effect of LPS combined to metformin in two GBM cell lines, U87MG and A172. Metformin (MET), a known medication for diabetic patients, sensitizes insulin receptor, increases mitochondrial ROS by inhibition of complex I of oxidative phosphorylation, decreases ATP level, and activates AMPK (adenosine monophosphate (AMP)-activated protein kinase). AMPK activation, in turn, inhibits NF- κ B pathway, leading to anti-tumor response by decreasing pro-inflammatory cytokines. We analyzed the impact of MET in GBM cells in TLR4 activated condition by RNA-Seq. This study was published in *Cancers* (63), where methodology, results and discussion were detailed. In brief, the transcriptomic analysis in the designed experimental conditions revealed different gene expression signature in U87MG and A172 cells in response to LPS+MET. U87MG cells were more prone to oxidative stress, mitochondrial damage and cell death than A172. On the other hand, A172 exhibited minor change after LPS, however, MET treatment downregulated a set of genes related to cell cycle, corroborating the cell cycle arrest observed after MET+TMZ combined treatment. Moreover, A172 cells presented an upregulation of antioxidant genes, explaining the low apoptotic rate presented by these cells after MET+TMZ treatment. According to Garofanos's proposed GBM stratification U87MG cell line presented a glycolytic/multimetabolic subtype profile, while A172 presented a mitochondrial subtype profile (44). Interestingly, the *in silico* analysis of the TCGA-GBM-RNASeq dataset showed upregulation of antioxidant genes in the MTC subtype and activation of the TLR4 pathway in GPM subtype, suggesting that GPM-GBM subtype will be eligible for MET treatment, but MTC-GBM subtype will require a combinatory treatment with an anti-oxidant inhibitor to get anti-tumor effect. The publication 2 (PMID: 36765551) is presented next.

Publication 2

GBM Cells Exhibit Susceptibility to Metformin Treatment
According to TLR4 Pathway Activation and Metabolic
and Antioxidant Status

Article

GBM Cells Exhibit Susceptibility to Metformin Treatment According to TLR4 Pathway Activation and Metabolic and Antioxidant Status

Isabele Fattori Moretti ^{1,*} , Antonio Marcondes Lerario ², Paula Rodrigues Sola ¹, Janaína Macedo-da-Silva ³, Mauricio da Silva Baptista ⁴ , Giuseppe Palmisano ³, Sueli Mieko Oba-Shinjo ¹  and Suely Kazue Nagahashi Marie ^{1,*} 

¹ Laboratory of Molecular and Cellular Biology (LIM 15), Department of Neurology, Faculdade de Medicina FMUSP, Universidade de Sao Paulo, Sao Paulo 01246-903, SP, Brazil

² Department of Internal Medicine, Division of Metabolism, Endocrinology and Diabetes, University of Michigan, Ann Arbor, MI 48108, USA

³ GlycoProteomics Laboratory, Department of Parasitology, ICB, University of Sao Paulo, São Paulo 05508-000, SP, Brazil

⁴ Biochemistry Department, Institute of Chemistry, Universidade de Sao Paulo, São Paulo 05508-900, SP, Brazil

* Correspondence: imortetti@usp.br (I.F.M.); sknmarie@usp.br (S.K.N.M.); Tel.: +55-11-3061-7458 (S.K.N.M.)

Simple Summary: An analysis of metformin (MET) treatment in combination with temozolomide (TMZ) in two glioblastoma cell lines, U87MG and A172, stimulated with lipopolysaccharide (LPS), a TLR4 agonist was conducted. Both cells presented blunted mitochondrial respiration leading to oxidative stress after MET treatment, and decreased cell viability after MET + TMZ treatment. U87MG cells presented increased apoptosis after MET + LPS + TMZ treatment by increment of ER stress, and downregulation of BLC2. A172, with an upregulated antioxidant background, including *SOD1*, exhibited cell cycle arrest after MET + TMZ treatment. The observed differential response was associated with a distinct metabolic status: glycolytic/plurimetabolic (GPM) subtype in U87MG and mitochondrial (MTC) in A172. TCGA-GBM-RNASeq in silico analysis showed that GPM-GBM cases with an activated TLR4 pathway might respond to MET, but the concomitant *CXCL8/IL8* upregulation may demand a combination treatment with an IL8 inhibitor. MET combined with an antioxidant inhibitor, such as anti-*SOD1*, may be indicated for MTC-GBM cases.

Abstract: Glioblastoma (GBM) is an aggressive brain cancer associated with poor overall survival. The metabolic status and tumor microenvironment of GBM cells have been targeted to improve therapeutic strategies. TLR4 is an important innate immune receptor capable of recognizing pathogens and danger-associated molecules. We have previously demonstrated the presence of TLR4 in GBM tumors and the decreased viability of the GBM tumor cell line after lipopolysaccharide (LPS) (TLR4 agonist) stimulation. In the present study, metformin (MET) treatment, used in combination with temozolomide (TMZ) in two GBM cell lines (U87MG and A172) and stimulated with LPS was analyzed. MET is a drug widely used for the treatment of diabetes and has been repurposed for cancer treatment owing to its anti-proliferative and anti-inflammatory actions. The aim of the study was to investigate MET and LPS treatment in two GBM cell lines with different metabolic statuses. MET treatment led to mitochondrial respiration blunting and oxidative stress with superoxide production in both cell lines, more markedly in U87MG cells. Decreased cell viability after MET + TMZ and MET + LPS + TMZ treatment was observed in both cell lines. U87MG cells exhibited apoptosis after MET + LPS + TMZ treatment, promoting increased ER stress, unfolded protein response, and BLC2 downregulation. LPS stimulation of U87MG cells led to upregulation of *SOD2* and genes related to the TLR4 signaling pathway, including *IL1B* and *CXCL8*. A172 cells attained upregulated antioxidant gene expression, particularly *SOD1*, *TXN* and *PRDX1-5*, while MET treatment led to cell-cycle arrest. In silico analysis of the TCGA-GBM-RNASeq dataset indicated that the glycolytic plurimetabolic (GPM)-GBM subtype had a transcriptomic profile which overlapped with U87MG cells, suggesting



Citation: Moretti, I.F.; Lerario, A.M.; Sola, P.R.; Macedo-da-Silva, J.; Baptista, M.d.S.; Palmisano, G.; Oba-Shinjo, S.M.; Marie, S.K.N. GBM Cells Exhibit Susceptibility to Metformin Treatment According to TLR4 Pathway Activation and Metabolic and Antioxidant Status. *Cancers* **2023**, *15*, 587. <https://doi.org/10.3390/cancers15030587>

Academic Editor: Edward Pan

Received: 20 December 2022

Revised: 10 January 2023

Accepted: 14 January 2023

Published: 18 January 2023



Copyright: © 2023 by the authors. Licensee MDPI, Basel, Switzerland. This article is an open access article distributed under the terms and conditions of the Creative Commons Attribution (CC BY) license (<https://creativecommons.org/licenses/by/4.0/>).

GBM cases exhibiting this metabolic background with an activated inflammatory TLR4 pathway may respond to MET treatment. For cases with upregulated *CXCL8*, coding for IL8 (a pro-angiogenic factor), combination treatment with an IL8 inhibitor may improve tumor growth control. The A172 cell line corresponded to the mitochondrial (MTC)-GBM subtype, where MET plus an antioxidant inhibitor, such as anti-SOD1, may be indicated as a combinatory therapy.

Keywords: GBM; U87MG; A172; Metformin; LPS; antioxidant; cell cycle arrest; apoptosis

1. Introduction

Glioblastoma (GBM), a WHO grade 4 astrocytoma, is the most aggressive and malignant brain tumor [1], with an overall survival (OS) of 15 months [2], despite the current standard of care treatment consisting of surgical tumor macroresection followed by radiotherapy and chemotherapy with the alkylating agent temozolomide (TMZ) [3]. The limited effectiveness of therapeutic modalities available has been attributed to tumor invasiveness and high tumor heterogeneity [4]. Moreover, metabolic plasticity guarantees tumor fitness, where a blockade of metabolic pathways has been a focus of combination therapy strategies [5].

Metformin (MET), 1,1-dimethylbiguanide hydrochloride, known for its hypoglycemic action and widely used as the first-line medication for the treatment of type 2 diabetes [6], has been repurposed for cancer therapy. Known MET actions include regulation of AMPK pathway activity and mitochondria oxidative stress through inhibition of the oxidative phosphorylation (OXPHOS) complex I [7]. MET can also inhibit hexokinase activity and reduce cell glucose consumption, as well as act on the NF κ B canonical pathway decreasing IL8 [8], IL6, and TNF expression [9]. Moreover, recent studies have shown the role of MET in inhibiting NLRP3 inflammasome activation and IL1 β production in alveolar macrophages [10]; involving inhibition of NF κ B-NLRP3-mediated endothelial cell pyroptosis [11]; and of fatty acid synthase (FASN) with suppression of the proinflammatory response through the FASN/AKT pathway [12]. Additionally, inhibition of tumor growth using MET treatment has been described for several types of cancer, including colon, breast, prostate, pancreatic, lung, endometrial carcinomas, melanoma, and leukemia [13–18]. In particular, MET is a promising therapeutic option for brain tumors, given its hydrophilic property and permeability across the blood–brain barrier, as demonstrated in animal models [19,20]. In fact, the effects of MET on GBM cell viability have been studied previously [21–23], and several clinical trials of combination treatment with MET for GBM patients have been conducted [24].

We have previously demonstrated activation of the TLR4 signaling pathway in GBM, mainly the mesenchymal subtype, and upregulation of IL1 β and DNA repair genes through late activation of NF κ B in GBM cells stimulated with lipopolysaccharide (LPS). The LPS-stimulated GBM cells had decreased tumor cell viability with the use of treatment combining DNA repair inhibitor and TMZ, which proved more effective than treatment with TMZ alone [25].

In the present study, MET treatment, used in combination with TMZ in two GBM cell lines (U87MG and A172) and stimulated using LPS, was analyzed. The aims were to analyze the signaling pathways activated by MET, LPS and TMZ treatment used alone and in combination, and to identify predictive markers of treatment response.

2. Materials and Methods

2.1. Cell Culture

GBM cellular lines U87MG and A172 were acquired from ATCC. Lineages authentication by short tandem repeats analysis was performed using the GenePrint 10 System (Promega, Madison, WI, USA). Cells were maintained in DMEM (Dulbecco's Modified Eagle's Medium) (Thermo Fisher Scientific, Waltham, MA, USA) with the addition of 10%

fetal bovine serum (FBS) (Cultilab, Campinas, Brazil), streptomycin (100 µg/mL), and penicillin (100 IU/mL) (Thermo Fisher Scientific). Cells were incubated at 37 °C with 5% CO₂ and were routinely tested for mycoplasma contamination.

2.2. Cell Treatment

The following reagents: LPS from *Escherichia coli* O55:B5, MET and TMZ (Merck, Readington Township, NJ, USA) were used in U87MG and A172 cell cultures in single or combination treatments. Controls consisted of non-treated cells or treated with DMSO when TMZ was used. Proliferation curves with PrestoBlue reagent (Thermo Fisher Scientific) were performed to determine the half maximal inhibitory concentration (IC₅₀) dose of a single treatment. The IC₅₀ was used for all assays. Assays before (time 0) and after 24 and/or 48 h of treatment were analyzed, according to Figure 1, which shows the schematic experimental design with the time points of the cellular functional analysis: cell viability, apoptosis, cell cycle, mitochondria respiration and superoxide measurements, and transcriptomic analysis.

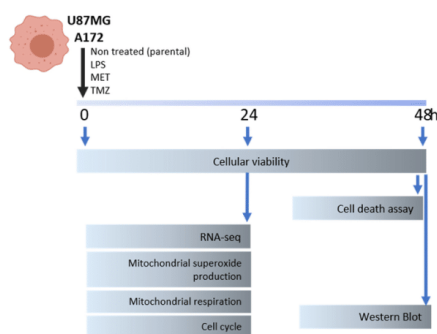


Figure 1. The schematic presentation of the experimental design.

2.3. Cell Viability and Apoptosis Assays

For the cell viability analyses, cells were plated in 96 wells plate (2×10^3 cells/well) and analyzed at different time points (24, 48 h). PrestoBlue Cell Viability Reagent was used according to the manufacturer's instructions (Thermo Fisher Scientific). Glomax equipment (Promega) was used to evaluate the fluorescence intensity after incubation (excitation at 540 nm, emission at 560 nm). Treatments were done in octuplicate, and two wells without the cell culture medium were used to access the background for each time point to be subtracted from each measurement value.

Cell-death assays of U87MG and A172 cell lines were analyzed after 48h of treatment. Cells were trypsinized, and the medium containing possible necrotic and late apoptotic cells was collected. The Dead Cell Apoptosis Kit (Thermo Fischer Scientific) containing Annexin V conjugated with FITC and propidium iodide (PI) was used following the instructions of the manufacturer. Cell death measurements were performed in the flow cytometry system BD FACSCanto (Beckton Dickinson, East Rutherford, NJ, USA). The analysis was done by FlowJo version 10 (Beckton Dickinson). For the analysis, a non-stained population of cells was used to set the percentage of alive cells. Positivity only for Annexin V was considered as early apoptosis, double positivity for Annexin V and PI was considered as late apoptosis, and positivity only for PI was considered as necrotic cells.

2.4. Mitochondrial Superoxide Assay

Production of superoxide by mitochondria after 24 h of treatment in U87MG and A172 cells was assessed by flow cytometry and compared to non-treated cells, in triplicate for each treatment. The MitoSOX Red Mitochondrial Superoxide Indicator kit was used following the instructions of the manufacturer (Thermo Fischer Scientific). MitoSOX fluorescence

was assessed in the flow cytometer FACSCanto (Beckton Dickinson). MitoSOX positivity was analyzed by FlowJo version 10.

2.5. Mitochondrial Respiration Analysis

The Seahorse XFe24 Analyzer (Agilent Technology, Santa Clara, CA, USA) equipment was used for mitochondrial respiration analysis of U87MG and A172 cell lines after treatment. The Cell Mito Stress Test Kit was used to assess mitochondria viability. Cells were plated in the Seahorse plate and treated with MET and LPS single and combined, in triplicate for each treatment, for 24 h, at 37 °C and 5% CO₂. Next, cells were washed, and the medium was changed to an un-buffered medium and maintained in a 37 °C incubator free of CO₂. The oxygen consumption rate (OCR) was measured following the Mito Stress program, and treatment was as follows: 2 μM oligomycin, for inhibiting ATP synthase (OXPHOS complex V), and decreasing OCR; 2 μM carbonyl cyanide 3-chlorophenylhydrazone (CCCP), for collapsing the proton gradient, disrupting the mitochondrial membrane, and maximizing OCR through OXPHOS complex IV; 5 μM antimycin A for inhibiting complex III and rotenone for inhibiting complex I, leading to a mitochondria shutdown.

2.6. Cell Cycle Analysis

Analyses of U87MG and A172 cell cycle phases were accessed by flow cytometry. Previously to treatment with LPS, MET, and TMZ, cells were synchronized by incubation with FBS-free DMEM with 0.5% bovine serum albumin for 24 h. Subsequently, cells were treated for 24 h in triplicate and fixed with cold ethanol in increasing concentrations (25, 50, 75, 90%). After fixation, cells were washed and incubated with PI. PI fluorescence was accessed by flow cytometry FACSCanto (Beckton Dickinson). Analysis was performed using FlowJo version 10, using the cell cycle interface.

2.7. High-Throughput Sequencing for Transcriptome Analysis

Total RNA of U87MG and A172 cells after 24 h of treatment with LPS and/or MET was extracted using the RNeasy mini kit (Qiagen, Hilden, Germany) for the transcriptomic analysis. Untreated cells were considered as the control. Two independent experiments in duplicate were performed for each condition. RNA integrity and concentration were accessed using RNA screentape in the 4200 TapeStation system (Agilent Technologies). The QuantSeq 3' mRNA-Seq Library Prep kit FWD for Illumina (Lexogen, Vienna, Austria) was used for library construction from 500 ng of total RNA following the recommendations of the manufacturer. The library concentration was measured using the Qubit dsDNA HS Assay Kit (Thermo Fisher Scientific), and the size distribution was determined using the Agilent D1000 ScreenTape System on TapeStation 4200 (Agilent Technologies). Sequencing was performed using the NextSeq 500 platform (Illumina, San Diego, CA, USA) at the next-generation sequencing facility core (SELA) at Faculdade de Medicina da Universidade de São Paulo (FMUSP). Sequencing data were aligned to the GRCh38 version of the human genome and quantified using the R-Bioconductor package QuasR using HISAT2 as the aligner [26]. The GFF file containing the gene models was obtained from ftp.ensembl.org (accessed on 20 November 2022). Sequencing quality and alignment metrics were assessed with FastQC and RNASEQC, respectively. Downstream analyses were performed in R using specific Bioconductor and CRAN tools, and briefly described. Normalization was performed with edgeR using the trimmed-mean (TMM) method. We used sva to remove occult/unwanted sources of variation from the data. The R-Bioconductor package limma was used to assess differential gene expression in each group, and to perform log₂ counts per million reads mapped (CPM) in the transformation of the data. Principal component analysis was performed using the prcomp function from R-stats, and graphically depicted as biplots constructed using ggplot2. To identify modules of co-regulated genes among the differentially expressed genes, we used heatmap and cutree to perform hierarchical clustering and to build heatmaps displaying these modules. We used Pearson correlation as the similarity metric, and the ward D2 clustering algorithm. We used clusterProfiler to

perform gene set enrichment analysis for each module of co-regulated genes. Expression data were centered on the mean of each gene. Additional gene set enrichment analyses were performed by online tools such as Gene Ontology [27–29] resources and String consortium [30,31]. The metabolic subtype for the cell lines was determined by the analysis of a combined score of marker gene expressions for glycolytic plurimetabolic (GPM) and mitochondrial (MTC subtypes described by Garofano et al. (2021) [32]. We used GSVA [33] to calculate these scores. For the heatmaps, the data were normalized by z-score. The logCPM for each gene was subtracted by the mean and divided by the standard deviation.

2.8. Western Blot

Protein extraction of U87MG and A172 cells was performed after 48 h of treatment using the lysis buffer (10 mM Hepes, 1% SDS, 1.5 mM MgCl₂, 1 mM KCl, 1 mM DTT, and 0.1% NP-40), protease and phosphatase inhibitors (Sigma-Aldrich, St. Louis, MO, USA). Samples were quantified by Qubit protein Assay kit platform (Thermo Fisher Scientific) and solubilized in sample buffer containing 60 mM Tris-HCl, 2% SDS, 10% glycerol, and 0.01% bromophenol blue. A total of 25 µg of proteins were separated by SDS-PAGE and electro-transferred to PVDF membranes, which were directly incubated with blocking buffer (5% bovine serum albumin (BSA) in Tris-buffered saline (TBS) and 0.05% Tween-20 (TBST)) for 1h. Subsequently, samples were incubated with primary antibodies: anti-BCL2 (2876, Cell signaling, Denver, MA, USA) and anti-β-actin (Sigma-Aldrich, A2228, 1:10,000) for loading control, followed by secondary antibody conjugated with horseradish peroxidase for anti-mouse diluted 1:4000 (Abcam, Cambridge, MA, USA) was used for detection of proteins. Immunoreactive bands were detected with the ChemiDoc XRS Imaging System equipment and protein quantification was performed using the ImageJ software (version 1.53t).

2.9. In Silico Analysis

The astrocytoma dataset from The Cancer Genome Atlas (TCGA) was downloaded from Genomics Data Commons Data Portal [34], and the data were normalized by DEseq software. GBM cases with clinical follow-up data were selected for the analysis. Data analysis was done by heatmap for visualization using z-score to normalize RPKM values.

2.10. Statistical Analysis

Statistical analysis was performed using the program SPSS version 23.0 (IBM Corporation, Armonk, NY, USA), Graph Pad Prism (GraphPad Software Inc., San Diego, CA, USA), and R studio [35]. The Kolmogorov–Smirnov test was applied to verify the normal distribution of the results. For non-parametric analysis, Kruskal–Wallis and post hoc Dunn test were used to assess the differences among three or more groups. For two groups comparison, the Mann–Whitney test was used. For parametric analysis, One-way ANOVA and Tukey post hoc test was used, and for multiple variables comparison, two-way ANOVA and Bonferroni or Tukey were used as post hoc tests. Correlation analysis was done by Pearson's test when parametric, and Spearman's when non-parametric. The Corrplot package was used for correlation visualization [36]. Statistical significance was considered when $p < 0.05$. The Kaplan–Meier estimator was applied for the TCGA-GPM-GBM subtype using *SOD2* and *CXCL8* expression ratio, where the cases were stratified as high and low according to the mean value for the ratio. Statistical analysis for the survival distribution was performed by Logrank test.

3. Results

3.1. Characterization of U87MG and A172 GBM Cell Lines

The effect of LPS and MET treatment, used alone and in combination, on U87MG and A172 GBM cell lines, was analyzed given that both present TLR4 expression [37] (Supplementary Figure S1A), and the fact that an increased apoptotic rate with the use of LPS and TMZ co-treatment in U87MG cells has been previously demonstrated by our group [24]. Also, U87MG and A172 cell lines were selected for an additional metabolic

3.2. U87MG and A172 Cell Viability and Cell Death with LPS, MET and TMZ Treatment

Cell viability and cell death assays were performed to analyze U87MG and A172 cell proliferation after use of LPS, MET, and TMZ treatment alone and in combination. In a previous study, we described a decrease in U87MG cell viability following the use of LPS + TMZ treatment [25]. By comparison, MET + TMZ treatment after 48 h in the present study led to a more significant decrease in cell viability (53%) ($p < 0.001$, one-way ANOVA post hoc Tukey test, relative to parental cells treated with DMSO), while MET alone led to a decrease of 19%, TMZ alone 37% or LPS + MET 12% ($p < 0.05$, one-way ANOVA post hoc Tukey test, relative to parental cells with DMSO) (Figure 2B). Analyses were performed at 24 and 48 h, and higher differences for the treatments group was observed after 48 h (Supplementary Figure S2A). The cell death assay revealed a significant increase in initial apoptosis only with the use of the LPS + MET + TMZ treatment combination after 48 h (57%) ($p < 0.001$, two-way ANOVA post hoc Tukey test, relative to parental cells + vehicle DMSO) (Figure 2C and Supplementary Figure S2B).

A172 cells also showed a significant decrease in cell viability (48%, $p < 0.001$, one-way ANOVA post hoc Tukey test, after 48 h) for the MET + TMZ treatment combination (Figure 2D), yielding similar results to the LPS + MET + TMZ treatment (49%). Moreover, no difference in the cell death assay was observed for treatment alone or combined in A172 cells (Figure 2E). Interestingly, treatment with TMZ alone resulted in a 42% increase in initial apoptosis of A172 cells compared to control cells (A172 cells + vehicle DMSO) (Figure 2E). In both cell lines, no differences were observed in late apoptosis (Supplementary Figure S2C).

3.3. Altered Signaling Pathways in U87MG and A172 Cells after LPS and MET Treatment Alone and in Combination

The results of the cell viability assay and cell death for the signaling pathways involved were analyzed by high-throughput sequencing of the transcriptome of both cell lines treated with LPS and MET, alone and in combination.

The RNASeq of U87MG cells yielded 12,396 genes with 212 differentially expressed genes (DEGs) for LPS treatment, 362 DEGs for MET treatment and 1810 DEGs for combined LPS + MET treatment with an adjusted p ($\text{adj } p$) < 0.1 compared to non-treated cells. To identify the clusters of DEGs, a Pearson's correlation analysis was performed, which identified 6 different clusters for the comparison of the four groups (U87MG parental cells, LPS alone, MET alone and LPS + MET treated cells) (Figure 3A). The clusters included enrichment of DEGs associated with different signaling pathways (Figure 3B). Cluster 1 showed upregulated genes after combined treatment (LPS + MET), whereas cluster 2 included upregulated genes only after MET treatment, while both clusters were related to apoptotic signaling pathway on the gene ontology enrichment analysis. Additionally, Cluster 1 included genes related to endoplasmic reticulum (ER) stress response and Cluster 2 to a process of import into cell pathways. Clusters 3 and 6 included genes downregulated after MET treatment, where the genes in Cluster 3 were related to response to wound and regulation of ERK1 and ERK2 cascade pathways, while the genes in Cluster 6 were related to actin filament assembly with increment of downregulation after combined (LPS + MET) treatment. Cluster 4 included upregulated genes after LPS treatment with enrichment for regulation of inflammatory response and vasculature development, and Cluster 5 included downregulated genes after LPS treatment enriched for ion transport and regulation (Figure 3A,B).

The RNASeq of A172 cells detected 13,059 genes, with 1278 DEGs after MET treatment and 1204 DEGs after LPS + MET combined treatment compared to non-treated cells, with an $\text{adj } p < 0.1$. Interestingly, LPS stimulation promoted no alteration in DEG profile relative to non-treated cells. The Pearson's correlation analysis for the DEGs showed four clusters of correlation (Figure 3C). Cluster 1 included upregulated genes after MET treatment with enrichment of genes related to the amino acid metabolic process and import into the cell pathways, while Cluster 2 included downregulated genes after MET treatment

related to chromosome segregation and mitotic nuclear division. Cluster 3 also included downregulated genes after MET treatment associated with the reactive oxygen metabolic process. Cluster 4 presented no significant enriched pathway (Figure 3C,D).

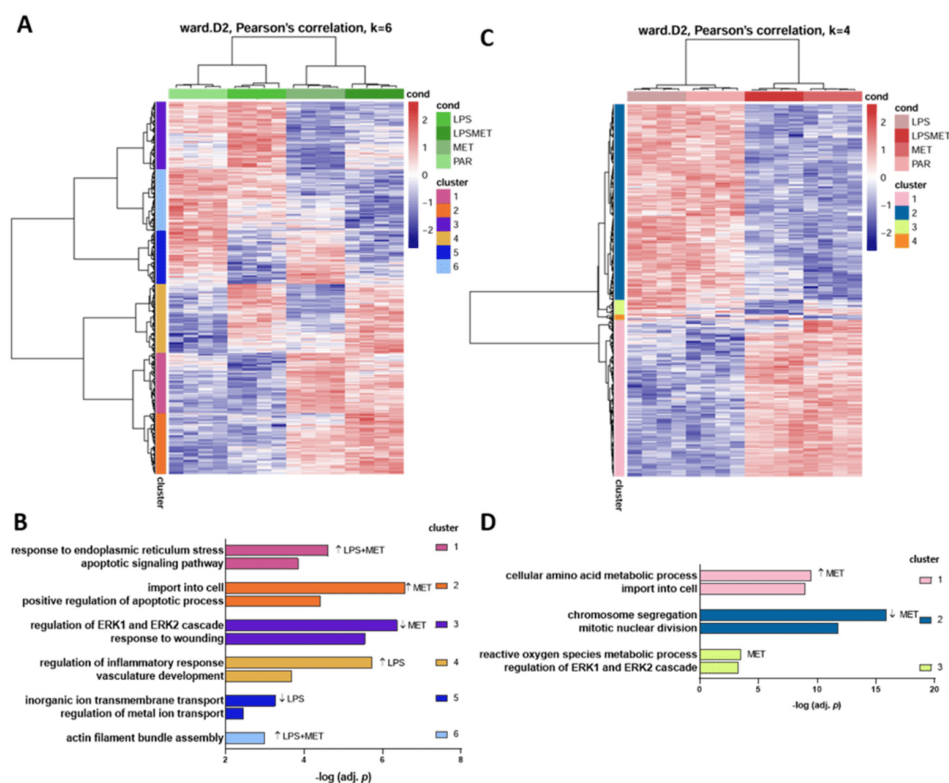


Figure 3. Transcriptome analysis for U87MG and A172 at 24 h after LPS and MET single and combined treatments compared to non-treated cells. A heatmap for the expression values after each treatment is presented and Pearson's correlation analysis for clusterization of the different groups showed six different clusters for U87MG (A) and four clusters for A172 (C). The top two gene ontology enrichment pathways identified in each cluster are shown in bars with the $-\log \text{adj } p$ for U87MG (B) and A172 (D).

3.4. U87MG Cells Were Prone to Mitochondrial Stress after MET Treatment

With regard to MET inhibition at the level of complex I of OXPHOS with consequent increase in reactive oxygen species (ROS) production, the MitoSOX assay was performed under the different treatment conditions.

An increase in mitochondrial superoxide production was observed in U87MG cells, as 100% of cells were positive for mitochondrial superoxide after MET treatment, a result replicated for the treatments combining TMZ or LPS ($p < 0.0001$ compared to non-treated condition, one-way ANOVA, post-hoc Tukey test) (Figure 4A and Supplementary Figure S3A). By contrast, A172 cells showed only 50% positivity when treated with MET, a rate unchanged by the treatment combination with TMZ or LPS ($p < 0.0001$ compared to non-treated cells, one-way ANOVA, post-hoc Tukey test) (Figure 4A and Supplementary Figure S3B).

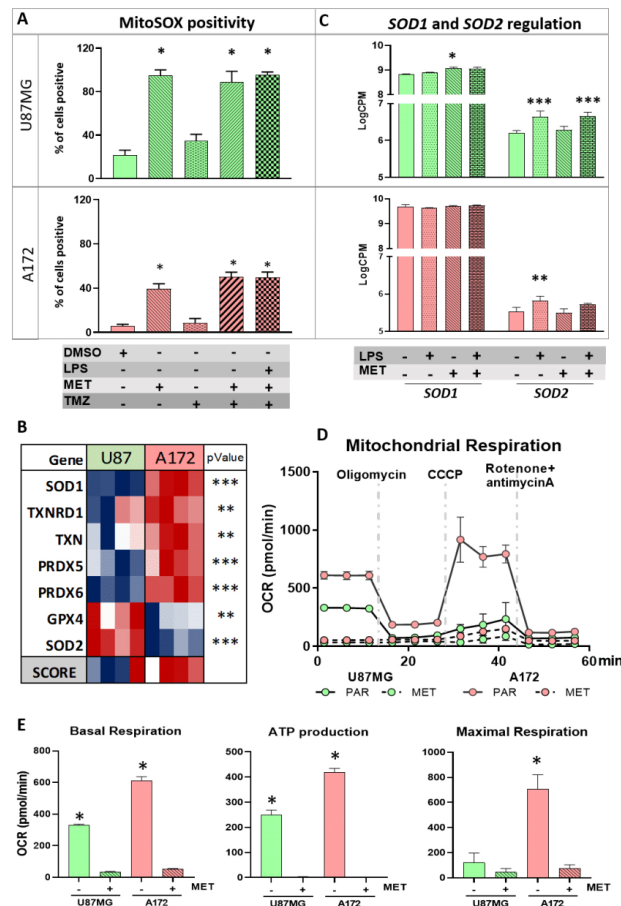


Figure 4. Mitochondrial stress. (A) The superoxide production in mitochondria after LPS, MET, and TMZ single and combined treatments for U87MG and A172. Graph bars represent the percentage of positive cells for MitoSOX. (*) $p < 0.0001$, One-wayANOVA post hoc Tukey test; (B) heatmap presenting the expression levels of antioxidant-related genes in U87MG and A172 cells. Presenting score values for the pathway for both cells (**) $p < 0.01$, and (***) $p < 0.001$, Limma t -test; (C) values for logCPM for *SOD1* and *SOD2* represented by the graph bars for U87MG and A172 after LPS, MET and LPS + MET treatment (*) $p < 0.05$, (**) $p < 0.01$, and $p < 0.001$, Limma t -test; (D) mitochondrial respiration by Seahorse, following the mitochondrial stress analysis. The oxygen consumption rate (OCR) curves along the time interval up to 60 min are presented according to applied drugs; and (E) histograms of basal respiration calculated by OCR before oligomycin incubation; ATP production evaluated by oligomycin-OCR subtracted from baseline cellular rate and maximal mitochondria respiration calculated as the value after CCCP-OCR subtracted from the value after rotenone- and antimycin A-OCR for U87MG and A172 in non-treated and MET treated. (*) $p < 0.0001$, one-way ANOVA followed by Tukey test. Red (parental-PAR), blue (MET treated) for U87MG and lilac (PAR), green (MET treated) for A172.

The antioxidant genes expressed in mitochondria were evaluated in U87MG and A172 parental cells to better understand the observed difference between the two cell lines.

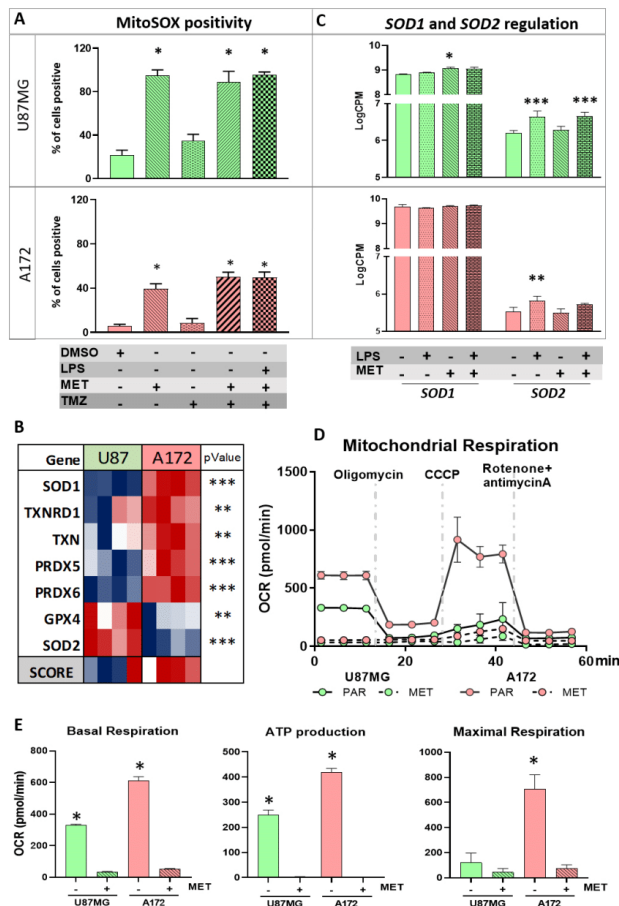


Figure 4. Mitochondrial stress. (A) The superoxide production in mitochondria after LPS, MET, and TMZ single and combined treatments for U87MG and A172. Graph bars represent the percentage of positive cells for MitoSOX. (*) $p < 0.0001$, One-wayANOVA post hoc Tukey test; (B) heatmap presenting the expression levels of antioxidant-related genes in U87MG and A172 cells. Presenting score values for the pathway for both cells (**) $p < 0.01$, and (***) $p < 0.001$, Limma t -test; (C) values for logCPM for *SOD1* and *SOD2* represented by the graph bars for U87MG and A172 after LPS, MET and LPS + MET treatment (*) $p < 0.05$, (**) $p < 0.01$, and $p < 0.001$, Limma t -test; (D) mitochondrial respiration by Seahorse, following the mitochondrial stress analysis. The oxygen consumption rate (OCR) curves along the time interval up to 60 min are presented according to applied drugs; and (E) histograms of basal respiration calculated by OCR before oligomycin incubation; ATP production evaluated by oligomycin-OCR subtracted from baseline cellular rate and maximal mitochondria respiration calculated as the value after CCCP-OCR subtracted from the value after rotenone- and antimycin A-OCR for U87MG and A172 in non-treated and MET treated. (*) $p < 0.0001$, one-way ANOVA followed by Tukey test. Red (parental-PAR), blue (MET treated) for U87MG and lilac (PAR), green (MET treated) for A172.

The antioxidant genes expressed in mitochondria were evaluated in U87MG and A172 parental cells to better understand the observed difference between the two cell lines.

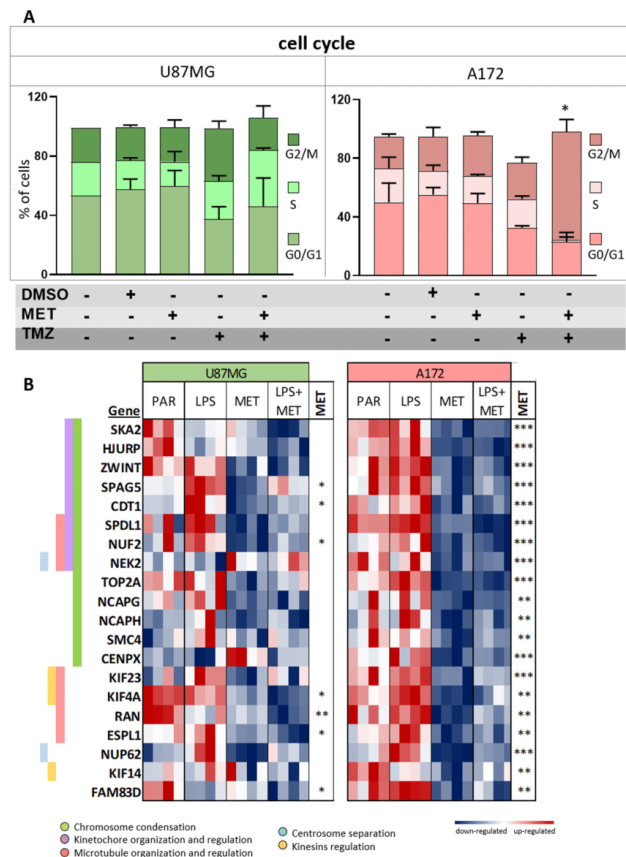


Figure 5. Cell cycle analysis and expression of genes related to chromosome segregation. (A) Cell cycle analysis for U87MG and A172 after MET and TMZ single and combined treatments. The bars represent each treatment condition. (*) $p < 0.0001$, two-way ANOVA post hoc Tukey test. G0/G1 phase (bottom bar), S phase (medium bar), G2/M phase (top bar); and (B) heatmap of chromosome segregation-related gene expressions after LPS and MET single and combined treatments in U87MG and A172 cells relative to non-treated controls. (*) $p < 0.05$, (**) $p < 0.01$, and (***) $p < 0.001$, Limma t -test for MET in comparison to PAR.

3.6. U87MG and A172 Cells Showed Upregulation of ER Stress and U87MG Cells Proved Prone to Apoptosis after MET Treatment

ER stress-related genes *ATF4*, *ATF6* and *DDIT3* (coding for CHOP), were upregulated in both cell lines after treatment with MET or LPS + MET. Additionally, pro-apoptotic genes *CHAC*, *TRIB3*, *PMAIP1*, *BBC3* and *BAX* were also upregulated in both cell lines, but more significantly in U87MG cells and after combined LPS + MET treatment ($3.2 \times 10^{-11} < p < 0.02$, compared to non-treated cells). Additionally, after MET or LPS + MET treatment, U87MG cells exhibited significant downregulation of anti-apoptotic genes, including *MCL1*, *PDK1* and *BCL2* ($p < 0.005$) (Figure 6A). Notably, the decrease in *BCL2* expression was confirmed at the protein level by Western blot in U87MG cells after MET + LPS treatment (Figure 6B, original Western blot is in Supplementary information

original images). By contrast, none of these anti-apoptotic genes were downregulated in A172 cells after treatment with MET or LPS + MET.

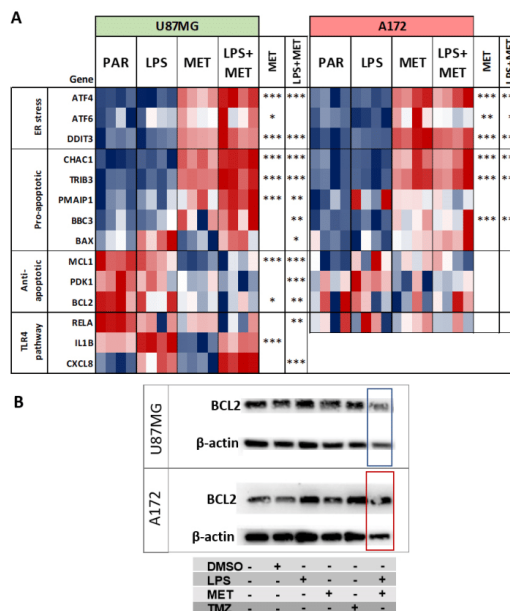


Figure 6. ER stress, pro- and anti-apoptotic and TLR4 pathway related gene expressions. (A) Heatmap for expression values of genes related to ER stress, pro-apoptotic, anti-apoptotic and TLR4 pathway in U87MG cells and A172 cells after LPS and MET single and combined treatments, (*) $p < 0.05$, (**) $p < 0.01$, and (***) $p < 0.001$, Limma *t*-test for LPS + MET combined and MET single treatment compared to non-treated cells; and (B) Western blot results for BCL2 of U87MG and A172 parental, DMSO, LPS, TMZ, MET single treated cells. β -actin was used for protein loading control.

Another difference between U87MG and A172 cells involved TLR4 signaling pathway activation. Expression of *RELA*, coding for p65 subunit of NF κ B, and of *IL1B*, was downregulated in U87MG after MET treatment, most significantly for *IL1B* expression. However, higher upregulation of *CXCL8*, coding for IL8, was observed after LPS + MET treatment compared to LPS treatment alone. By contrast, A172 cells showed no differential expression for *RELA*, while no *CXCL8* and *IL1B* expression was detected for any of the treatment conditions (Figure 6A).

3.7. In Silico Validation of the Results in the TCGA-GBM-RNASeq Dataset

Of the 160 GBM cases in the TCGA-RNASeq dataset, 77 were stratified according to the metabolic classification proposed by Garofano et al. (2021) [32] into GPM ($n = 34$) subtype with similarities to the U87MG cell line, and MTC ($n = 43$) subtype with similarities to the A172 cell line. Interestingly, antioxidant genes, including *SOD1*, *TXN* and *PRDX1-5*, were upregulated in MTC cases (Figure 7A and Supplementary Figure S5), whereas *SOD2* (Figure 7A) and *TXNRD1* were upregulated in GPM ($p < 0.05$, Mann-Whitney test). Moreover, expression levels of antioxidant genes were significantly correlated to *SOD1* expression in MTC ($p < 0.05$, Spearman's test) (Figure 7B). In contrast, genes related to the TLR4 signaling pathway, including *TLR4*, *MYD88*, *TRAF6*, subunits of NF κ B (*REL*, *RELA*, *RELB*, *NFKB1*) and *CXCL8*, were upregulated in GPM ($p < 0.05$, Mann-Whitney test) (Figure 7A and Supplementary Figure S5). More specifically, expression of *SOD2* and *CXCL8*

was higher in GPM-GBM than in MTC-GBM (Figure 7C) and the analysis of the impact of upregulation of these two genes, according to the Kaplan–Meier estimator, showed that *CXCL8* upregulation was more negative than *SOD2* upregulation, as GPM-GBM cases with lower *SOD2*/*CXCL8* ratio had an OS of 7.72 months compared to 22.26 months for cases with a higher ratio ($p = 0.002$, Logrank test) (Figure 7D). Taken together, this in silico analysis of the MTC-GBM subtype revealing upregulation of antioxidant genes, especially *SOD1*, and the GPM-GBM subtype showing upregulation of *SOD2* and TLR4 pathway-related genes, mirrors the findings observed for A172 and U87MG cells, respectively.

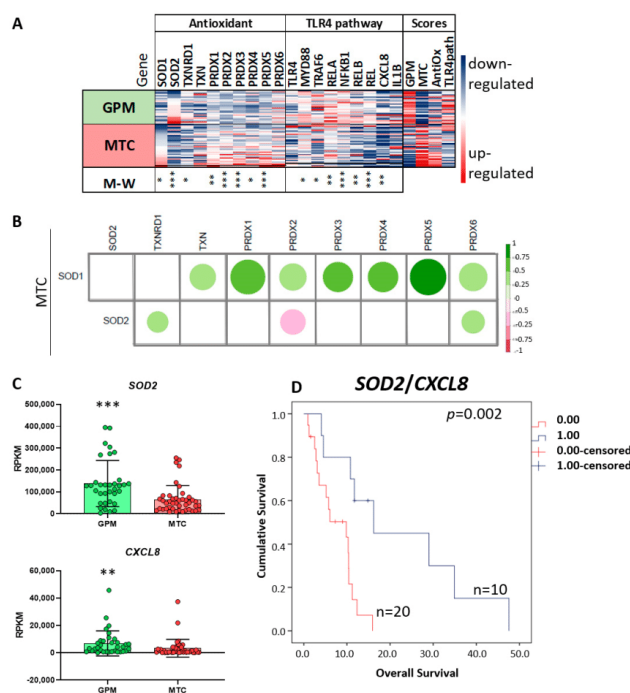


Figure 7. In silico validation of antioxidant and TLR4 pathway-related gene expressions in TCGA GBM-RNASeq dataset. (A) Heatmap of antioxidant and TLR4 pathway-related gene expressions normalized by z-score in 34 GPM and 43 MTC GBM subtypes according to Garofano's classification. The gene signatures for each case were calculated, and a score value was designated and normalized by z-score. (*) $p < 0.05$, (**) $p < 0.01$ (***), $p < 0.001$ (Mann–Whitney test); (B) in MTC, Spearman's correlation analysis showed strong correlation between the expression of *SOD1* and other antioxidant genes. The size of the circles is proportional to the p values, and positive (green) and negative (pink) correlations are presented according to the rho values in the bar scale at right. (C) RPKM values of *SOD2* and *CXCL8* for GPM- and MTC-GBM subtypes, graph bar presenting the mean values. Each circle represents a GBM case. (**) $p < 0.01$ (***), $p < 0.001$ (Mann–Whitney test); (D) in GPM, longer OS was presented by GBM cases with higher *SOD2*/*CXCL8* ratio in a Kaplan–Meier graph, $p = 0.002$ by log rank test (four cases were censored).

4. Discussion

GBM heterogeneity is a major factor limiting the effectiveness of therapeutic strategies available, creating the need to identify biomarkers to better stratify these tumors for specific combination therapies. We analyzed the response of two GBM cell lines to treatment with MET, LPS and TMZ, used alone and in combination. The U87MG cell line harboring the

NF1 mutation and A172 cell line with *RB1* mutation, classified as the mesenchymal GBM subtype with the worst prognosis, were selected to investigate the effects of these treatment conditions. These two specific cell lines were also chosen for their distinct metabolic profile, where U87MG has a GPM profile and A172 a MTC profile, according to Garofano's proposed GBM stratification based on metabolic pathways [32]. Differences of response to MET were already associated to mutational status of GBM cell lines [40]. Herein, we investigated MET response associated with the metabolic status of GBM cell lines.

Decreased cell viability was detected after MET + TMZ and MET + LPS + TMZ treatments in both cell lines, corroborating previous reports of anti-tumor effects of MET + TMZ [41,42]. Combined LPS + MET treatment has been previously tested in a mouse model of colon rectal cancer, with decreased tumor cell migration and longer OS in this animal model [13]. However, to our knowledge, this is the first study of LPS + MET treatment in gliomas.

A MET effect on mitochondrial respiration was confirmed in U87MG and A172 cells. Although A172 cells exhibited mostly oxidative respiration, with higher expression of genes coding for complex I of OXPHOS compared with U87MG cells, MET treatment reduced ATP production and oxygen consumption in both cell lines. The decoupling of electron transport induced by MET led to oxidative stress with superoxide production, ER stress and unfolded protein response (UPR) activation in both cell lines. Elevated superoxide after MET treatment was previously described in hepatocellular carcinoma [43], and pancreatic cancer cells, where superoxide accumulation in the mitochondrial matrix was associated with alteration of superoxide dismutase (SOD) expression [16]. SODs are antioxidant proteins responsible for converting superoxide radicals into hydrogen peroxide. SOD1 is localized in cytosol and mitochondrial intermembrane space and SOD2 in mitochondrial matrix [39,44]. Interestingly, A172 cells exhibited high expression of SOD1 and of several other antioxidant genes coding for proteins located in the organelle, possibly explaining the lower production of mitochondrial ROS detected after MET treatment. Moreover, A172 cells had upregulated expression of pro-apoptotic genes, with no change in expression of anti-apoptotic genes and, consequently, no increase in apoptosis after MET treatment. Nevertheless, in A172 cells, MET treatment promoted cell-cycle alteration with G2/M arrest due to downregulation of several genes related to chromosome segregation. In particular, genes related to kinetochore (*HJURP*, *ZWINT*), centromere (*NUF2*, *NEK2*, *CENPX*), mitotic spindle (*SPDL1*, *SPAG5*), chromatid separation (*TOP2A*, *NCAPG*), chromosome assembly (*NCAPH*, *SMC4*) and microtubule binding (*CDT1*, *FAM83D*), were downregulated. The kinetochore is built in the centromere and connects the chromosome to microtubules. The NDC80 complex (coded by *NUF2*), the kinetochore structural component, maintains microtubule attachment, and its blockage affects chromosome segregation stability [45]. *CDT1* is associated with the stable attachment of microtubule to kinetochore in the formation of the pre-DNA replication complex [46]. *RAN* [47], *NEK2* [48], *SPDL1* are related to microtubule positioning, where the latter plays this role by recruiting dynein for kinetochore [49]. Kinesins, *KIF4*, *KIF23* and *KIF14*, are important molecules responsible for microtubule transportation and positioning [50], which were also downregulated in A172 cells after MET treatment. Therefore, treatment with MET alone led to cell-cycle arrest, but this intervention proved insufficient to induce cell death of A172 cells. In a bid to identify an analogy of these findings with human GBM cases, the GBM-RNASeq dataset of the TCGA was analyzed. The MTC-GBM subtype, corresponding to the A172 cell line expression profile, showed upregulation of *SOD1* expression and significant correlation with antioxidant gene expressions, predominantly with the *PRDX* family, *PRDX1-5*, and with *TXNRD1*. Given this increased antioxidant state may blunt the apoptotic response, antioxidant inhibitors may represent an alternative combination therapy for the MTC-GBM subtype. Previous studies have demonstrated suppression of the ROS signaling pathway and triggering of apoptosis by a specific SOD1 inhibitor LD100 [51], an efficient copper-chelating agent [52]. Therefore, SOD1 inhibitors, or other antioxidant drugs, may be eligible for use in combination treatment with MET for the MTC-GBM subtype to induce cell-cycle arrest and

activation of the apoptotic pathway. Under this condition, SOD1 expression level may be used as an eligibility parameter for this combination therapy.

By contrast, U87MG cells showed upregulation of *SOD2*, with increased expression following LPS stimulation. However, the upregulation of this antioxidant proved insufficient to buffer the massive production of superoxide after MET treatment, exacerbated by the low expression of other mitochondrial antioxidant genes. ER response and UPR activation due to this oxidative stress resulted in increased apoptosis after MET treatment (33%), an increase which was significantly higher with MET + LPS + TMZ treatment (57%). The upregulation of pro-apoptotic genes and downregulation of anti-apoptotic genes, mainly *MCL1*, *PDK1* and *BCL2*, after MET and MET + LPS treatments contributed to the tumor cell death observed. In fact, a previous U87MG *in vivo* study showed delayed tumor growth with daily MET treatment [40], and better OS with MET + TMZ combined treatment [41]. MET treatment also induced TMZ sensitivity to a resistant GBM cell line [53]. In U251 and T98G GBM cell lines, a decrease of *BCL2* and an increase of pro-apoptotic proteins were observed after MET treatment with enhancement of TMZ effect [54].

Additionally, unlike A172 cells, U87MG cells showed activation of the NF κ B pathway leading to increased *IL1B* expression after LPS stimulation, confirming our previous evidence [25]. Notably, *IL1B* upregulation persisted after LPS + MET treatment, a phenomenon that might also control tumor growth, as a pyroptotic type of cell death via the cGAS-STING pathway was triggered by persistent stimulation of *IL1 β* [55]. However, LPS treatment also increased *CXCL8*, coding for IL8, a known pro-angiogenic factor in the tumor microenvironment [56], where neovascularization is one of the main characteristics of GBM responsible for its aggressiveness. Moreover, *SOD2* upregulation has been associated with poor prognosis in several tumors [57] and was associated with TMZ resistance in GBM cells and in xenograft models [58]. In fact, the transcriptomic analysis of the human GBM cases of the TCGA RNASeq dataset showed the GPM-GBM subtype had upregulation of *SOD2* and genes related to the TLR4 signaling pathway, including *CXCL8*, in comparison to the MTC-GBM subtype. The analysis of the impact of the two pro-tumoral genes, *SOD2* and *CXCL8*, showed a shorter OS for the GPM-GBM cases with lower *SOD2/CXCL8*, indicating that increased *CXCL8* expression may be more deleterious. Increased *CXCL8* (IL8) expression may be addressed by a neutralizing IL8 monoclonal antibody, which has been tested in a phase I clinical trial for metastatic or unresectable solid tumors and in ongoing studies evaluating its effect in reducing mesenchymal features in tumor cells, rendering them less resistant to treatment [59]. To date, no *SOD2* pharmacological inhibitors have been tested. Further *in vivo* studies are needed to determine the efficacy of the suggested combination therapies for GBM treatment.

5. Conclusions

In conclusion, U87MG, a mesenchymal GBM cell line with GPM metabolic background, responded with increased apoptosis after MET + LPS + TMZ treatment via increased ER stress and UPR response and downregulation of *BCL2*. A172; however, a mesenchymal GBM cell line with an MTC metabolic background, also attained an upregulated antioxidant status and MET treatment led to cell-cycle arrest. The present *in vitro* findings suggest that the GPM-GBM subtype with activated inflammatory TLR4 pathway may respond to MET treatment and that combination treatment with *CXCL8/IL8*-inhibitor may improve tumor growth control. The use of MET treatment, in combination with an antioxidant inhibitor such as anti-SOD1, may be an eligible approach for cases with the MTC-GBM subtype. The efficacy of the suggested combination therapies needs to be tested in *in vivo* studies.

Supplementary Materials: The following supporting information can be downloaded at: <https://www.mdpi.com/article/10.3390/cancers15030587/s1>. Figure S1:(A) Immunofluorescence analysis exhibiting the presence of TLR4 (in red) in U87MG and A172 cells; (B) Heatmap showing the differential expression in U87MG and A172 cell lines for marker genes for glycolytic plurimetabolic (GPM) and mitochondrial (MTC) according to Garofano's classification (2021). Figure S2: U87MG and A172 cell death analyzed by flow cytometry. Figure S3: Superoxide production in mitochondria

after LPS, MET, and TMZ single and combined treatments for U87MG. Figure S4: Cell cycle analysis for U87MG and A172 after LPS, MET and TMZ single and combined treatments. Figure S5: Heatmap of antioxidant genes, TLR4 pathway-related genes, marker genes for glycolytic plurimetabolic (GPM) and mitochondrial (MTC) subtypes. Original images: Western blot original figure. See Ref. [60].

Author Contributions: Conceptualization, I.F.M. and S.K.N.M.; methodology, I.F.M., A.M.L., P.R.S., J.M.-d.-S. and G.P.; validation, I.F.M., J.M.-d.-S. and A.M.L.; formal analysis, I.F.M. and S.K.N.M.; investigation, I.F.M. and S.K.N.M.; writing—original draft preparation, I.F.M. and S.K.N.M.; writing—review and editing, I.F.M., S.M.O.-S. and S.K.N.M.; supervision, S.K.N.M.; funding acquisition, S.M.O.-S., S.K.N.M., M.d.S.B. and G.P. All authors have read and agreed to the published version of the manuscript.

Funding: This research was supported by Conselho Nacional de Pesquisa (CNPq) “Bolsa de Produtividade”: #304541/2020-6 (S.K.N.M.), #307854/2018-3 (G.P.), #317214/2021-7 (S.M.O.-S.); Sao Paulo Research Foundation (FAPESP, grants #04/12133-6 (S.K.N.M.), #2013/07937-8 (M.S.B.), #2020/02988-7 (S.K.N.M., S.M.O.-S.), #2018/18257-1 (G.P.), #2020/04923-0 (G.P.), #2021/00140-3 (J.M.-d.-S.); Coordenação de Aperfeiçoamento de Pessoal de Nível Superior—Brasil (CAPES/PROEX) grants #23038.018285/2019-21 (S.K.N.M., S.M.O.-S.), #88887.600107/2021-00 (I.F.M.) and (CAPES/NUFFIC) grants #062/15, 9999.001625 (S.K.N.M.), 88887.351607/2019-00 (I.F.M.); Fundação Faculdade de Medicina (FFM); and Faculdade de Medicina da USP (FMUSP).

Institutional Review Board Statement: The present study was approved by the HCFMUSP (process number: 059/15) and the FMUSP, ethical committee (process number: 278/15).

Informed Consent Statement: Not applicable.

Data Availability Statement: Not applicable.

Acknowledgments: We are grateful to Esper Kallas, coordinator of the FMUSP flow cytometry facility, for the use of the equipment and excellent assistance provided by their staff. We also would like to thank Marisa Passarelli for Metformin reagent donation. We thank Alicia J Kowaltowski for the Seahorse equipment use and the technical support of Camille C. Caldeira da Silva. We also thank the SELA Facility Core of School of Medicine, University of Sao Paulo (Fapesp grant #2014/50137-5), for assistance with sequencing.

Conflicts of Interest: The authors declare no conflict of interest.

References

- Louis, D.N.; Perry, A.; Wesseling, P.; Brat, D.J.; Cree, I.A.; Figarella-Branger, D.; Hawkins, C.; Ng, H.K.; Pfister, S.M.; Reifenberger, G.; et al. The 2021 WHO Classification of Tumors of the Central Nervous System: A summary. *Neuro Oncol.* **2021**, *23*, 1231–1251. [[CrossRef](#)]
- Villano, J.L.; Seery, T.E.; Bressler, L.R. Temozolomide in malignant gliomas: Current use and future targets. *Cancer Chemother. Pharmacol.* **2009**, *64*, 647–655. [[CrossRef](#)]
- Stupp, R.; Mason, W.P.; van den Bent, M.J.; Weller, M.; Fisher, B.; Taphoorn, M.J.; Belanger, K.; Brandes, A.A.; Marosi, C.; Bogdahn, U.; et al. Radiotherapy plus concomitant and adjuvant temozolomide for newly diagnosed glioblastoma. *N. Engl. J. Med.* **2005**, *352*, 987–996. [[CrossRef](#)]
- Louis, D.N.; Ohgaki, H.; Wiestler, O.D.; Cavenee, W.K.; Burger, P.C.; Jouvet, A.; Scheithauer, B.W.; Kleihues, P. The 2007 WHO Classification of Tumours of the Central Nervous System. *Acta Neuropathol.* **2007**, *114*, 97–109. [[CrossRef](#)]
- Mazurek, M.; Litak, J.; Kamiński, P.; Kulesza, B.; Jonak, K.; Baj, J.; Grochowski, C. Metformin as Potential Therapy for High-Grade Glioma. *Cancers.* **2020**, *12*, 210. [[CrossRef](#)]
- Fujita, Y.; Inagaki, N. Metformin: New Preparations and Nonglycemic Benefits. *Curr. Diabetes Rep.* **2017**, *17*, 5. [[CrossRef](#)]
- Wang, Y.; An, H.; Liu, T.; Qin, C.; Sesaki, H.; Guo, S.; Radovick, S.; Hussain, M.; Maheshwari, A.; Wondisford, F.E.; et al. Metformin Improves Mitochondrial Respiratory Activity through Activation of AMPK. *Cell Rep.* **2019**, *29*, 1511–1523.e5. [[CrossRef](#)]
- Xiao, Z.; Wu, W.; Poltoratsky, V. Metformin Suppressed CXCL8 Expression and Cell Migration in HEK293/TLR4 Cell Line. *Mediat. Inflamm.* **2017**, *2017*, 6589423. [[CrossRef](#)]
- Kim, J.; Kwak, H.J.; Cha, J.Y.; Sesaki, H.; Guo, S.; Radovick, S.; Hussain, M.; Maheshwari, A.; Wondisford, F.E.; O'Rourke, B.; et al. Metformin suppresses lipopolysaccharide (LPS)-induced inflammatory response in murine macrophages via activating transcription factor-3 (ATF-3) induction. *J. Biol. Chem.* **2014**, *289*, 23246–23255. [[CrossRef](#)]
- Xian, H.; Liu, Y.; Nilsson, A.R.; Gatchalian, R.; Crother, T.R.; Tourtellotte, W.G.; Zhang, Y.; Aleman-Muench, G.R.; Lewis, G.; Chen, W.; et al. Metformin inhibition of mitochondrial ATP and DNA synthesis abrogates NLRP3 inflammasome activation and pulmonary inflammation. *Immunity* **2021**, *54*, 1463–1477.e11. [[CrossRef](#)]
- Zhang, Y.; Zhang, H.; Li, S.; Huang, K.; Jiang, L.; Wang, Y. Metformin Alleviates LPS-Induced Acute Lung Injury by Regulating the SIRT1/NF-κB/NLRP3 Pathway and Inhibiting Endothelial Cell Pyroptosis. *Front. Pharmacol.* **2022**, *13*, 801337. [[CrossRef](#)]

12. Xiong, W.; Sun, K.-Y.; Zhu, Y.; Zhang, X.; Zhou, Y.-H.; Zou, X. Metformin alleviates inflammation through suppressing FASN-dependent palmitoylation of Akt. *Cell Death Dis.* **2021**, *12*, 934. [CrossRef]
13. Wu, X.; Qian, S.; Zhang, J.; Feng, J.; Luo, K.; Sun, L.; Zhao, L.; Ran, Y.; Sun, L.; Wang, J.; et al. Lipopolysaccharide promotes metastasis via acceleration of glycolysis by the nuclear factor- κ B/snail/hexokinase3 signaling axis in colorectal cancer. *Cancer Metab.* **2021**, *9*, 23. [CrossRef]
14. Xue, C.; Wang, C.; Sun, Y.; Meng, Q.; Liu, Z.; Huo, X.; Sun, P.; Sun, H.; Ma, X.; Ma, X.; et al. Targeting P-glycoprotein function, p53 and energy metabolism: Combination of metformin and 2-deoxyglucose reverses the multidrug resistance of MCF-7/Dox cells to doxorubicin. *Oncotarget* **2017**, *8*, 8622–8632. [CrossRef]
15. Khan, A.S.; Frigo, D.E. A spatiotemporal hypothesis for the regulation; role; and targeting of AMPK in prostate cancer. *Nat. Rev. Urol.* **2017**, *14*, 164–180. [CrossRef]
16. Warkad, M.S.; Kim, C.H.; Kang, B.G.; Park, S.H.; Jung, J.S.; Feng, J.H.; Inci, G.; Kim, S.C.; Suh, H.W.; Lim, S.S.; et al. Metformin-induced ROS upregulation as amplified by apigenin causes profound anticancer activity while sparing normal cells. *Sci. Rep.* **2021**, *11*, 14002. [CrossRef]
17. Takahashi, A.; Kimura, F.; Yamanaka, A.; Takebayashi, A.; Kita, N.; Takahashi, K.; Murakami, T. Metformin impairs growth of endometrial cancer cells via cell cycle arrest and concomitant autophagy and apoptosis. *Cancer Cell Int.* **2014**, *14*, 53. [CrossRef]
18. Tseng, H.-W.; Li, S.-C.; Tsai, K.-W. Metformin Treatment Suppresses Melanoma Cell Growth and Motility Through Modulation of microRNA Expression. *Cancers* **2019**, *11*, 209. [CrossRef]
19. Markowicz-Piasecka, M.; Sikora, J.; Szydłowska, A.; Skupień, A.; Mikiciuk-Olasik, E.; Huttunen, K.M. Metformin—A Future Therapy for Neurodegenerative Diseases. *Pharm. Res.* **2017**, *34*, 2614–2627. [CrossRef]
20. Łabuzek, K.; Suchy, D.; Gabryel, B.; Bielecka, A.; Liber, S.; Okopień, B. Quantification of metformin by the HPLC method in brain regions; cerebrospinal fluid and plasma of rats treated with lipopolysaccharide. *Pharmacol. Rep.* **2010**, *62*, 956–965. [CrossRef]
21. Albayrak, G.; Konac, E.; Akin Dere, U.; Emmez, H. Targeting Cancer Cell Metabolism with Metformin; Dichloroacetate and Memantine in Glioblastoma (GBM). *Turk. Neurosurg.* **2021**, *31*, 233–237. [CrossRef]
22. Soraya, H.; Sani, N.A.; Jabbari, N.; Rezaie, J. Metformin Increases Exosome Biogenesis and Secretion in U87 MG Human Glioblastoma Cells: A Possible Mechanism of Therapeutic Resistance. *Arch. Med. Res.* **2021**, *52*, 151–162. [CrossRef]
23. Rezaei, N.; Neshasteh-Riz, A.; Mazaheri, Z.; Koosha, F.; Hoormand, M. The Combination of Metformin and Disulfiram-Cu for Effective Radiosensitization on Glioblastoma Cells. *Cell J.* **2020**, *22*, 263–272. [CrossRef]
24. Ohno, M.; Kitanaka, C.; Miyakita, Y.; Tanaka, S.; Sonoda, Y.; Mishima, K.; Ishikawa, E.; Takahashi, M.; Yanagisawa, S.; Ohashi, K.; et al. Metformin with Temozolomide for Newly Diagnosed Glioblastoma: Results of Phase I Study and a Brief Review of Relevant Studies. *Cancers* **2022**, *14*, 4222. [CrossRef]
25. Moretti, I.F.; Lerario, A.M.; Trombetta-Lima, M.; Sola, P.R.; da Silva Soares, R.; Oba-Shinjo, S.M.; Marie, S.K.N. Late p65 nuclear translocation in glioblastoma cells indicates non-canonical TLR4 signaling and activation of DNA repair genes. *Sci. Rep.* **2021**, *11*, 1333. [CrossRef]
26. Kim, D.; Langmead, B.; Salzberg, S.L. HISAT: A fast spliced aligner with low memory requirements. *Nat. Methods* **2015**, *12*, 357–360. [CrossRef]
27. The Gene Ontology Consortium. The Gene Ontology Resource: 20 years and still GOing strong. *Nucleic Acids Res.* **2019**, *47*, D330–D338. [CrossRef]
28. The Gene Ontology Consortium. The Gene Ontology resource: Enriching a GOLD mine. *Nucleic Acids Res.* **2021**, *49*, D325–D334. [CrossRef]
29. Carbon, S.; Ireland, A.; Mungall, C.J.; Shu, S.; Marshall, B.; Lewis, S.; AmiGO Hub; Web Presence Working Group. AmiGO: Online access to ontology and annotation data. *Bioinformatics* **2009**, *25*, 288–289. [CrossRef]
30. Snel, B.; Lehmann, G.; Bork, P.; Huynen, M.A. STRING: A web-server to retrieve and display the repeatedly occurring neighbourhood of a gene. *Nucleic Acids Res.* **2000**, *28*, 3442–3444. [CrossRef]
31. Szklarczyk, D.; Gable, A.L.; Nastou, K.C.; Lyon, D.; Kirsch, R.; Pyysalo, S.; Doncheva, N.T.; Legeay, M.; Fang, T.; Bork, P.; et al. The STRING database in 2021: Customizable protein-protein networks; and functional characterization of user-uploaded gene/measurement sets. *Nucleic Acids Res.* **2021**, *49*, D605–D612. [CrossRef]
32. Garofano, L.; Migliozi, S.; Oh, Y.T.; D'Angelo, F.; Najac, R.D.; Ko, A.; Frangaj, B.; Caruso, F.P.; Yu, K.; Yuan, J.; et al. Pathway-based classification of glioblastoma uncovers a mitochondrial subtype with therapeutic vulnerabilities. *Nat. Cancer* **2021**, *2*, 141–156. [CrossRef]
33. Hänzelmann, S.; Castelo, R.; Guinney, J. GSEA: Gene set variation analysis for microarray and RNA-seq data. *BMC Bioinform.* **2013**, *14*, 7. [CrossRef]
34. Cerami, E.; Gao, J.; Dogrusoz, U.; Gross, B.E.; Sumer, S.O.; Aksoy, B.A.; Jacobsen, A.; Byrne, C.J.; Heuer, M.L.; Larsson, E.; et al. The cBio cancer genomics portal: An open platform for exploring multidimensional cancer genomics data. *Cancer Discov.* **2012**, *2*, 401–404. [CrossRef]
35. R Studio Team. *RStudio: Integrated Development Environment for R*; RStudio, PBC: Boston, MA, USA, 2020. Available online: <http://www.rstudio.com/> (accessed on 3 November 2022).
36. Wei, T.; Simko, V.; Levy, M.; Xie, Y.; Jin, Y.; Zemla, J. Package 'corrplot'. *Statistician* **2017**, *56*, 316–324.
37. Moretti, I.F.; Franco, D.G.; de Almeida Galatro, T.F.; Oba-Shinjo, S.M.; Marie, S.K.N. Plasmatic membrane toll-like receptor expressions in human astrocytomas. *PLoS ONE* **2018**, *13*, e0199211. [CrossRef]

38. Baek, Y.; Woo, T.-G.; Ahn, J.; Lee, D.; Kwon, Y.; Park, B.J.; Ha, N.C. Structural analysis of the overoxidized Cu/Zn-superoxide dismutase in ROS-induced ALS filament formation. *Commun. Biol.* **2022**, *5*, 1085. [[CrossRef](#)]
39. Candas, D.; Li, J.J. MnSOD in oxidative stress response-potential regulation via mitochondrial protein influx. *Antioxid. Redox Signal.* **2014**, *20*, 1599–1617. [[CrossRef](#)]
40. Sesen, J.; Dahan, P.; Scotland, S.J.; Saland, E.; Dang, V.T.; Lemarié, A.; Tyler, B.M.; Brem, H.; Toulas, C.; Cohen-Jonathan Moyal, E.; et al. Metformin Inhibits Growth of Human Glioblastoma Cells and Enhances Therapeutic Response. *PLoS ONE* **2015**, *10*, e0123721. [[CrossRef](#)]
41. Xiong, Z.S.; Gong, S.F.; Si, W.; Jiang, T.; Li, Q.L.; Wang, T.J.; Wang, W.J.; Wu, R.Y.; Jiang, K. Effect of metformin on cell proliferation, apoptosis, migration and invasion in A172 glioma cells and its mechanisms. *Mol. Med. Rep.* **2019**, *20*, 887–894. [[CrossRef](#)]
42. Lee, J.E.; Lim, J.H.; Hong, Y.K.; Yang, S.H. High-Dose Metformin Plus Temozolomide Shows Increased Anti-tumor Effects in Glioblastoma In Vitro and In Vivo Compared with Monotherapy. *Cancer Res. Treat.* **2018**, *50*, 1331–1342. [[CrossRef](#)]
43. Gou, S.; Qiu, L.; Yang, Q.; Li, P.; Zhou, X.; Sun, Y.; Zhou, X.; Zhao, W.; Zhai, W.; Li, G.; et al. Metformin leads to accumulation of reactive oxygen species by inhibiting the NFE2L1 expression in human hepatocellular carcinoma cells. *Toxicol. Appl. Pharmacol.* **2021**, *420*, 115523. [[CrossRef](#)]
44. Okado-Matsumoto, A.; Fridovich, I. Subcellular Distribution of Superoxide Dismutases (SOD) in Rat Liver: Cu/Zn-SOD in mitochondria. *J. Biol. Chem.* **2001**, *276*, 38388–38393. [[CrossRef](#)]
45. Vorozhko, V.V.; Emanuele, M.J.; Kallio, M.J.; Stukenberg, P.T.; Gorbisky, G.J. Multiple mechanisms of chromosome movement in vertebrate cells mediated through the Ndc80 complex and dynein/dynactin. *Chromosoma* **2008**, *117*, 169–179. [[CrossRef](#)]
46. Varma, D.; Chandrasekaran, S.; Sundin, L.J.; Reidy, K.T.; Wan, X.; Chasse, D.A.; Nevis, K.R.; DeLuca, J.G.; Salmon, E.D.; Cook, J.G. Recruitment of the human Cdt1 replication licensing protein by the loop domain of Hec1 is required for stable kinetochore-microtubule attachment. *Nat. Cell Biol.* **2012**, *14*, 593–603. [[CrossRef](#)]
47. Oh, D.; Yu, C.-H.; Needleman, D.J. Spatial organization of the Ran pathway by microtubules in mitosis. *Proc. Natl. Acad. Sci. USA* **2016**, *113*, 8729–8734. [[CrossRef](#)]
48. Fry, A.M.; O'Regan, L.; Sabir, S.R.; Bayliss, R. Cell cycle regulation by the NEK family of protein kinases. *J. Cell Sci.* **2012**, *125*, 4423–4433. [[CrossRef](#)]
49. Griffis, E.R.; Stuurman, N.; Vale, R.D. Spindly, a novel protein essential for silencing the spindle assembly checkpoint; recruits dynein to the kinetochore. *J. Cell Biol.* **2007**, *177*, 1005–1015. [[CrossRef](#)]
50. Liang, Y.J.; Yang, W.X. Kinesins in MAPK cascade: How kinesin motors are involved in the MAPK pathway? *Gene* **2019**, *684*, 1–9. [[CrossRef](#)]
51. Li, X.; Chen, Y.; Zhao, J.; Shi, J.; Wang, M.; Qiu, S.; Hu, Y.; Xu, Y.; Cui, Y.; Liu, C.; et al. The Specific Inhibition of SOD1 Selectively Promotes Apoptosis of Cancer Cells via Regulation of the ROS Signaling Network. *Oxidative Med. Cell. Longev.* **2019**, *2019*, 9706792. [[CrossRef](#)]
52. Dong, X.; Zhang, Z.; Zhao, J.; Lei, J.; Chen, Y.; Li, X.; Chen, H.; Tian, J.; Zhang, D.; Liu, C.; et al. The rational design of specific SOD1 inhibitors via copper coordination and their application in ROS signaling research. *Chem. Sci.* **2016**, *7*, 6251–6262. [[CrossRef](#)]
53. Yang, S.H.; Li, S.; Lu, G.; Xue, H.; Kim, D.H.; Zhu, J.J.; Liu, Y. Metformin treatment reduces temozolomide resistance of glioblastoma cells. *Oncotarget* **2016**, *7*, 78787–78803. [[CrossRef](#)] [[PubMed](#)]
54. Valtorta, S.; Dico, A.L.; Raccagni, L.; Gaglio, D.; Belloli, S.; Politi, L.S.; Martelli, C.; Diceglie, C.; Bonanomi, M.; Ercoli, G.; et al. Metformin and temozolomide, a synergic option to overcome resistance in glioblastoma multiforme models. *Oncotarget* **2017**, *8*, 113090–113104. [[CrossRef](#)] [[PubMed](#)]
55. Aarreberg, L.D.; Esser-Nobis, K.; Driscoll, C.; Shuvarikov, A.; Roby, J.A.; Gale, M., Jr. Interleukin-1 β Induces mtDNA Release to Activate Innate Immune Signaling via cGAS-STING. *Mol Cell* **2019**, *74*, 801–815.e6. [[CrossRef](#)]
56. De Palma, M.; Bizziato, D.; Petrova, T.V. Microenvironmental regulation of tumour angiogenesis. *Nat. Rev. Cancer* **2017**, *17*, 457–474. [[CrossRef](#)] [[PubMed](#)]
57. Miar, A.; Hevia, D.; Muñoz-Cimadevilla, H.; Astudillo, A.; Velasco, J.; Sainz, R.M.; Mayo, J.C. Manganese superoxide dismutase (SOD2/MnSOD)/catalase and SOD2/GPx1 ratios as biomarkers for tumor progression and metastasis in prostate, colon, and lung cancer. *Free Radic. Biol. Med.* **2015**, *85*, 45–55. [[CrossRef](#)]
58. Chang, K.Y.; Hsu, T.I.; Hsu, C.C.; Tsai, S.Y.; Liu, J.J.; Chou, S.W.; Liu, M.S.; Liou, J.P.; Ko, C.Y.; Chen, K.Y.; et al. Specificity protein 1-modulated superoxide dismutase 2 enhances temozolomide resistance in glioblastoma; which is independent of O(6)-methylguanine-DNA methyltransferase. *Redox Biol.* **2017**, *13*, 655–664. [[CrossRef](#)]
59. Bilusic, M.; Heery, C.R.; Collins, J.M.; Donahue, R.N.; Palena, C.; Madan, R.A.; Karzai, F.; Marté, J.L.; Strauss, J.; Gatti-Mays, M.E.; et al. Phase I trial of HuMax-IL8 (BMS-986253), an anti-IL-8 monoclonal antibody; in patients with metastatic or unresectable solid tumors. *J. Immunother. Cancer* **2019**, *7*, 240. [[CrossRef](#)]
60. Verhaak, R.G.W.; Hoadley, K.A.; Purdom, E.; Wang, V.; Qi, Y.; Wilkerson, M.D.; Miller, C.R.; Ding, L.; Golub, T.; Mesirov, J.P.; et al. Integrated Genomic Analysis Identifies Clinically Relevant Subtypes of Glioblastoma Characterized by Abnormalities in PDGFRA, IDH1, EGFR, and NF1. *Cancer Cell* **2010**, *17*, 98–110. [[CrossRef](#)]

Disclaimer/Publisher's Note: The statements, opinions and data contained in all publications are solely those of the individual author(s) and contributor(s) and not of MDPI and/or the editor(s). MDPI and/or the editor(s) disclaim responsibility for any injury to people or property resulting from any ideas, methods, instructions or products referred to in the content.

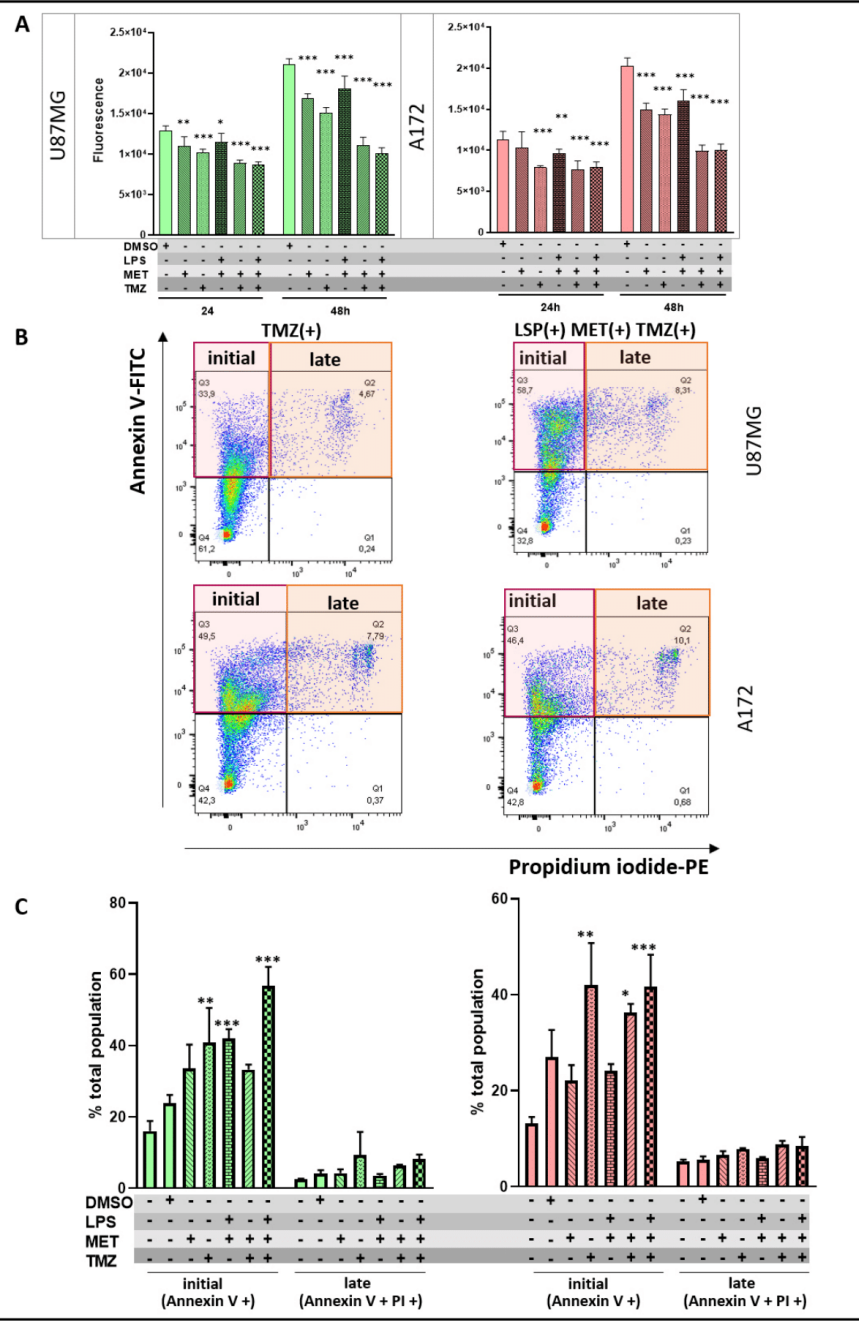


Figure S2. U87MG and A172 cell death analyzed by flow cytometry. (A) Graph bars representing the viability plotted for the single and combined treatments for LPS, MET, and TMZ in U87MG and A172 at two different time points (24 and 48 h) (* $p < 0.05$, (**) $p < 0.01$, (***) $p < 0.001$ (Two-way ANOVA post hoc Tukey test) (B) Representation of different cell populations observed in the apoptosis assay of U87MG and A172 cells treated for TMZ alone and LPS+MET+TMZ combination. Initial

and late apoptosis are highlighted in red and orange bars, respectively. (C) The values in percentage for initial and late apoptosis are presented in bar-graphs for each treatment condition, where annexin V positive and propidium iodide (PI) negative corresponds to initial apoptosis and annexin V and PI positive to late apoptosis. (*) $p < 0.05$, (**) $p < 0.01$, (***) $p < 0.001$ (Two-way ANOVA post hoc Tukey test).

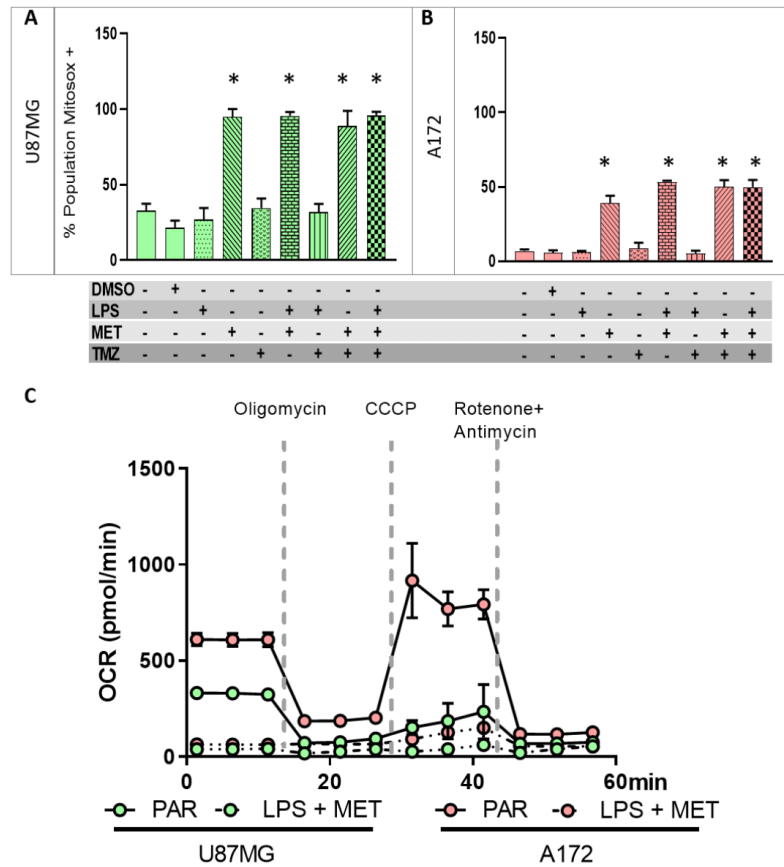


Figure S3. Superoxide production in mitochondria after LPS, MET, and TMZ single and combined treatments for U87MG (A) and A172 (B). Bar-graphs represent the percentage of positive cells for MitoSOX. (*) $p < 0.0001$, one-way-ANOVA post hoc Tukey test. (C) Mitochondrial respiration analysis, following the mitochondrial stress analysis. The curves of the oxygen consumption rate (OCR) along the time interval up to 60 minutes are presented according to drug treatment. The analysis was performed for the LPS and MET single and combined treatments compared to non-treated cells (PAR). CCCP, carbonyl cyanide 3-chlorophenylhydrazone.

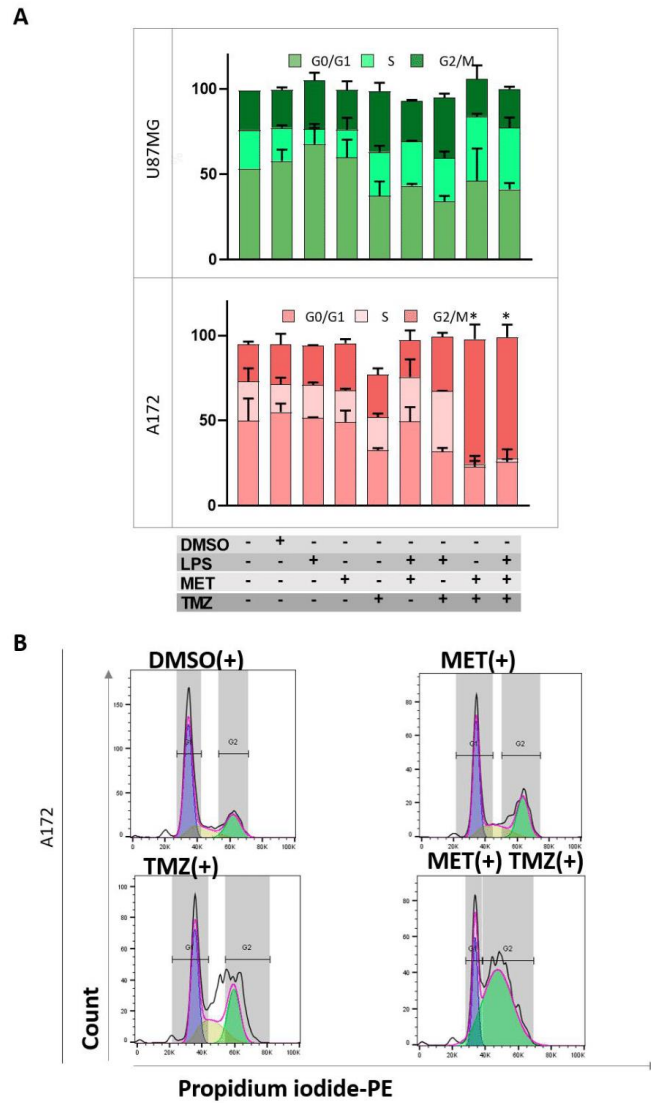


Figure S4. (A) Cell cycle analysis for U87MG and A172 after LPS, MET and TMZ single and combined treatments. The bars represent the percentage of cells in the corresponding cell cycle phase in each treatment condition. (*) $p < 0.0001$, two-way-ANOVA post hoc Tukey test. G0/G1 phase (bottom bar), S phase (medium bar), G2/M phase (top bar) (B) Cell cycle curves for DMSO, MET and TMZ single and combined treatments of A172 cells. The areas under the curve represent G0/G1 (lilac), S (yellow), and G2/M (green).

A

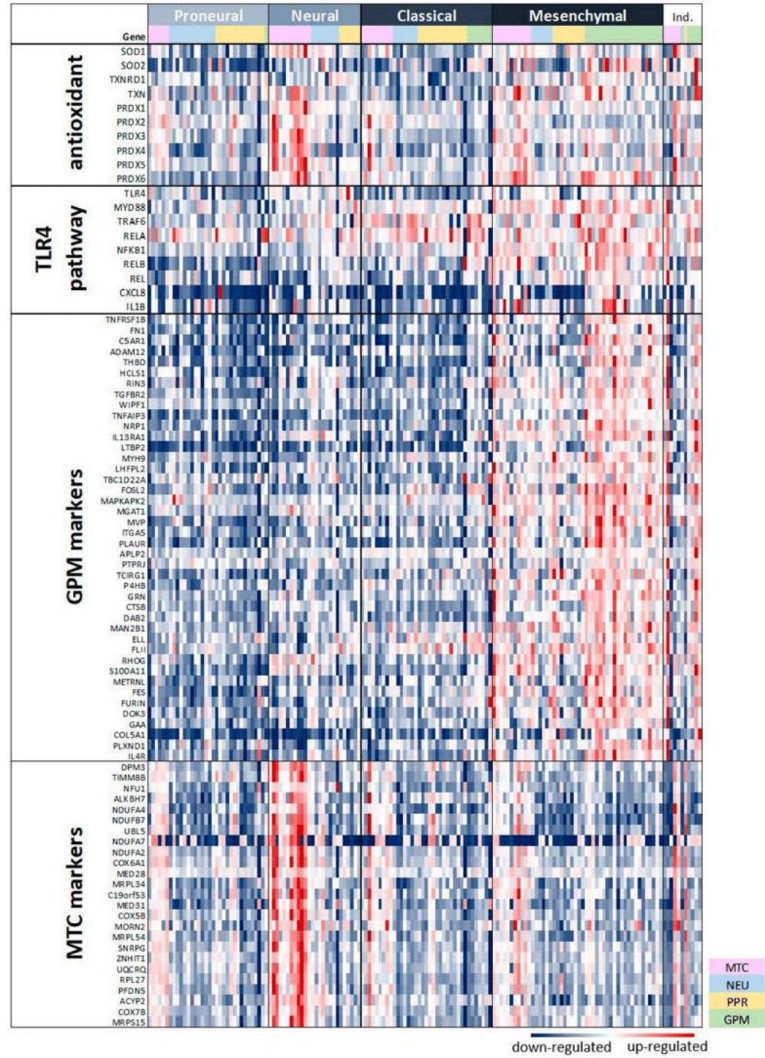
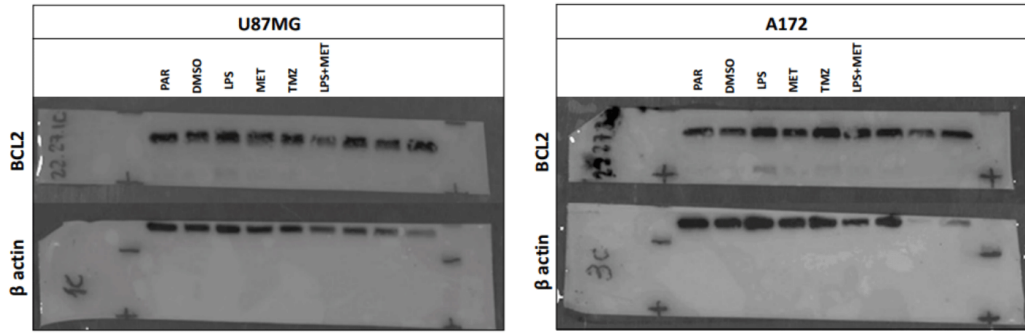


Figure S5. Heatmap of antioxidant genes, TLR4 pathway-related genes, marker genes for glycolytic plurimetabolic (GPM) and mitochondrial (MTC) subtypes according to Garofano's, 2021 [32] in 160 GBM cases of the TCGA-GBM-RNASeq dataset classified according to Verhaak, 2010 [60] in proneural, neural, classical and mesenchymal molecular subtypes and according to Garofano's MTC, neural (NEU), proliferative/progenitor (PPR), and GPM metabolic subtypes. The gene expression levels are normalized by z-score, and up-regulated genes are in red, and down-regulated in blue.



Western Blot images for U87MG and A172 cells. Proteins extracted from each cell line in the designated treatment condition were loaded in one gel. The membrane was cropped to avoid antibodies cross reaction.

Discussion

TLR4 and Glioblastoma - final remarks

6 Discussion- TLR4 and Glioblastoma – final remarks

In the present work, we analyzed the signaling pathways involved in TLR4 activation in GBM, based on *in vitro* experiments with GBM cell lines with transcriptomic approach and *in silico* validation in the TCGA GBM RNASeq dataset. First, in the publication 1 we confirmed the TLR4 expression in human astrocytoma samples and in human GBM derived cell lines. The Mesenchymal (MES) GBM subtype exhibited the highest TLR4 expression, and also upregulation of important TLR4 downstream signaling targets. The TLR4 agonist, LPS, was used to track the involved signaling pathways in MES-GBM cell line, U87MG. TLR4-agonists have been tested in several clinical trials and have proved to improve the outcome in several types of cancers. These trials aimed to activate inflammatory responses (64) by enhancing the recruitment of lymphocytes (65) or increasing antigen presentation by concomitant intratumoral injection of immature dendritic cells (66). Moreover, the safety of immune checkpoint blockage together with TLR4-agonists was confirmed in phase I clinical trials, and lymphoma patients with upregulated TLR4 presenting better outcome in phase II clinical trial (67).

The demonstration of TLR4 in GBM tumor cells pointed this receptor as a potential therapeutic target in GBM. As TLR4 recognizes self-molecules, as damage associated molecules and promotes pro-inflammatory response (68), it may be triggered by GBM necrotic cell debris (34) to activate immune response. The GBM tumor microenvironment is immunosuppressed (7), devoid from lymphocytes (69), and the major immune population of macrophages derived from monocytes and microglia present immunosuppressed and pro-tumor survival profiles (70, 71). Macrophages co-cultured with GBM cells exhibited downregulation of TLR4 (72). Thus, a therapeutic strategy to activate TLR4 in GBM is justified in this context. However, in parallel to a pro-inflammatory response with upregulation of *IL1B*, we observed upregulation of pro-proliferative gene expressions, such as *SRF* and *JUN*, and also of DNA repair related genes after LPS stimulation of U87MG cells. In fact, a correlation of TLR4 with DNA repair genes has also been observed in kidney clear cell carcinoma, melanoma, and stomach adenocarcinoma (73). Upregulation of DNA repair pathway may contribute to TMZ therapy resistance (12). Regulation of TLR4 by miR-23b-5p was described in GBM,

where TMZ resistant cells presented downregulation of this miR, and its overexpression increased tumoral cell death (13). TLR4 was also associated to radiation resistance through upregulation of DNA repair, by a mechanism involving activation of MYD88 and NF- κ B (16). Among the upregulated DNA repair genes detected in this study, RAD51 is the central enzyme for homologous recombination of double strand break repair (74) and there was a commercial pharmacological compound, Amuvatinib (18), that has already been tested in clinical trials, including a phase I trial in GBM (18-21). Although, the compound was well tolerated, in the phase II clinical trial including small cell lung carcinoma the pre-established endpoint was not complied (20). Amuvatinib has also downregulated activation of c-MET receptor tyrosine kinase. The protein c-MET is associated with cell survival and proliferation (75). *In vitro* study with glioma cells, a specific antibody blocking RAD51 caused DNA damage accumulation and cell death (76). In our study, U87MG cells stimulated with LPS, RAD51 inhibition with Amuvatinib, led to significant decrease in tumor cell viability at the rate of TMZ treated cells. *FEN1* was another upregulated DNA repair gene after LPS treatment of U87MG cells, that was correlated with *RAD51* expression. Similarly, *FEN1* upregulation was observed in TMZ resistant cells, and in glioma patients associated with poor overall survival (12). Pharmacological inhibition of *FEN1* increased double strand breaks leading to genome instability and cell death (12), reverted TMZ resistance, and downregulated *RAD51* in glioma mouse model. Therefore, *FEN1* inhibition may be another option for combined therapy in GBM, Nevertheless, specificity of these compounds for inhibition of tumor cells-only still needs to be proven to avoid undesired effect on DNA repair essential for the survival of normal cells (17).

Interestingly, in U87MG cells, TLR4 activation led to apoptosis, but TLR4 inhibition also led to cell cycle arrest, cell death and decreased migration (77). Therefore, the comprehension of the involved pathways in TLR4 activation and inhibition will help to refine the options for combinatory therapy in GBM. Curcumin was reported as owing pharmacological effect to downregulate TLR4 and its downstream cascade targets as p65, IL-1 β and IL-6 (50), decreasing U87MG cell viability. TAK-242, a more specific inhibitor of TLR4, decreased migration and invasion of ovarian and breast cancer cells (78). Metformin (MET) decreased LPS response and NF- κ B activation in immune cells (27). Repurposing MET for GBM

treatment is compelling, as MET is a well-known medication for diabetes, well tolerated already tested for long-term usage.

Therefore, as the next step of the study we analyzed the role of MET associated with LPS treatment in GBM cells. Two different GBM cell lines, U87MG and A172, were used to this end, for both being MES-subtype but with distinct metabolic profile, according to Garofano's recent report (44). U87MG cells presented glycolytic / plurimetabolic (GPM) phenotype and A172 presented upregulation of complex I of oxidative phosphorylation related genes, being classified with mitochondrial (MTC) phenotype. Transcriptomic analysis of both cell lineages treated for LPS, MET and LPS+MET showed upregulation of ER stress genes. Additionally, differences in the antioxidant status was identified. A172 cells presenting an upregulation of anti-oxidative genes, as *SOD1*, peroxiredoxins, and *TRX*, were less prone to mitochondrial oxidative stress that hindered an increment of apoptosis after LPS+MET treatment. Instead of apoptosis, A172 cells presented downregulation of chromosome segregation related genes, and cell cycle arrest in G2/M phase after MET+TMZ treatment. U87MG cells with GPM profile presented increased cell death, through reduced BCL-2, a cell survival gene, suggesting an increment of autophagic apoptosis after LPS+MET+TMZ treatment. Schematic main findings of these combined treatments of U87MG and A172 cells are presented in figure 1.

The validation of the transcriptomic findings was performed *in silico* in GBM RNASeq dataset of the TCGA. In this dataset, GPM-GBM subtype showed TLR4 activation with downstream pathway genes, presenting eligibility characteristics for MET treatment. However, such cases also presented upregulation of *IL8*, a pro-angiogenic factor, suggesting that a combination treatment for MET and IL-8 inhibition may be more effective. Upregulation of anti-oxidative genes was validated in MTC-GBM subtype at the TCGA-GBM RNASeq dataset, and for those cases an

inhibition of antioxidant factors, specially SOD1 inhibitor, may be indicated.

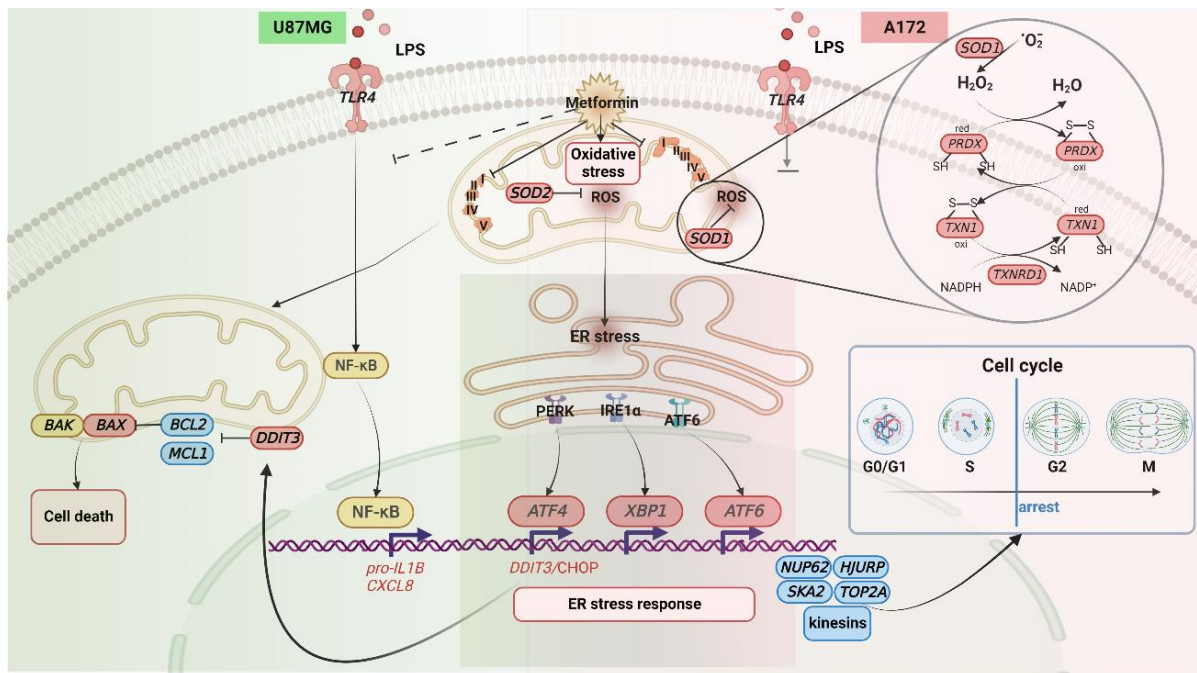


Figure 1. Graphical abstract. U87MG and A172 cells, two GBM cell lines, exhibited different responses after Metformin (MET) and Lipopolysaccharide (LPS) treatment. U87MG cells exhibited upregulation of *SOD2*, while A172 presented upregulation of *SOD1*, peroxiredoxins, and thioredoxin genes. U87MG presented activation of the TLR4 pathway, leading to upregulation of *CXCL8* and *IL1B* after LPS stimulation, whereas A172 showed no response to LPS. In both cell lines, MET treatment blunted mitochondrial respiration and increased mitochondrial superoxide production, leading to upregulation of genes related to ER stress. U87MG exhibited upregulation of pro-apoptotic genes and downregulation of anti-apoptotic genes, resulting in increased apoptosis after MET+LPS+TMZ combination treatment. A172 exhibited downregulation of cell cycle genes, leading to cell cycle arrest after MET treatment. The graphical abstract was produced using [BioRender.com](https://www.biorender.com).

Enthusiasm for MET in cancer therapies is increasing. New studies since the publication 2 were released and will be discussed next. Two studies, one in breast cancer cells and another in colon cancer cells, observed improvement of outcome with MET combined therapy with other drugs. MET was responsible to increase oxidative stress, cell cycle arrest and cell death (79, 80). Oxidative stress due to MET induced DNA damage and cell death (80). In colorectal cancer cells, a phosphoproteomic approach identified alterations in cell cycle regulation proteins with cell cycle arrest in MET treated cells after 24hrs. The combined therapy with MET and inhibitor of BCL-2 or BCL-XL improved the anti-survival effect of MET (81). These findings were convergent with our study presented in publication 2, and highlight the multiomics approach to refine the search for potential targets to improve MET therapy.

Additionally, CAR-T cell was prepared in a hydrogel scaffold containing MET,

and injected in a gastric cancer animal model. The CAR-T cells were more proliferative with better metabolic fitness than tumor cells, and no tumor growth was observed in the animals after 60 days (32).

7 Conclusion

In conclusion, TLR4 proved to be an interesting therapeutic target in GBM. As GBM is a very heterogeneous tumor, the combination therapy needs to be featured according to characteristics of each subtype described so far. Taking into account the molecular mesenchymal (MES) subtype, and the metabolic phenotypes: glycolytic / plurimetabolic (GPM) and mitochondrial (MTC) metabolic phenotype, the MES-GPM-GBM presented upregulation of TLR4 pathway with eligibility for metformin treatment, while the MES-MTC-GBM presented gene expression profile prone to anti-oxidative inhibitor therapy, as anti-SOD1. Combinatory therapy with anti-DNA repair, as anti-RDA51, and anti-angiogenic factor, as anti-IL8 may be beneficial for MES-GPM-GBM.

8 References for introduction and discussion

1. O'Neill LAJ, Golenbock D, Bowie AG. The history of Toll-like receptors - redefining innate immunity. *Nat Rev Immunol.* 2013;13(6):453-60.
2. Silke J, Rickard JA, Gerlic M. The diverse role of RIP kinases in necroptosis and inflammation. *Nat Immunol.* 2015;16(7):689-97.
3. Hanahan D, Weinberg Robert A. Hallmarks of Cancer: The Next Generation. *Cell.* 2011;144(5):646-74.
4. Hambardzumyan D, Gutmann DH, Kettenmann H. The role of microglia and macrophages in glioma maintenance and progression. *Nat Neurosci.* 2015;19(1):20-7.
5. Ye K, Wu Y, Sun Y, Lin J, Xu J. TLR4 siRNA inhibits proliferation and invasion in colorectal cancer cells by downregulating ACAT1 expression. *Life Sci.* 2016;155:133-9.
6. Liu Y, Li T, Xu Y, Xu E, Zhou M, Wang B, et al. Effects of TLR4 gene silencing on the proliferation and apoptosis of hepatocarcinoma HEPG2 cells. *Oncol Lett.* 2016;11(5):3054-60.
7. Sarrazy V, Vedrenne N, Billet F, Bordeau N, Lepreux S, Vital A, et al. TLR4 signal transduction pathways neutralize the effect of Fas signals on glioblastoma cell proliferation and migration. *Cancer Lett.* 2011;311(2):195-202.
8. Moretti IF, Franco DG, de Almeida Galatro TF, Oba-Shinjo SM, Marie SKN. Plasmatic membrane toll-like receptor expressions in human astrocytomas. *PLOS ONE.* 2018;13(6):e0199211.
9. Pradere JP, Dapito DH, Schwabe RF. The Yin and Yang of Toll-like receptors in cancer. *Oncogene.* 2014;33(27):3485-95.
10. Rakoff-Nahoum S, Medzhitov R. Toll-like receptors and cancer. *Nat Rev Cancer.* 2009;9(1):57-63.
11. Botos I, Segal DM, Davies DR. The Structural Biology of Toll-like Receptors. *Structure.* 2011;19(4):447-59.
12. Takeda K, Kaisho T, Akira S. Toll-like receptors. *Annu Rev Immunol.* 2003;21:335-76.
13. Yu M, Wang HC, Ding AH, Golenbock DT, Latz E, Czura CJ, et al. HMGB1 signals through toll-like receptor (TLR) 4 and TLR2. *Shock.* 2006;26(2):174-9.
14. Galluzzi L, Vacchelli E, Eggermont A, Fridman WH, Galon J, Sautes-Fridman C, et al. Trial Watch Experimental Toll-like receptor agonists for cancer therapy. *Oncoimmunology.* 2012;1(5):699-716.
15. Taylor RC, Cullen SP, Martin SJ. Apoptosis: controlled demolition at the cellular level. *Nat Rev Mol Cell Biol.* 2008;9(3):231-41.
16. Chun KH, Seong SY. CD14 but not MD2 transmit signals from DAMP. *Int Immunopharmacol.* 2010;10(1):98-106.

17. Huang DB, Vu D, Cassidy LA, Zimmerman JM, Maher LJ, 3rd, Ghosh G. Crystal structure of NF-kappaB (p50)₂ complexed to a high-affinity RNA aptamer. *Proc Natl Acad Sci U S A*. 2003;100(16):9268-73.
18. Hayden MS, Ghosh S. Signaling to NF-kappaB. *Genes Dev*. 2004;18(18):2195-224.
19. Karin M, Ben-Neriah Y. Phosphorylation meets ubiquitination: the control of NF-[kappa]B activity. *Annu Rev Immunol*. 2000;18:621-63.
20. Hedayat M, Takeda K, Rezaei N. Prophylactic and therapeutic implications of toll-like receptor ligands. *Medicinal Research Reviews*. 2012;32(2):294-325.
21. Beutler B. Microbe sensing, positive feedback loops, and the pathogenesis of inflammatory diseases. *Immunol Rev*. 2009;227(1):248-63.
22. Guttridge DC, Albanese C, Reuther JY, Pestell RG, Baldwin AS, Jr. NF-kappaB controls cell growth and differentiation through transcriptional regulation of cyclin D1. *Mol Cell Biol*. 1999;19(8):5785-99.
23. Lai J-l, Liu Y-h, Liu C, Qi M-p, Liu R-n, Zhu X-f, et al. Indirubin Inhibits LPS-Induced Inflammation via TLR4 Abrogation Mediated by the NF-kB and MAPK Signaling Pathways. *Inflammation*. 2017;40(1):1-12.
24. David A, Arnaud N, Fradet M, Lascaux H, Ouk-Martin C, Gachard N, et al. c-Myc dysregulation is a co-transforming event for nuclear factor-kappaB activated B cells. *Haematologica*. 2017;102(5):883-94.
25. Grivennikov S, Karin E, Terzic J, Mucida D, Yu GY, Vallabhapurapu S, et al. IL-6 and Stat3 are required for survival of intestinal epithelial cells and development of colitis-associated cancer. *Cancer Cell*. 2009;15(2):103-13.
26. Holani R, Babbar A, Blyth GAD, Lopes F, Jijon H, McKay DM, et al. Cathelicidin-mediated lipopolysaccharide signaling via intracellular TLR4 in colonic epithelial cells evokes CXCL8 production. *Gut Microbes*. 2020;12(1):1785802.
27. Erdogan O, Xie L, Wang L, Wu B, Kong Q, Wan Y, et al. Proteomic dissection of LPS-inducible, PHF8-dependent secretome reveals novel roles of PHF8 in TLR4-induced acute inflammation and T cell proliferation. *Sci Rep*. 2016;6:24833.
28. He Y, Hara H, Núñez G. Mechanism and Regulation of NLRP3 Inflammasome Activation. *Trends in Biochemical Sciences*. 2016;41(12):1012-21.
29. Aksoy E, Taboubi S, Torres D, Delbauve S, Hachani A, Whitehead MA, et al. The p110[delta] isoform of the kinase PI(3)K controls the subcellular compartmentalization of TLR4 signaling and protects from endotoxic shock. *Nat Immunol*. 2012;13(11):1045-54.
30. Li J, Lee DSW, Madrenas J. Evolving Bacterial Envelopes and Plasticity of TLR2-dependent Responses: Basic Research and Translational Opportunities. *Frontiers in Immunology*. 2013;4.
31. Kawai T, Akira S. The role of pattern-recognition receptors in innate immunity: update on Toll-like receptors. *Nature Immunology*. 2010;11(5):373-84.
32. Vanlangenakker N, Vanden Berghe T, Vandenabeele P. Many stimuli pull the necrotic

- trigger, an overview. *Cell Death Differ.* 2012;19(1):75-86.
33. Hasan UA, Caux C, Perrot I, Doffin AC, Menetrier-Caux C, Trinchieri G, et al. Cell proliferation and survival induced by Toll-like receptors is antagonized by type I IFNs. *Proc Natl Acad Sci U S A.* 2007;104(19):8047-52.
 34. Louis DN, Ohgaki H, Wiestler OD, Cavenee WK, Burger PC, Jouvet A, et al. The 2007 WHO Classification of Tumours of the Central Nervous System. *Acta Neuropathology.* 2007 july:97-109.
 35. Stupp R, Mason WP, van den Beuf MJ. Radiotherapy plus concomitant and adjuvant temozolomide for newly diagnosed glioblastoma (vol 352, pg 19, 2005). *Annals of Oncology.* 2005;16(6):949-.
 36. Appin CL, Brat DJ. Molecular Genetics of Gliomas. *Cancer Journal.* 2014;20(1):66-72.
 37. Omuro A, DeAngelis LM. Glioblastoma and other malignant gliomas: A clinical review. *JAMA.* 2013;310(17):1842-50.
 38. Ohgaki H, Kleihues P. The Definition of Primary and Secondary Glioblastoma. *Clinical Cancer Research.* 2013;19(4):764-72.
 39. Phillips HS, Kharbanda S, Chen R, Forrest WF, Soriano RH, Wu TD, et al. Molecular subclasses of high-grade glioma predict prognosis, delineate a pattern of disease progression, and resemble stages in neurogenesis. *Cancer Cell.* 2006;9(3):157-73.
 40. Colman H, Zhang L, Sulman EP, McDonald JM, Shooshtari NL, Rivera A, et al. A multigene predictor of outcome in glioblastoma. *Neuro Oncol.* 2010;12(1):49-57.
 41. Verhaak RG, Hoadley KA, Purdom E, Wang V, Qi Y, Wilkerson MD, et al. Integrated genomic analysis identifies clinically relevant subtypes of glioblastoma characterized by abnormalities in PDGFRA, IDH1, EGFR, and NF1. *Cancer Cell.* 2010;17(1):98-110.
 42. Louis DN, Perry A, Reifenberger G, von Deimling A, Figarella-Branger D, Cavenee WK, et al. The 2016 World Health Organization Classification of Tumors of the Central Nervous System: a summary. *Acta Neuropathologica.* 2016;131(6):803-20.
 43. Louis DN, Perry A, Wesseling P, Brat DJ, Cree IA, Figarella-Branger D, et al. The 2021 WHO Classification of Tumors of the Central Nervous System: a summary. *Neuro Oncol.* 2021;23(8):1231-51.
 44. Garofano L, Migliozi S, Oh YT, D'Angelo F, Najac RD, Ko A, et al. Pathway-based classification of glioblastoma uncovers a mitochondrial subtype with therapeutic vulnerabilities. *Nat Cancer.* 2021;2(2):141-56.
 45. Zu Y, Ping W, Deng T, Zhang N, Fu X, Sun W. Lipopolysaccharide-induced toll-like receptor 4 signaling in esophageal squamous cell carcinoma promotes tumor proliferation and regulates inflammatory cytokines expression. *Dis Esophagus.* 2016.
 46. Cai G, Ma X, Chen B, Huang Y, Liu S, Yang H, et al. Galectin-3 induces ovarian cancer cell survival and chemoresistance via TLR4 signaling activation. *Tumour Biol.* 2016.
 47. Lopes JA, Borges-Canha M, Pimentel-Nunes P. Innate immunity and hepatocarcinoma: Can toll-like receptors open the door to oncogenesis? *World J Hepatol.* 2016;8(3):162-82.

48. Dong YQ, Lu CW, Zhang L, Yang J, Hameed W, Chen W. Toll-like receptor 4 signaling promotes invasion of hepatocellular carcinoma cells through MKK4/JNK pathway. *Mol Immunol.* 2015;68(2 Pt C):671-83.
49. Bedini A, Baiula M, Vincelli G, Formaggio F, Lombardi S, Caprini M, et al. Nociceptin/orphanin FQ antagonizes lipopolysaccharide-stimulated proliferation, migration and inflammatory signaling in human glioblastoma U87 cells. *Biochemical Pharmacology.* 2017;140:89-104.
50. Bi F, Wang J, Zheng X, Xiao J, Zhi C, Gu J, et al. HSP60 participates in the anti-glioma effects of curcumin. *Exp Ther Med.* 2021;21(3):204.
51. Li H, Li J, Zhang G, Da Q, Chen L, Yu S, et al. HMGB1-Induced p62 Overexpression Promotes Snail-Mediated Epithelial-Mesenchymal Transition in Glioblastoma Cells via the Degradation of GSK-3 β . *Theranostics.* 2019;9(7):1909-22.
52. Grauer OM, Molling JW, Bennink E, Toonen LWJ, Suttmuller RPM, Nierkens S, et al. TLR Ligands in the Local Treatment of Established Intracerebral Murine Gliomas. *Journal of Immunology.* 2008;181(10):6720-9.
53. Goto Y, Arigami T, Kitago M, Nguyen SL, Narita N, Ferrone S, et al. Activation of Toll-like receptors 2, 3, and 4 on human melanoma cells induces inflammatory factors. *Mol Cancer Ther.* 2008;7(11):3642-53.
54. Jin H, Peng X, He Y, Ruganzu JB, Yang W. Tanshinone IIA suppresses lipopolysaccharide-induced neuroinflammatory responses through NF- κ B/MAPKs signaling pathways in human U87 astrocytoma cells. *Brain Research Bulletin.* 2020;164:136-45.
55. Ma WW, Li CQ, Zhao L, Wang YS, Xiao R. NF- κ B-mediated inflammatory damage is differentially affected in SH-SY5Y and C6 cells treated with 27-hydroxycholesterol. *Food Sci Nutr.* 2019;7(5):1685-94.
56. Hu F, OD AD, Hahn A, Yu Y, Scavetta RJ, Dittmar G, et al. Glioma-derived versican promotes tumor expansion via glioma-associated microglial/macrophages Toll-like receptor 2 signaling. *Neuro Oncol.* 2015;17(2):200-10.
57. Chicoine MR, Zahner M, Won EK, Kalra RR, Kitamura T, Perry A, et al. The in vivo antitumoral effects of lipopolysaccharide against glioblastoma multiforme are mediated in part by toll-like receptor 4. *Neurosurgery.* 2007;60(2):372-80.
58. Ferrandez E, Gutierrez O, Segundo DS, Fernandez-Luna JL. NF κ B activation in differentiating glioblastoma stem-like cells is promoted by hyaluronic acid signaling through TLR4. *Scientific Reports.* 2018;8(1):6341.
59. Megías J, Martínez A, San-Miguel T, Gil-Benso R, Muñoz-Hidalgo L, Albert-Bellver D, et al. Pam3CSK4, a TLR2 ligand, induces differentiation of glioblastoma stem cells and confers susceptibility to temozolomide. *Investigational New Drugs.* 2020;38(2):299-310.
60. Alvarado AG, Thiagarajan PS, Mulkearns-Hubert EE, Silver DJ, Hale JS, Alban TJ, et al. Glioblastoma Cancer Stem Cells Evade Innate Immune Suppression of Self-Renewal through Reduced TLR4 Expression. *Cell Stem Cell.* 2017;20(4):450-61.e4.
61. Dzaye O, Hu F, Derkow K, Haage V, Euskirchen P, Harms C, et al. Glioma Stem Cells

- but Not Bulk Glioma Cells Upregulate IL-6 Secretion in Microglia/Brain Macrophages via Toll-like Receptor 4 Signaling. *J Neuropathol Exp Neurol.* 2016;75(5):429-40.
62. Moretti IF, Lerario AM, Trombetta-Lima M, Sola PR, da Silva Soares R, Oba-Shinjo SM, et al. Late p65 nuclear translocation in glioblastoma cells indicates non-canonical TLR4 signaling and activation of DNA repair genes. *Scientific Reports.* 2021;11(1):1333.
 63. Moretti IF, Lerario AM, Sola PR, Macedo-da-Silva J, Baptista MDS, Palmisano G, et al. GBM Cells Exhibit Susceptibility to Metformin Treatment According to TLR4 Pathway Activation and Metabolic and Antioxidant Status. *Cancers (Basel).* 2023;15(3).
 64. Lin MJ, Svensson-Arvelund J, Lubitz GS, Marabelle A, Melero I, Brown BD, et al. Cancer vaccines: the next immunotherapy frontier. *Nature Cancer.* 2022;3(8):911-26.
 65. Bhatia S, Miller NJ, Lu H, Longino NV, Ibrani D, Shinohara MM, et al. Intratumoral G100, a TLR4 Agonist, Induces Antitumor Immune Responses and Tumor Regression in Patients with Merkel Cell Carcinoma. *Clin Cancer Res.* 2019;25(4):1185-95.
 66. Endo H, Saito T, Kenjo A, Hoshino M, Terashima M, Sato T, et al. Phase I trial of preoperative intratumoral injection of immature dendritic cells and OK-432 for resectable pancreatic cancer patients. *J Hepatobiliary Pancreat Sci.* 2012;19(4):465-75.
 67. Melero I, Castanon E, Alvarez M, Champiat S, Marabelle A. Intratumoural administration and tumour tissue targeting of cancer immunotherapies. *Nature Reviews Clinical Oncology.* 2021;18(9):558-76.
 68. Land WG. Role of DAMPs and cell death in autoimmune diseases: the example of multiple sclerosis. *Genes & Immunity.* 2023.
 69. Karimi E, Yu MW, Maritan SM, Perus LJM, Rezanejad M, Sorin M, et al. Single-cell spatial immune landscapes of primary and metastatic brain tumours. *Nature.* 2023;614(7948):555-63.
 70. Lee AH, Sun L, Mochizuki AY, Reynoso JG, Orpilla J, Chow F, et al. Neoadjuvant PD-1 blockade induces T cell and cDC1 activation but fails to overcome the immunosuppressive tumor associated macrophages in recurrent glioblastoma. *Nature Communications.* 2021;12(1):6938.
 71. Andersen BM, Faust Akl C, Wheeler MA, Chiocca EA, Reardon DA, Quintana FJ. Glial and myeloid heterogeneity in the brain tumour microenvironment. *Nature Reviews Cancer.* 2021;21(12):786-802.
 72. da Cruz LLP, de Souza PO, Dal Prá M, Falchetti M, de Abreu AM, Azambuja JH, et al. TLR4 expression and functionality are downregulated in glioblastoma cells and in tumor-associated macrophages: A new mechanism of immune evasion? *Biochimica et Biophysica Acta (BBA) - Molecular Basis of Disease.* 2021;1867(8):166155.
 73. Hu J, Xu J, Feng X, Li Y, Hua F, Xu G. Differential Expression of the TLR4 Gene in Pan-Cancer and Its Related Mechanism. *Front Cell Dev Biol.* 2021;9:700661.
 74. Groelly FJ, Fawkes M, Dagg RA, Blackford AN, Tarsounas M. Targeting DNA damage response pathways in cancer. *Nature Reviews Cancer.* 2023;23(2):78-94.

75. Phillip CJ, Zaman S, Shentu S, Balakrishnan K, Zhang J, Baladandayuthapani V, et al. Targeting MET kinase with the small-molecule inhibitor amuvatinib induces cytotoxicity in primary myeloma cells and cell lines. *Journal of Hematology & Oncology*. 2013;6(1):92.
76. Turchick A, Liu Y, Zhao W, Cohen I, Glazer PM. Synthetic lethality of a cell-penetrating anti-RAD51 antibody in PTEN-deficient melanoma and glioma cells. *Oncotarget*. 2019;10(13):1272-83.
77. Liu Y, Ju Y, Liu J, Chen Y, Huo X, Liu L. Inhibition of proliferation and migration and induction of apoptosis in glioma cells by silencing TLR4 expression levels via RNA interference. *Oncol Lett*. 2021;21(1):13.
78. Zandi Z, Kashani B, Poursani EM, Bashash D, Kabuli M, Momeny M, et al. TLR4 blockade using TAK-242 suppresses ovarian and breast cancer cells invasion through the inhibition of extracellular matrix degradation and epithelial-mesenchymal transition. *Eur J Pharmacol*. 2019;853:256-63.
79. Fatehi R, Rashedinia M, Akbarizadeh AR, zamani M, Firouzabadi N. Metformin enhances anti-cancer properties of resveratrol in MCF-7 breast cancer cells via induction of apoptosis, autophagy and alteration in cell cycle distribution. *Biochemical and Biophysical Research Communications*. 2023;644:130-9.
80. Kang BG, Shende M, Inci G, Park SH, Jung JS, Kim SB, et al. Combination of metformin/efavirenz/fluoxetine exhibits profound anticancer activity via a cancer cell-specific ROS amplification. *Cancer Biol Ther*. 2023;24(1):20-32.
81. Salovska B, Gao E, Müller-Dott S, Li W, Cordon CC, Wang S, et al. Phosphoproteomic analysis of metformin signaling in colorectal cancer cells elucidates mechanism of action and potential therapeutic opportunities. *Clin Transl Med*. 2023;13(2):e1179.

9 Anexos

FACULDADE DE MEDICINA DA
UNIVERSIDADE DE SÃO
PAULO - FMUSP



PARECER CONSUBSTANCIADO DO CEP

DADOS DO PROJETO DE PESQUISA

Título da Pesquisa: Expressões dos Receptores do Tipo Toll em Astrocitomas Humanos de Diferentes Graus de Malignidade

Pesquisador: Suely Kazue Nagahashi Marie

Área Temática:

Versão: 1

CAAE: 42280015.9.0000.0065

Instituição Proponente: Faculdade de Medicina da Universidade de São Paulo

Patrocinador Principal: Hospital das Clínicas da Faculdade de Medicina da USP
FUNDAÇÃO DE AMPARO A PESQUISA DO ESTADO DE SÃO PAULO

DADOS DO PARECER

Número do Parecer: 974.633

Data da Relatoria: 04/03/2015

Apresentação do Projeto:

Trata-se projeto de mestrado para detecção da expressão de receptores Toll em astrocitomas humanos, usando tecido parafinado estocado. O projeto é bem apresentado e envolve apenas uso retrospectivo de tecido.

Objetivo da Pesquisa:

Adequado, a identificação de marcadores celulares diferencial nos astrócitos tumorais, além do conhecimento direto e suporte diagnóstico, pode sugerir receptores para futuras terapias, já que os receptores Toll são expressos na superfície celular.

Avaliação dos Riscos e Benefícios:

Futuras terapias

Comentários e Considerações sobre a Pesquisa:

Adequada

Considerações sobre os Termos de apresentação obrigatória:

Não há necessidade

Recomendações:

Nenhuma

Endereço: DOUTOR ARNALDO 251 21º andar sala 36

Bairro: PACAEMBU

CEP: 01.246-903

UF: SP

Município: SAO PAULO

Telefone: (11)3893-4401

E-mail: cep.fm@usp.br

FACULDADE DE MEDICINA DA
UNIVERSIDADE DE SÃO
PAULO - FMUSP



Continuação do Parecer: 974.633

Conclusões ou Pendências e Lista de Inadequações:

Nenhuma

Situação do Parecer:

Aprovado

Necessita Apreciação da CONEP:

Não

Considerações Finais a critério do CEP:

SAO PAULO, 05 de Março de 2015

Assinado por:
Roger Chammas
(Coordenador)

Endereço: DOUTOR ARNALDO 251 21º andar sala 36
Bairro: PACAEMBU **CEP:** 01.246-903
UF: SP **Município:** SAO PAULO
Telefone: (11)3893-4401 **E-mail:** cep.fm@usp.br

APROVAÇÃO

O Comitê de Ética em Pesquisa da Faculdade de Medicina da Universidade de São Paulo, em sessão de 04/03/2015, APROVOU o Protocolo de Pesquisa nº 059/15 intitulado: “EXPRESSÕES DOS RECEPTORES DO TIPO TOLL EM ASTROCITOMAS HUMANOS DE DIFERENTES GRAUS DE MALIGNIDADE” apresentado pelo Departamento de NEUROLOGIA.

Cabe ao pesquisador elaborar e apresentar ao CEP-FMUSP, os relatórios parciais e final sobre a pesquisa (Resolução do Conselho Nacional de Saúde nº 466/12, inciso IX.2, letra "c").

Pesquisador (a) Responsável: Suely Kazue Nagahashi Marie

Pesquisador (a) Executante: Isabele Fattori Moretti

CEP-FMUSP, 06 de Março de 2015.



Prof. Dr. Paulo Eurípedes Marchiori
Vice-Coordenador
Comitê de Ética em Pesquisa